Faculty of Engineering

Electrophoretic Deposition of Carbon Nanotubes onto Carbon Fiber Laminated Composites: Effect of Suspension Medium, Deposition Voltage, and Time

Nur – Azzah Afifah binti Taib

Master of Engineering
2023

Electrophoretic Deposition of Carbon Nanotubes onto Carbon Fiber Laminated Composites: Effect of Suspension Medium, Deposition Voltage, and Time

Nur – Azzah Afifah binti Taib

A thesis submitted

In fulfillment of the requirements for the degree of Master of Engineering

(Chemical Engineering)

Faculty of Engineering
UNIVERSITI MALAYSIA SARAWAK

2023

DECLARATION

I declare that the work in this thesis was carried out in accordance with the regulations of Universiti Malaysia Sarawak. Except where due acknowledgements have been made, the work is that of the author alone. The thesis has not been accepted for any degree and is not concurrently submitted in candidature of any other degree.

....

Signature

Name: Nur–Azzah Afifah binti Taib

Matric No.: 19020097

Faculty of Engineering

Universiti Malaysia Sarawak

Date : 26/12/2023

ACKNOWLEDGEMENT

My highest praise to Allah S.W.T, the Most Gracious and the Most Merciful, for His blessing, strength, and guidance in completing this thesis. All problems and challenges were able to be surpassed by His allowance. My sincere gratitude to my supervisor, Dr. Md. Rezaur Rahman for his supervision, advice, and support. This research was completed with his consistent guidance and valuable critics throughout the work. Next, I would like to express my highest gratitude to my family, especially my parents, whose continuous support and trust in me have played a vital role in my study career—also, deepest thanks to all my friends for helping me in many aspects of my study life. Finally, I would like to thank the Department of Chemical Engineering, Faculty of Engineering, and Universiti Malaysia Sarawak for making it possible for me to complete my study here. Thank you all.

ABSTRACT

Multiwalled carbon nanotubes-Carbon Fiber (MWCNT–CF/) epoxy laminated composites are widely used in many applications, and electrophoretic deposition (EPD) is a hybridisation method that is often used. This research focuses on improving the technique by optimising the input parameters to obtain composites with enhanced tensile properties. Various studies have utilized the EPD method, but there hardly any study utilized the water-methanol mixture as the medium. This study showed that the input parameters (volume ratio of suspension medium, deposition voltage, and time) influenced the responses of the research (tensile strength and Young's modulus). Firstly, the optical observation showed good distribution of MWCNTs throughout the medium. Secondly, the analyses of Fourier Transform Infra-Red (FTIR), Scanning Electron Microscopy (SEM), and tensile properties demonstrated that the input factors directly influenced the composites. Thirdly, the ideal factors that correspond to the desired responses were obtained through the optimization. For the first design of experiment (DoE) (0% water, 100% methanol and 100% water,0% methanol), the optimum conditions were a volume ratio of 99.99% water, a voltage of 20V, and time of 8.88 minutes, producing maximum tensile strength and young's modulus of 7.983 N/mm^2 and 268.558 N/mm^2, respectively. For the second DoE (20% water,80% methanol and 80% water, 20% methanol), tensile strength and young's modulus of 7.2766 N/mm^2 and 266.78 N/mm^2, respectively, were achieved when the ideal conditions were: volume ratio of 79.99 % water, voltage of 20V, and time of 5.22 minutes.

Keywords: MWCNTs, CF, epoxy, EPD, tensile properties

Pemendapan Electroforetik Karbon Nanotiub pada Komposit Berlapis Gentian Karbon: Kesan Media Ampaian, Voltan dan Masa Pemendapan

ABSTRAK

"Multiwalled "Karbon Nanotiub-Gentian Karbon (MWCNT–CF) epoksi komposit berlamina digunakan dalam banyak aplikasi, dan pemendapan elekrtoforetik (EPD) ialah kaedah hibridisasi yang kerap digunakan. Kajian ini berfokuskan peningkatan teknik dengan mengoptimum parameter input bagi mendapatkan komposit dengan sifat tegangan dipertingkat. Pelbagai kajian telah menggunakan EPD, tetapi hampir tiada kajian menggunakan campuran air-metanol sebagai media. Kajian ini menunjukkan bahawa parameter input (nisbah isipadu medium ampaian, voltan dan masa pemendapan) mempengaruhi respon kajian (kekuatan tegangan dan modulus "Young"). Pertama, pemerhatian optikal menunjukkan pengedaran MWCNTs yang bagus di keseluruhan medium. Kedua, analisis spektroskopi inframerah fourier transformasi (FTIR), pengimbasan mikroskop electron (SEM) dan sifat tegangan menunjukkan bahawa faktor input mempengaruhi komposit secara langsung. Ketiga, faktor ideal yang sepadan dengan respon diingini diperolehi daripada pengoptimuman. Bagi desain eksperimen (DoE) pertama (0% air,100% methanol dan 100% air,0% metanol), kondisi optimum ialah nisbah isipadu 99.99% air, voltan 20V, dan masa 8.88 minit, menghasilkan kekuatan tegangan dan modulus "Young" maksima 7.983N/mm^2 dan 268.558N/mm^2, masing-masing. Bagi DoE kedua (20% air,80% methanol dan 80% air,20% metanol), kekuatan tegangan dan modulus "Young" 7.2766N/mm^{2}dan 266.78 N/mm^2, masing–masing, diperolehi apabila keadaan ideal: nisbah isipadu 79.99% air, voltan 20V, dan masa 5.22 minit.

Kata kunci: *MWCNTs, CF, Epoksi, EPD, Sifat Tegangan*

TABLE OF CONTENTS

LIST OF TABLES

LIST OF FIGURES

LIST OF ABBREVIATIONS

2D	Two dimensional
3D	Three dimensional
AC	Alternating Current
ANOVA	Analysis of Variance
AP	Adequate Precision
ASTM	American Society for Testing and Materials
BA	Bioactive Glass
BBD	Box-Behnken Design
CCC	Circumscribed Central Composite Design
CCD	Central Composite Design
CCF	Face-centred Central Composite Design
CCI	Inscribed Central Composite Design
CF	Carbon Fiber
CFRP	Carbon Fiber Reinforced Polymer
CMC	Ceramic Matrix Composite
CNT	Carbon Nanotube
CNT–CF	Carbon Nanotube-Carbon Fiber
CO_2	Carbon Dioxide
C.V.	Coefficient of Variance
CVD	Chemical Vapor Deposition
DC	Direct Current
DE	Design Expert
DoE	Design of Experiment

DOM	Methodology of Desirability
E	Young's modulus
EM	Electrophoretic Mobility
EPD	Electrophoretic Deposition
FFD	Full Factorial Design
FRP	Fiber Reinforced Polymer
FTIR	Fourier Transform Infrared
HA	Hydroxyapatite
IR	Infra-Red
LED	Light-Emmiting Diode
LIBs	Lithium Ion Batteries
LOF	Lack-of-Fit
MeOH	Methanol
MFC	Microbial Fuel Cells
MWCNT	Multiwalled Carbon Nanotube
MWCNT-CF	Multiwalled Carbon Nanotube-Carbon Fiber
NHST	Null Hypothesis Significance Testing
PA	Polyamide
PANI	Polyaniline
PE	Polyethylene
PEDOT	Poly-(3,4-ethylenedioxythiophene)
PEEK	Polyetheretherketone
PEI	Polyetherimide
pH	Potential of Hydrogen
PMC	Polymer matrix composite

PP	Polypropylene
PP	Polypyrrole
PRESS	Prediction error sums of squares
PVA	Polyvinyl alcohol
R^2_{Adj}	Adjusted R^2
R^2_{Pred}	Predicted R^2
RSM	Response Surface Methodology
SEM	Scanning Electron Microscopy
SSA	Specific Surface Area
Std. Dev.	Standard Deviation
SWCNT	Single-walled Carbon Nanotubes
TAI	Turkish Aerospace Industries
TiO_2	Titanium Dioxide
TS	Tensile Strength
UPR	Unsaturated Polymer Resin
VE	Vinyl Ester
W	Water

CHAPTER 1

INTRODUCTION

1.1 Background of study

Carbon fiber (CF)/epoxy composite, also known as carbon fiber–reinforced polymer composites (CFRPs), has been used extensively in fields such as automotive, aerospace, marine, and energy to replace conventional metal materials. High strength and stiffness combined with moderately low density have increased the demand for CFRPs in the industries (Rodríguez-González & Rubio-González, 2019). The interfacial interactions of the CFs and epoxy matrix greatly influenced the performance of CFRPs, especially their mechanical properties (Park & Park, 2020). However, interaction between the matrix and fiber for CF and resin epoxy is not favored as the CF surface is non–polar while the epoxy resins are polar (Keyte et al., 2019). Additionally, CF surfaces that are chemically inert, hydrophobic, and intrinsically smooth have caused low interfacial bonding strength between the CF and the polymer matrix (Yao et al., 2018). Hence, the modification must be done at the fibre surface to overcome the CF's inertness and obtain strong fiber/matrix interfacial adhesion (Salahuddin et al., 2021).

Studies have shown that the CFRPs' interfacial properties can be improved by introducing carbon nanotubes (CNTs) onto the reinforcing CF (Sheth et al., 2020). Owing to their excellent mechanical properties, the addition of CNT may effectively enhance the CF–matrix interaction (Moaseri et al., 2016). In addition, the CFs' surface roughness is improved with the presence of CNT and subsequently increases the CF–matrix interfacial adhesion (Zakaria et al., 2020a). Not only taking advantage of the excellent properties of

CNTs, but the reinforced FRP material also maintained the superiority of the conventional fiber reinforcements (J. Li et al., 2021).

CNT-CF hybrids can be fabricated via several methods such as spray coating, chemical vapor deposition (CVD), electrophoretic deposition (EPD), dip coating, etc. Then, the nanoparticles are successfully deposited or attached to the CF surface. Among these methods, EPD has several advantages compared to the other techniques, which allowed this method to be used for CF surface modification (Yao et al., 2018). It is essential to use stable suspension media throughout the EPD process to ensure that the particles are dispersed stably (Chavez-Valdez et al., 2013). Water is commonly used in the EPD process for several reasons: cost effective, low requirement of electric field, easy to regulate throughout the process, and environmentally compatible (Ervina et al., 2019). Despite that, water electrolysis may occur when high voltage is applied in the process, which compromises the depositions' quality. Organic solvents such as alcohol are used to overcome the issue. However, a high applied voltage is needed for pure organic solvents. Apart from that, their particle mobility is low due to the little electric charge on the particles. It can be overcome by combining organic solvent and water as the solvent for the EPD process (Ouedraogo & Savadogo, 2013).

Table 1.1 lists some of the previous works in which EPD was used to deposit materials and their limitation in comparison to this research study. Based on the articles and previous works related to EPD, the number of investigations into the usage of mixture suspension medium, especially those involving the usage of methanol and water for the MWCNT deposition using the EPD method, is still relatively low. Therefore, this huge research gap in working with a methanol-water mixture suspension medium that had not yet been highlighted gives the researcher an opportunity to makes improvements in this area of study. Not only can the issue of the MWCNTs' stability in medium with various ratios be resolved, but the impact of the EPD parameters on the tensile properties of composites can also be resolved. Apart from that, the optimized values for the input parameters could also be obtained. This study investigate the effects of mixture suspension medium for the EPD process in enhancing the tensile properties of the composites.

This study is done in combination with the Response Surface Methodology (RSM) paired with the central composite design (CCD) to help optimize the obtained data. The interaction of the parameters used in the research was observed and optimized using RSM. Combining mathematical and statistical methods, RSM was able to build models by evaluating the effects of multiple independent variables to find the best value for each variable and get good results (Breig & Luti, 2021).

Table 1.1: Previous works related to EPD, and their limitation compared to this study

	Author (s)	**Brief description of parameter studied in the article**	**Limitation/Gap compared to this study**
1	J.Guo et al. (2012)	CNT/CF hybrid materials prepared using ultrasonically assisted EPD by using deionized water as medium. Parameter of EPD: 20V for 15 minutes	Only single solvent is used (Deionized water) Only single deposition voltage and time
2	Li et al. (2013)	Coating of two different CF with two types of functionalized MWCNTs using aqueous suspension deposition method in deionized water as medium. Parameter of deposition: 20 minutes; with and without additional of surfactant.	Single solvent used (Deionized water) Used different types of deposition (no electric field applied) Only one immersion time

Table 1.1 continued

3	Cordero-Arias et al (2013)	Chitosan composite coating using titania (n-TiO_2) nanoparticles by EPD using ethanol-water mixture as medium. Parameter of EPD: Voltage (2 to 50V), time (15s to 5 minutes)	Different types of materials of deposition Uses trial-and-error approach for parameter, i.e., ratio of medium, deposition voltage and time (wide range of parameter's value)
4	Moaseri et al. (2016)	Effect of electrostatic repulsion of MWCNT-CF hybrid epoxy composite on the mechanical properties using ethanol as medium Parameter of EPD: 10V for 20 minutes	Using single solvent (Ethanol) Fixed/ single deposition voltage and time Presence of electrostatic during molding
5	C.Xiao et al. (2018)	CF coated with MWCNTs using aqueous suspension deposition method in deionized water as medium. Parameter of deposition: 20 minutes	Single solvent used (Deionized water) Used different types of deposition (no electric field applied) Only one immersion time
6	Ervina et al. (2019)	EPD of MWCNT onto CF using deionized water, and testing of colloidal stability of MWCNT in medium (with and without presence of voltage) Parameter of EPD: Voltage (10 to 60V), time (3 to 30 minutes)	Only used single solvent (deionized water) Wide range of deposition voltage and time. More focus on the colloidal stability of suspension medium

Based on the table, it was proven that there is a huge gap in the study of the use of mixture suspension medium in depositing MWCNTs via the EPD process, providing opportunities for researchers to find out more about this area of study.

1.2 Research Problems

Firstly, the study involving the EPD process commonly utilized water as a single suspension medium, as shown in **Table 1.1**. However, water electrolysis might occur during the process when the voltage used is too high, which affects the deposition's quality (Ouedraogo & Savadogo, 2013). This will directly impact the properties of the composites produced. Hence, using a mixture of alcohol and water as an EPD medium is encouraged, as alcohol by itself requires a high deposition voltage (Ouedraogo & Savadogo, 2013). As a result, in this study, methanol and water are used as both a single suspension medium and a mixture suspension medium to compare the tensile properties of composites prepared using these mediums.

Secondly, when alcohol is used in the EPD process, ethanol is chosen as the medium. However, the ideal suspension medium had a low viscosity but a high dielectric constant, which is demonstrated by another type of alcohol, namely methanol. In a book chapter by Amrollahi et al., methanol was listed as having better properties as a suspension medium compared to ethanol (Amrollahi et al., 2016). Because of that, methanol was selected as the organic solvent for the study in order to find out its capability as an EPD suspension medium.

Thirdly, most of the previous studies, as shown in **Table 1.1**, are either using trial-and-error approaches or using repetitive values for the parameters in the study. The tabulated data is commonly generated based on previous studies. For instance, in the study by Li et al. in 2013, Moaseri et al. in 2016, and Xiao et al. in 2018, all three studies used 20 minutes of deposition time. Meanwhile, a study in 2013 by Cordero-Arias et al. used the trial-and-error method for their selection of parameters values. Hence, for this reason, in the study, RSM is paired with CCD to give more targeted parameters values as well as save time in terms of the experimental runs to be done.

1.3 Null and Research/Alternative Hypothesis

The null hypothesis is that "*Changes and interaction of the input parameters of EPD (volume ratio of water-methanol, deposition voltage and time) has no influence on the tensile properties of MWCNT-CF/Epoxy laminated composites.*"

The research/ alternative hypothesis is that *"The changes and interaction of the input parameters of EPD (volume ratio of water-methanol, deposition voltage and time) would have significant influence on the tensile properties of MWCNT-CF/Epoxy laminated composites."*

1.4 Aim and Objectives

The study aims to analyse the tensile properties of MWCNT-CF/epoxy laminated composites when the parameters of EPD, i.e., the volume ratios of the suspension medium, deposition voltage, and time, are varied. To achieve the aim of the study, there are several objectives, which are:

i. To determine stability of the MWCNTs when it was dispersed in single and mixture suspension medium before starting the EPD using optical observation method.
ii. To investigate the effects of various medium's ratios (single and mixture medium), deposition voltage and time on the tensile properties of the MWCNT–CF/epoxy laminated composites.
iii. To optimize the EPD's input parameters in order to get the maximum tensile properties of composites by using RSM.

1.5 Chapter Summary

This chapter discusses the overview of this research study, which includes the background of the study, the problem gap and statement, the hypothesis and also the aim and objectives of the research. The objectives act as guidelines to solve the problem arising which is the main reason for this research study.

CHAPTER 2

LITERATURE REVIEW

2.1 Overview

This chapter contains the literature review for this research. Information on electrophoretic deposition (EPD), carbon nanotubes (CNTs), epoxy laminated composites and Response Surface Methodology (RSM) is discussed. Basic information regarding the EPD process is explained in detail, such as history, mechanisms, and applications. Apart from that, information such as background, history, and applications CNTs are also elaborated on the chapter. The variation of epoxy laminated composites is also discussed in this chapter. Additionally, the information related to RSM such as model design, Analysis of Variance (ANOVA) and optimization is also elaborated in the chapter.

2.2 Electrophoretic Deposition (EPD)

Indian scientist G.M. Bose, was the first person to conduct EPD experiments in the 1740s. After that, at the beginning of the 19^{th} century, the Russian scientist, Ruess, introduced the electrophoresis phenomenon when it was discovered that by including the electric field in water, there were movement observed in the clay particles. EPD was first used industrially to deposit ceramic tiles onto zinc drums (Avcu et al., 2019). But before being applied in industry, this method was first practically used or applied in 1933 for the deposition of thoria particles onto a platinum cathode to be used as the electron tube's emitter. Since then, this technique has progressed to being used in the processing of advance materials such as polymers, metals, carbides, and so on (Ma et al., 2018).

2.2.1 Definition of EPD

The EPD method is a colloidal process where, under the influence of electric field, the compactly packed particles in a suspension medium would be impelled onto the substrate (Hu et al., 2020; Ma et al., 2018). There are four distinct parts of an EPD cell setting, i.e., the substrate and counter electrode (working electrodes), colloidal suspension medium, and the power supply (either AC or DC) (Amrollahi et al., 2016). This method relies on two subprocess: electrophoresis and deposition. Two electrodes are used in this process, where one acts as counter electrode while the other substrate is to be deposited with the particles. The suspension medium contained charged particles, and both of the electrodes are submerged in the medium. Electrophoresis occurs when an electric field (DC voltage is commonly used) is applied, the charged particles will move towards a substrate that is oppositely charged. The electric field acts as a directional force that moves the particles suspended in the medium. The particles are then accumulated near the surface of the substrate, creating a solid packing film. This is known as the deposition process (Chen et al., 2018). EPD is also known as an electrokinetic phenomenon as both electrophoresis and deposition occur during the process (Obregón et al., 2019). **Figure 2.1** illustrates the EPD process in a simple schematic diagram, meanwhile in **Figure 2.2**, the four steps of the EPD process are shown. **Figure 2.2** shows that (a) colloidal particles are well distributed in the solvent suspension and capable of moving independently and spontaneously, (b) the surface charge of particles is due to the solvent's electrochemical equilibrium, (c) the particles in the suspension travel electrophoretically to the substrate (the oppositely charged electrode), and (d) a firm, neutralized layer of particles is observed deposited on the substrate. In EPD, particles and ions moves because of electrostatic force, but the liquid stays still (Amrollahi et al., 2016).

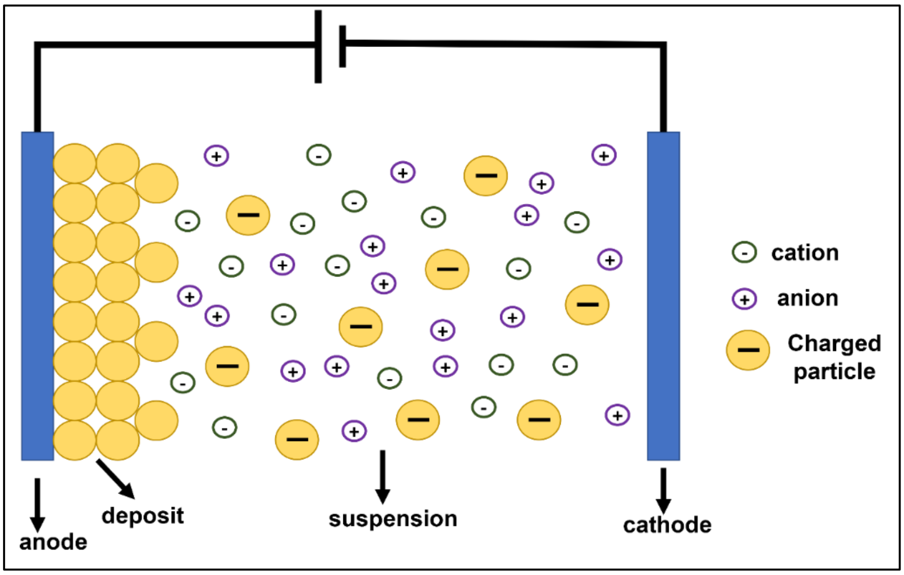

Figure 2.1: Simple schematic diagram of the EPD process (Hu et al., 2020)

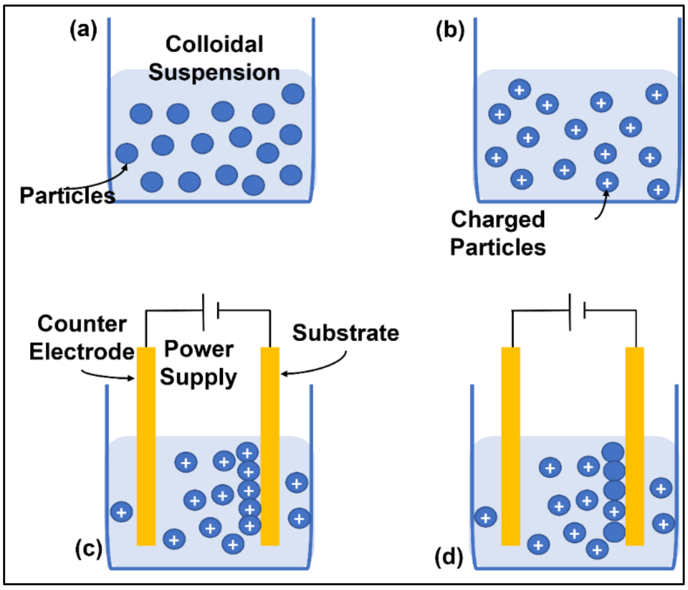

Figure 2.2: The four steps in EPD process (a) dispersion, (b) electrochemical charging, (c) electrophoresis, and (d) deposition (Amrollahi et al., 2016)

Additionally, the EPD coating can be classified into two kinds depending on the charged particles and electrode on which the deposition occurred, i.e., cathodic, and anodic EPD. For the anodic EPD, the negatively charged particles would be deposited onto the anode or positive electrode. Meanwhile, as for cathodic EPD, the deposition would occur at the cathode (negative electrode) as the particles are positively charged (Ranjbar &

Bakhtiary-Noodeh, 2020). The schematic diagram of both types of EPD is depicted in **Figure 2.3**. Obtaining a stable suspension of the charged particles is essential in order to successfully perform the EPD process of particulate materials. Generally, for the EPD process to be efficiently deposit the particles, the suspensions need to remain stable throughout the whole process of deposition, even when electric field are introduced (Diba et al., 2016).

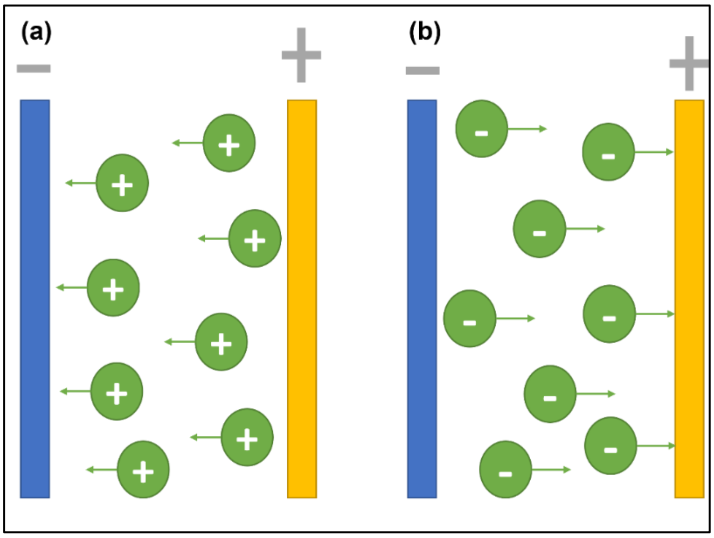

Figure 2.3: Schematic illustration of two types of EPD (a) cathodic and (b) anodic EPD (Ranjbar & Bakhtiary-Noodeh, 2020)

2.2.2 Factors that influence EPD

There are two categories of parameters that directly affect the EPD process, namely parameters that are related to the suspension stability and parameters that are related to the deposition process itself. Electrophoresis occurs when charged particles or molecules in a suspension migrate when an electric field is applied. There are several factors that are affecting charged particles' mobility, which are mostly related to the suspension's characteristics (Batool et al., 2021). There are six parameters that are related to the suspension, i.e., particle size, the dielectric constant of liquid, the conductivity of suspension, the suspension's viscosity, the zeta potential, and the suspension stability. The size of particles used can vary from 1 to 20 µm, but when larger particles are used in EPD process, there is concern as large particles tend to sediment in the suspension. Hence, to overcome this issue, it was either by increasing the size of electrical double layer regime or by reaching a resilient surface charge (Awasthi et al., 2019). It is crucial that the suspension have particles that are constantly stable and uniformly dispersed. Small-sized particles would have a large electrophoretic mobility (EM) value owing to their natural Brownian motion, whereby particles that are smaller than 1 µm would remain in the suspension instead of settling down. Hence, the obtained coating is thick and uniform with improved properties. As aforesaid, a strong electric field is essential for large-sized particles to have effective mobility (Batool et al., 2021).

The second parameter is the liquid's dielectric constant, which is generally correlated with EM, whereby when there is inadequate dissociative energy needed by the particles to produce good deposition, the mobility is slow. Meanwhile, the rate of EM at high dielectric constant values would be reduced due to high ionic concentration. This occurs when the size of the double layer decreased (Batool et al., 2021). For EPD process, the dielectric constant are deemed optimal in the range of 12 to 25, especially for organic solvents (Awasthi et al., 2019). Additionally, the suspension conductivity is also affecting the EPD process, as it is closely associated with the suspension properties. Flocculation happens when the particles are electronically charged due to the extremely low conductivity (Aznam et al., 2018). The charged particles lose their stability due to the electronic charging when the suspension is highly resistive. Meanwhile, the movement of particles would be at a slower rate when the suspension is highly conductive. Hence, there is a limited range of optimum conductivity values in which good deposition can be obtained. As for EM, it is inversely proportional to the suspension conductivity. EM is in favor at low ionic conduction, but when the conductivity value is high, there would be resistance in the particle motion (Batool et al., 2021). Thus, it can deduced that the suspension's conductivity directly effects the charged particles deposition behaviour (Hu et al., 2020).

Additionally, the viscosity of the suspension also influenced the EPD process. The suspension viscosity was affected by the amount, size and pH of the dispersed particles in suspension (Lee et al., 2018). For the EPD process, low viscosity is preferred (Amrollahi et al., 2016). Higher viscosity means lower EM, and higher mobility can be achieved when the solvent have a low viscosity, which in turn would produce good deposition (Batool et al., 2021). **Table 2.1** lists some of the commonly used media for the EPD process and their properties. An ideal suspension medium usually has low viscosity and conductivity but a high dielectric constant. According to **Table 2.1**, acetone and methanol are the most effective solvents to be used for deposition.

Table 2.1: Properties of commonly used solvent in EPD process (Amrollahi et al., 2016)

Solvents	Viscosity (cP) = 10^{-3} N.s.m^{-2}	Relative dielectric constant
Acetone	0.3087	20.7
Methanol	0.557	32.63
Water	0.890	78.2
Ethanol	1.0885	24.55
Acetylacetone	1.09	25.7
n-Propanol	1.9365	20.33
Iso-propanol	2.0439	19.92
n-Butanol	2.5875	17.51
Ethylene glycol	16.265	37.7

The next parameter is the zeta potential of the particles, which is one of the key factors in the EPD process. The zeta potential is defined as the potential difference between the liquid medium and the double layer region (interfacial double layer at the slipping region) (Aznam et al., 2018). Also known as the electrokinetic potential, this potential is the summation value of the initially generated surface charge and the charge of accumulated layers, and it is produced at the solid–liquid medium boundary (Batool et al., 2021). The suspension stability and the direction in which the particles move are shown by the value of zeta potential. When the other parameters are fixed, the mobility of the charged particles is directly proportional to the zeta potential. Hence, as the zeta potential (absolute value) increases, the deposition rate also increases. Denser green deposit are more likely to be obtained when the suspension is well-dispersed and has higher zeta potential values (Hu et al., 2020). By introducing charging agents such as bases, acids, and adsorbed ions in the suspension, zeta potential can be controlled (Lee et al., 2018). This is because manipulation of the pH condition of the suspension would have a direct effect on the zeta potential, and by using suitable charging agents, the pH value where the suspension is generally at stable state can be achieved (Aznam et al., 2018). The degree of ionization is determined by the pH values; the EM is elevated at increased ionization rates as there are more charged particles exists in the suspension produced by the acids or bases (Batool et al., 2021).

The last parameter that are related to the suspension is the suspension stability. A dense and strong adherence layer on a surface can be obtained when the suspension is stable because there would be no agglomeration by the particles besides the particles having a slow settling rate (Aznam et al., 2018). There are several factors that can affect the suspension stability, such as the size of charged particles, the particle size distribution, the Debye length (double layer thickness) of solution, zeta potential, and the presence of adsorbed species. Generally, there is no flocculation or sedimentation of particles shown by a stable suspension

(Lee et al., 2018). A large contact area with free ions is present in the suspension that have well–dispersed particles. This improves the EDL forces (Aznam et al., 2018).

Additionally, there are four parameters that influence the deposition process, namely the deposition time, concentration of solid in suspension, applied voltage, and substrate conductivity. At initial deposition time, the deposition is linear, but as the time is increased, the yield of thickness also increasing. But, the relationship between the deposition rate and time is inversely proportional; there is a reduction in the deposition rate as time increases, and eventually, after prolonged time, the rate of deposition will reached plateau (Lee et al., 2018). After that, no more particles would stick to the surface of the electrode because the existing deposit acts as an insulator and stops more particles from sticking (Batool et al., 2021).

The solid concentration in a suspension also plays a crucial role in the EPD process, especially in multi–component systems EPD. Theoretically, the deposition rate of the particles should be identical as they all have the same surface charges. Despite that, the deposition rate is influenced by the particles' volume fraction in the suspension (Batool et al., 2021). In a few cases, depending on the concentration of the solids in the suspension, different species of particles can be deposited at varying rate despite having similar surface charges (Lee et al., 2018). Particles with a higher volume fraction would deposit uniformly at a higher rate, but the rate of deposition for particles with a lower volume fraction depends on their unique EM (Batool et al., 2021).

Applied voltage and electric field have a direct relationship, which simultaneously affecting the particles' velocity. Hence, applied voltage is one of the main parameters that needs to be taken into consideration during the process (Obregón et al., 2019). The combination of electric field strength and particles' surface charge defined the driving force that are exerted onto the charged particles. Hence, the increment in the applied voltage would generally increases the yield of deposit as the driving force grows respectively (Hu et al., 2020). For the EPD process to set off, a substantial amount of applied field is required for there would be little to no movement from the particles when the electric field passed through the suspension are low. But when the electric field are too high, the quality of the deposited films would be compromised as the particles does not have sufficient time to uniformly deposit on the substrate due to rapid particles movement. Hence, it is important to select optimum range of applied field in which the EPD would be conducted (Batool et al., 2021).

Lastly, the conductivity of the substrate is important in producing deposits of great quality via EPD process. Low deposition yield is obtained when substrates with low conductivity are used, even at prolonged period of EPD. The thickness of deposited film would also be uneven (Batool et al., 2021). It can be concluded that careful consideration must be given when it comes to selecting or fixing the parameters of the suspension in order to obtain a satisfactory suspension so that an optimum EPD process can be achieved (Lee et al., 2018).

2.2.3 Applications of EPD

The EPD process offers many advantages and has resulted in a wide range of applications in which EPD is utilized (Chen et al., 2018).

2.2.3.1 Deposition of nanostructure materials

Carbon nanotubes (CNTs) are one of the nanomaterials that frequently utilize EPD, either to deposit pure CNT coatings or to prepare composite coating that are CNT-based. **Figure 2.4** lists the successful combination of various nanoparticles with CNTs using the EPD process. Simple alternating EPD from two or more single-phase dispersions can easily achieve layered composite materials (laminates). In addition, CNT has also been combined with materials such as ceramics and polymers in a single EPD step via co-deposition (Atiq Ur Rehman et al., 2020).

CNTs can also be used together with other carbon nanomaterial such as graphene. Agglomeration of graphene sheets can be avoided by incorporating well-dispersed CNTs in the process. Their large surface area can also be maintained, and the CNTs also served as conductive bridges that lessen the hybrid CNT/graphene transparent conductive films' resistance. Additionally, co-deposition of CNTs with polymeric components are also feasible to form composite structures. Polyacrylic acid (PAA), alginate, and chitosan are among the example of polymeric materials that are used together with CNTs (Atiq Ur Rehman et al., 2020).

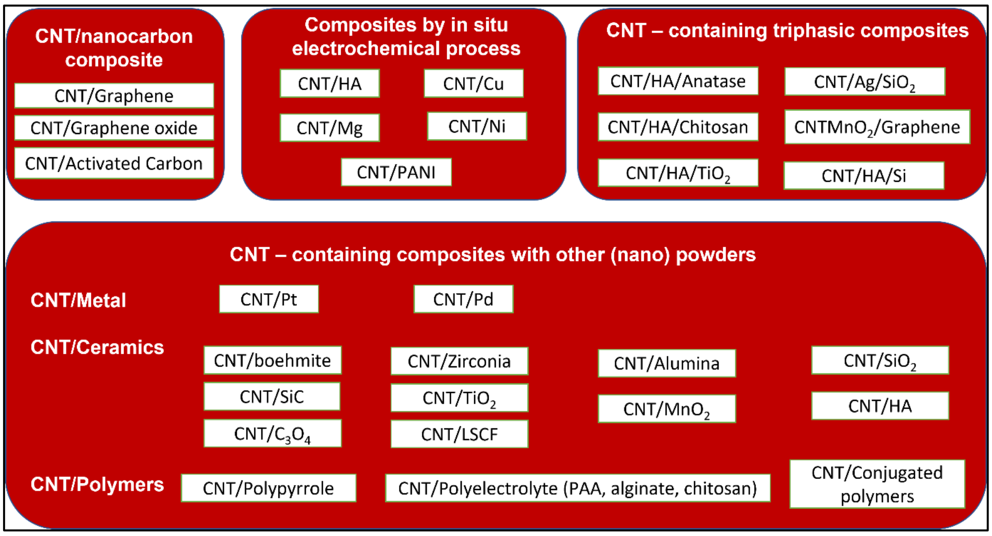

Figure 2.4: The various successful combination of CNT–nanoparticles via EPD methods (Atiq Ur Rehman et al., 2020)

2.2.3.2 Energy conversion and storage devices

Implementation of the EPD method in the production of energy storage and conversion devices allowed the active particles to be directly deposited on the current collector. It is a prerequisite to employ conductive substrates for both the EPD process and energy storage appliances. By utilizing EPD to fabricate films to be used in energy storage and conversion devices, the interfacial resistance can be decreased, and the mechanical flexibility can be improved. Hence, devices with high performance are attainable by using EPD (Ye et al., 2016).

The preparation of lithium-ion batteries (LIBs) electrodes can be done via the EPD technique instead of using traditional electrode materials that only allow a limited range of substrates to be used with the conducting carbon–active materials mixtures. Compared to other methods that are commonly used for coating, the EPD technique can accommodate a wider range of materials that can be coated and deposited as the materials that undergo the EPD process do not necessarily need to have defined properties (Lee et al., 2018). High performance cathode films can be obtained by the EPD method by depositing both the active materials and conductive agents at the same time (Ye et al., 2016). Additionally, EPD can also be used by nanoparticle suspensions to manufacture nanoscale films and nanostructured coatings with improved properties to be used in LIBs as anode electrodes. EPD eliminates the need for adding conductive additives or a cohesive polymer binder to active materials, thereby enhancing the electrochemical performance of the electrode (Lee et al., 2018).

Another type of energy storage device that benefited from the EPD method is supercapacitors, which, similar to batteries, are made of an electrolyte and two electrodes (Lee et al., 2018). High-performance supercapacitors are obtainable by fabricating materials such as CNTs, graphene and their composites via EPD into the capacitor electrode materials. For instance, CNTs are a promising candidate to be applied to supercapacitors because the EPD films of CNTs are highly porous. The open space between the intertwined nanotubes forms uniform nanoscale pores, making electrolyte readily accessible to the electrode. This is because electric double layer charging favours high accessible contact surface area. Thus, the assembly of the supercapacitor using EPD is demonstrated to be highly efficient (Ye et al., 2016).

2.2.3.3 Biomedical application

At early stages, the biomedical field is using EPD to deposit conventional bioactive ceramics such as hydroxyapatite (HA). Later, EPD is used to produce bioactiveglass (BA), titanium dioxide (TiO_2), wollastonite, and zirconia coatings and also their composites on titanium alloys and stainless steel (Avcu et al., 2019).

The biomaterials field commonly utilized EPD in their production, especially in the manufacturing of bioactive coatings. The deposition of coatings or thin films on porous biomedical structures (e.g., scaffolds) is a vital part of the medical field, especially in tissue engineering and regenerative medicine. Processing of both simple and complex form of micro-and nanostructured biomaterials is attainable via EPD. The deposition of bioactive layers and biological entities (polymers, cells, proteins, enzymes, etc.) with therapeutic metallic ions or drugs can be homogeneously coated onto numerous substrates when using EPD (Batool et al., 2021). Besides that, the EPD of bacterial biofilms and enzymes onto biomedicals appliances such as catheters, voice prostheses, and biosensors is done to form protective coatings on those appliances. EPD can also be used to develop anti–infective implant surfaces on metallic substrates because it makes it easier to deposit antimicrobial agents or drugs (like tetracycline, antifungal lipopeptide drug caspofungin, etc.) on the metallic substrates (Avcu et al., 2019).

By modifying the metallic implant surface with using the EPD process, the functionality and effect of treatment can be improved. For example, the coating of orthopaedic implants to improve their corrosion resistance, bioactivity, and biocompatibility is done by using EPD. Besides that, neural stimulating electrodes, which are used for stimulation and neural recording, also utilized this method to obtain lower impedance, higher charge capacity, and improved impedance stability. To get those properties, biomedical devices are coated with materials like carbon nanotube, platinum nanoparticles, polymer nanotubes or multilayer approaches of CNTs and conductive polymers (Chen et al., 2018).

2.3 Carbon Nanotubes (CNTs)

Carbon is one of the most common elements on the planet, and it can take on a wide range of crystalline structures. Since carbon has a tetravalency, it contains sp^3 hybridization. Carbon is a fascinating product because it occurs in eight different allotropes, one of which is carbon nanotubes (CNT), which belongs to the group of nanosized carbons or nanocarbons (Rahman et al., 2019; Raunika et al., 2017). Since it has a micrometre-sized volume and a nanometre-sized diameter, CNT has a length-to-diameter ratio of over 1000. Aside from that, it had the same atom composition as graphite, with hexagonally organized atoms. CNT is a carbon allotrope that exists between fullerenes and graphite (Aqel et al., 2012).

2.3.1 History of CNTs

Even though carbon has been used for over 6000 years, the next advances in carbon did not occur until the late 1980s. The discovery of other stable, ordered structures besides graphite and diamond sparked the quest for new sources of carbon. With their fortuitous observation of the C_{60} in 1985, it opened the way for the systematic analysis of carbon filaments of exceedingly small diameters, which has sparked a lot of interest in CNTs. The study has brought fullerenes into the spotlight with the synthesis of carbon clusters with various sizes, properties, and structures (Aqel et al., 2012; Ghasempour & Narei, 2018). This is since C_{60} was made using a basic arc evaporation apparatus that was widely available in all laboratories (Aqel et al., 2012). Sumio Iijima, a Japanese physicist, discovered carbon nanotubes in 1991 while studying carbon compounds under an electron microscope. These needle-like materials were later confirmed to have graphite structure and are now known as carbon nanotubes (Bera, 2017). The first observation of multi-walled carbon nanotubes

(MWCNTs) occurred when hard deposits on the cathode were formed using electric arc experiments to shape fullerenes. Meanwhile, two independently conducted experiments in 1993 confirmed the development of single-walled carbon nanotubes (SWCNTs) (Raunika et al., 2017). While carbon nanotubes had been known for a long time before Iijima's invention, CNT-related research only began when they discovered that these new fibres had a variety of unique properties. Since such tubes were structurally imperfect prior to this, their properties were not especially important (Aqel et al., 2012). As a result, recent studies and analysis have focused on improving the quality of CNTs generated. Due to their intriguing properties, carbon nanotubes are a major substance in nanotechnology fields and the future (Kaur et al., 2018).

2.3.2 Classifications of CNTs

Carbon nanotubes are divided into two types: (i) single-walled carbon nanotubes (SWCNTs). and (ii) multi-walled carbon nanotubes (MWCNTs). SWCNT is made up of just one sheet of graphene and has a simple structure that allows it to be twisted effortlessly. It also had a low purity (Kaur et al., 2018). SWCNT was created by rolling a single layer of graphite (a different term for graphene) into a smooth cylinder (long wrapped graphene sheets). Since the length to diameter ratio of CNT is about 1000, it is known to be a virtually one-dimensional object. As a result, the majority of SWCNTs had a diameter of 1–2 nm. This structure is often thinner than multi-walled tubes, with a circular outline rather than a linear one. The sidewall of the tube and the end cap of the tube are the next two distinct regions in the SWCNT. Each area had its own set of physical and chemical characteristics. SWCNTs are a more significant variation of a CNT than MWCNT variations. This is because they exhibit critical electric properties that the MWCNT varieties do not. Electric wire is the most fundamental building block of these devices, and SWCNT can be an outstanding conductor (Aqel et al., 2012). It can also be semiconducting or metallic based on their helical angle (χ). SWCNTs have thus been the focus of nanotechnology science for the past two decades (Rao et al., 2018). SWCNTs are also expensive to produce, and their synthesis necessitates the use of a catalyst. As a result, developing cost-effective synthesis methods is critical for the future of carbon nanotechnology (Aqel et al., 2012; Kaur et al., 2018).

The MWCNTs are the next kind. This arrangement is made up of two or more aligned rolled sheets of graphene, and it has a complicated structure that makes it difficult to twist in this shape. As a result, unlike SWCNT, MWCNT had a high purity (Ghasempour & Narei, 2018; Kaur et al., 2018). Multiple layers of graphite of varying diameters were rolled in on themselves to create the tube structure of the multi-walled, and both ends of such tubes were often closed. In other words, these multi-walled carbon tubes would be made up of a series of concentric SWCNTs. The outer diameter of these tubes varied between 3nm and 30nm. Since the length and diameter of these structures vary from those of single-walled carbon tubes, their properties often differ. MWCNTs have an interlayer spacing of around 3.3Å, which is similar to the distance between graphene layers in graphite (Aqel et al., 2012). Furthermore, no catalysts are needed in the production of these multi-walled carbon tubes (Kaur et al., 2018).

Figure 2.5 depicted the two kinds of carbon nanotubes, while **Table 2.2** compared the two types of CNTs. **Table 2.3** shows the properties of SWCNT and MWCNT in comparison with other carbon materials.

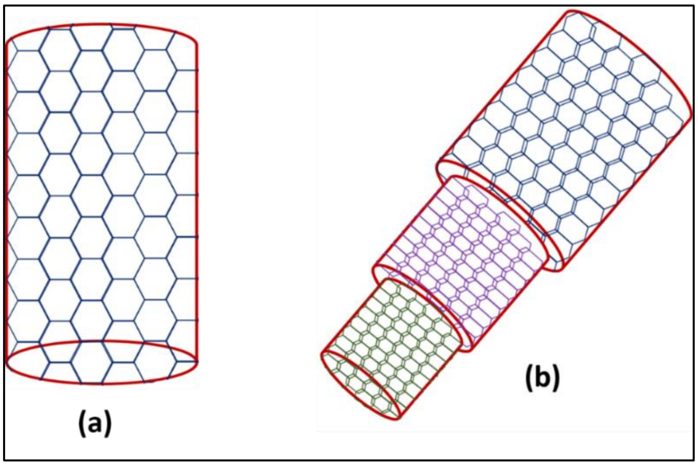

Figure 2.5: Two main types of carbon nanotubes, i.e. (a) SWCNT, and (b) MWCNT (Jafar et al., 2016)

Table 2.2: Comparison between single-walled and multi-walled CNT

Characteristics/ or basis of the properties	Single-walled CNT	Multi-walled CNT	Ref
Graphene presence in structure	Single layer of graphene	Multiple layers of graphene	(Saifuddin et al., 2013)
Presence of catalyst during synthesis	Catalyst is required for synthesis	Can be produced without catalyst	(Kaur et al., 2018)
Bulk synthesis	Bulk synthesis is difficult as it requires proper control overgrowth and atmospheric condition	Bulk synthesis is easy	(Saifuddin et al., 2013)
Structure of CNT	Not fully dispersed, and form bundled structures	Homogeneously dispersed with no apparent bundled formation	(Eatemadi et al., 2014; Saifuddin et al., 2013)
Resistivity range	Resistivity usually in the range of 10^{-4}–10^{3} Ω.m	Resistivity usually in the range of 1.8 x10^{-5}–6.1 x 10^{-5} Ω.m	(Deshpande & Mahendru, 2018; Saifuddin et al., 2013)

Table 2.2 continued

Purity of CNT	Purity is poor. Typical SWCNT content is as-prepared samples by chemical vapor deposition (CVD) method is about 30–50 wt%. However high purity up to 80% has been reported by using arc discharge synthesis method.	Purity is high. Typical MWCNT content is as-prepared samples by CVD method is about 35–90 wt%.	(Kaur et al., 2018; Saifuddin et al., 2013)
Defect in structure	A chance of defect is more during functionalization	A chance of defect is less especially when synthesized by arc-discharged method	(Eatemadi et al., 2014)
Characterization of structure	Characterization and evaluation are easy	It has very complex structure	(Eatemadi et al., 2014)
Flexibility of CNT	It can be easily twisted and are more pliable	It cannot be easily twisted	(Kaur et al., 2018)

Table 2.3: Properties comparison between SWCNT and MWCNT with other types of carbon materials (Imtiaz et al., 2018)

Property	**SWCNT**	**MWCNT**	**Graphite**	**Diamond**	**Fullerene**
Specific gravity (g/cm^3)	0.8	1.8	1.9–2.3	3.5	1.7
Electrical conductivity (S/cm)	10^2-10^6	10^3–10^5	4000^P, 3.3^C	10^{-2}–10^{-5}	10^{-5}
Electron mobility (cm^2/ (V.s))	~ 10^5	10^4–10^5	2.0×10^4	1800	0.5 × 6
Thermal conductivity (W/ (m.K))	6000	2000	298^P, 2.2^C	900–2320	0.4
Coefficient of thermal expansion (K^{-1})	Negligible	Negligible	-1×10^{-6p}, 2.9×10^{-5c}	$(1–3) \times 10^{-6}$	6.2×10^{-5}
Thermal stability in air (°C)	>600	>600	450–650	<600	~ 600

"P": in plane, "C": c - axis

2.3.3 Application of CNT

CNTs had a wide variety of possible applications due to their unusual anisotropic properties, and had piqued the interest of several different fields and industries (Shahidi & Moazzenchi, 2018).

2.3.3.1 Medical/Biomedical field

CNTs are a promising commodity in the biomedical field because they have several distinct characteristics, including an excellent structure that enhances the remarkable combination of mechanical, electrical, and optical properties. CNTs are used in biomedical applications such as biomolecule transfer, gene delivery to cells or organs, and tissue regeneration. CNTs are naturally hydrophobic materials, but they can be functionalized to accommodate specific applications. CNTs' appealing properties are what have led to their widespread use, i.e. (i) because of their hollowness and wide surface area, they are ideal for drug distribution, (ii) because of its hydrophobicity, it has increased functionality in the delivery of biomolecules, and (iii) for the combined use of contrast agent, photodynamic therapy, and photoacoustic imaging, great optical properties are needed (Alshehri et al., 2016; Lamberti et al., 2015; Prajapati et al., 2020). Drug and gene distribution are one of the medicinal systems that uses CNTs, and **Figure 2.6** shows how CNTs are currently used as drug carriers (Menezes et al., 2019).

The other use will be in biomedical imaging, which is the use of high-resolution imaging techniques to image the actions of cells, tissues, organs, or the whole body. CNTs are used to study and enhance imaging functionalities as well as their reaction to their surroundings (Alshehri et al., 2016). MWNTs and SWNTs are used as photothermal agents in this imaging since they both have a good near-infrared field (NIR) (Chen et al., 2017).

CNTs in composites may often be used to regenerate and engineer bone tissue, and they are classified as biomimetic nanocomposites of collagen fibers at the cell hierarchy stage. CNTs have a beneficial effect on cell adhesion by stimulating cell adhesion, as well as cell morphology modulation and stem cell differentiation acceleration due to their preferential affinity for cell binding, which facilitates new bone development when osteoblast differentiation and apatite mineralization are triggered. Conjugating moieties such as aptamers, peptides, and small molecules may be used to functionalize CNTs for use in diseased bone tissue aggregation, targeting the pathological site, and effectively delivering specific therapeutic agents (Pei et al., 2019).

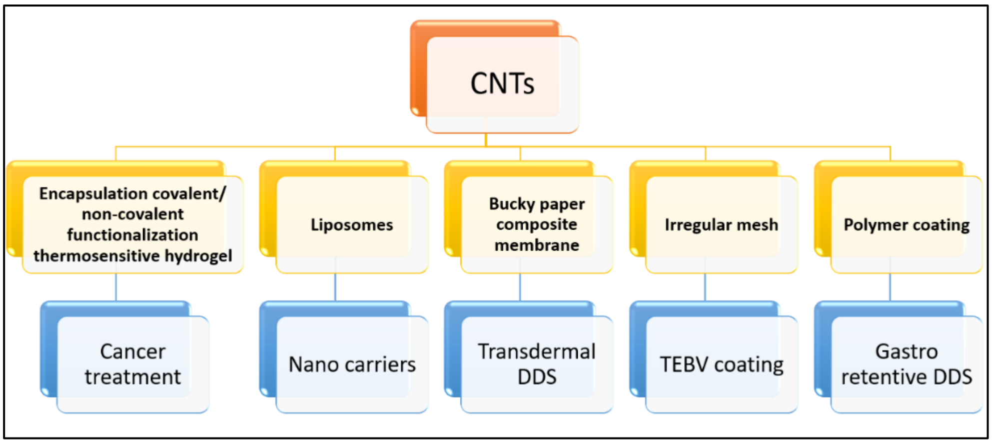

Figure 2.6: Current CNTs uses as drug carriers (Menezes et al., 2019)

2.3.3.2 Wastewater treatment application

CNTs can be a promising anode material for microbial fuel cells (MFC) because of their high conductivity and high surface-to-volume ratio. Microbial fuel cells are one of the most important, environmentally sustainable methods for wastewater treatment. Direct application of CNT, on the other hand, may induce cellular toxicity. As a result, CNTs can be used as an anode medium by coating them with conductive polymers including polyaniline and polypyrrole. The electrode specific surface area can be increased by adapting

CNTs in this process, thus improving charge transfer efficiency. Following that, a three-dimensional structure was obtained by evenly covering the CNT on a macroscale porous substrate, which demonstrates close contact with the microbial biofilm. The electron transfer from the exoelectrogens to the electrode surface had been aided by this. As a result, the charge transfer resistance was significantly reduced, resulting in improved MFC efficiency (Attar & Ranveer, 2015).

Additionally, CNT are also used for water filtration as anti-microbial materials. Strong antimicrobial activity was shown by CNTs especially SWCNTs. High bacterial retention was shown by SWCNT filter, while high viral removal is exhibited by MWCNT at low pressure, and both are done through size exclusion effect. Bacterial inactivation and viral preservation at low pressure can be accomplished by integrating all types of nanotubes as a hybrid filter. (Liu et al., 2013).

2.3.3.3 Structural reinforcement

CNTs are an ideal material for load-bearing reinforcement in composites and structural applications ranging from casual things like clothing to military jackets and space elevators, thanks to their mechanical properties. CNTs are used as a composite filler in structures such as tennis rackets, aircraft body parts, and even spacecraft. Polymers and epoxy resins are also used in conjunction with CNTs to improve properties such as durability, strength, and hardness (Jafari, 2018).

In composites, CNT is a promising filler material whereby when coupled with very large interfacial contact region, will exhibit excellent electrical, thermal, and mechanical properties. CNT-reinforced polymer composites have drawn a lot of interest for industrial applications like electronics, energy storage systems, and vehicles because of their compatibility with CNT. **Table 2.4** shows some of the applications for polymer/CNT composites. Apart from that, CNT-epoxy composites are widely used in commercial applications such as sporting equipment (i.e., badminton rackets, golf sticks, ski poles, and so on), electronic packaging, and aircraft. Epoxy composites are widely used in the aircraft and aerospace industries due to their high temperature tolerance and high strength-to-weight ratio. The mechanical efficiency of the composites can be increased further by using CNTs as epoxy fillers (Kausar et al., 2016; Mittal et al., 2015).

Table 2.4: Polymer/CNT composites application

Nanotube type	**Polymer type**	**Applications**	**Ref**
SWCNT, MWCNT	Polyamide	Electrostatic discharge, electronics and industrial, automotive	(Kingston et al., 2014)
MWCNT	Polyaniline (PANI), Polypyrrole (PP) and Poly-(3,4-ethylenedioxythiophene) (PEDOT)	Supercapacitor electrode materials	(Frackowiak et al., 2006)
MWCNT	Poly (vinyl alcohol), poly (2-acrylamido-2-methyl-1-propane sulfonic acid)	Sensors and actuators for biomedical applications	(Dai et al., 2009)
SWCNT	Poly (4-methyl-1-pentene)	Space vehicles, space stations, biomedical art	(Mohd Nurazzi et al., 2021)
SWCNT	Poly (methyl methacrylate)	Biocatalytic films	(Rege et al., 2003)

2.4 Carbon Fiber – Reinforced Polymer (CFRPs) composites

Fiber- reinforced polymers (FRPs) exceptional properties such as high stiffness and performance, better corrosion resistance, and lightweight, making them an excellent choice to be used in applications such as aeronautical, automobile, and other applications. Acting as the main load–bearing elements, the reinforcement fibers in FRPS are typically stiff, hard, and widely dispersed in the composite phases embedded within the matrix. Additionally, the matrix does not bear much of the loads compared to the reinforcement. It acts as a binder that surrounds the reinforcement and protects the structure from harsh environments and damage onto the structure's surface. Ductility and crack propagation protection from one fiber to another are also provided by the matrix. The combination of the two acts as compression resistance since the matrix opposes shear and the fibers resist tension (Aamir et al., 2019). In comparison with metals, composites with a polymer matrix are advantageous in terms of the manufacturing processes where production of parts with complex shapes and lower density is possible. Thus, for automobiles and aviation, fuel consumption are lower, and for competitive sports, higher speeds are achievable (Hsissou et al., 2021).

There are several types of FRPs, but carbon fiber–reinforced polymers (CFRPs) are more commonly used in applications involving high technology (Aamir et al., 2019). In most innovative applications, carbon fibers (CF) are favored reinforcements thanks to their exceptional properties such as lightweight, had superior stiffness, high strength, low thermal expansion, electrical conductivity, high thermal conductivity and corrosion resistance (Yassin & Hojjati, 2018).

Carbon fiber reinforced polymers (CFRP) are composites that are produced using polymers as the matrix and carbon fibers as the reinforcement materials. CFRPs had exceptional mechanical properties compared to conventional materials, such as being five times stronger than grade 1020 steel despite being five times lighter. Additionally, compared to 6061 aluminum, this type of composite is 1.5 times lighter but two times stiffer and seven times stronger. The mass of the produced product can also be reduced by 40% when CFRPs are used instead of aluminum, yet retaining the same mechanical properties (Ozkan et al., 2020).

Figure 2.7 illustrates the schematic structure of a composite material, while **Figure 2.8** listed the formulation of composite materials.

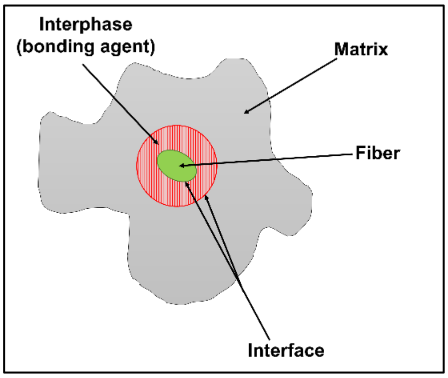

Figure 2.7: Schematic structure of a composite material (Altin Karataş & Gökkaya, 2018)

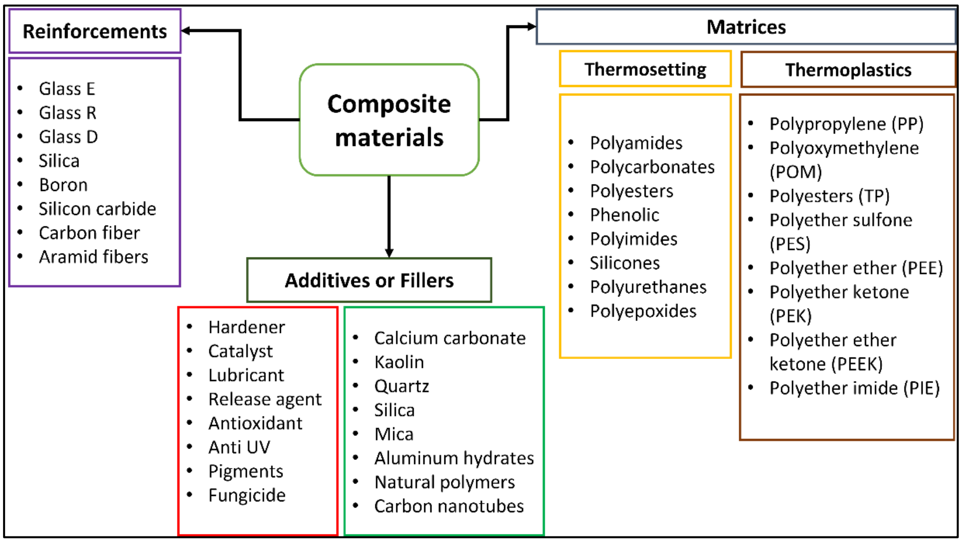

Figure 2.8: The formulation of composite materials (Hsissou et al., 2021)

2.4.1 Matrix materials

The matrix is responsible for the constraints' distribution, the link between the reinforcing fibers, as well as making sure the structure is resistant to chemical and helps the final product achieve the desired shape. The matrix used depends on the intended usage of the composite materials (Hsissou et al., 2021). In comparison with the other types of composites, polymeric composites, or polymer matrix composites (PMCs) are eminent due to their lightweightness. PMCs are further classified into three composites, i.e., thermoplastic, thermosets, and elastomeric. Generally, especially in the case of polymers, matrix is also considered as resin (Erden & Ho, 2017).

2.4.1.1 Thermoplastics

The fabrication of thermoplastic polymer–matrix composites utilize fully reacted high molecular weight resin. Polyethylene (PE), polypropylene (PP), polyamide (PA), polyetheretherketone (PEEK) and polyetherimide (PEI) are among the examples of thermoplastic resins. The recycling of thermoplastics to be reused or reprocessed is possible by reheating since thermoplastic does not cross–link during the processing. Additionally, compared to thermoset resins, the viscosity of thermoplastics is higher as the resin's molecular weight is high (Awais et al., 2021). Even though thermoplastics can be remelted and reprocessed, their polymer properties such as impact properties can degrade if the thermoplastic are exposed to too high of a temperature or a given temperature, the dwell time is too long (Akca & Gursel, 2015). The production of thermoplastic resins based composites typically utilizes traditional molding techniques such as injection molding, rotational molding, vacuum forming, extrusion molding and compression molding (Salahuddin et al., 2021).

2.4.1.2 Thermosets

Thermosets-based composites are usually made up of two or more components, such as resins and hardeners. The crosslinks of the materials are done by one of those components that act as multifunctional monomers. At the beginning, the composites are in viscous or soft solid state, but upon curing, they transform into an infusible, insoluble polymer network, forming high crosslinking density. Hence, despite having high impact resistance, after polymerization process, thermoset resins cannot be recycled and reshaped. Unsaturated polyesters resins (UPR), epoxy resins, phenolic, and vinyl ester (VE) are among the commonly used thermoset resins and their properties are listed in **Table 2.5** (Lee et al., 2021).

Among the thermosets resins, epoxy resins are widely utilized in highly developed composites. Coatings, adhesives, and structural composites are among the fields that use epoxy resins. The formation of epoxy resins is made up of long molecular chain with functional groups at both ends, with the exception of ester functional groups, hence making epoxy had better water resistance compared to VE. Hardener is essential for the curing process of epoxy resins (Lee et al., 2021). Epoxy resins have good thermal and mechanical resistance, as well as resistance to chemical agents. This thermoset also had exceptional adhesion to fibers and metals, besides very low uptake of humidity in immersion (Hsissou et al., 2021).

Table 2.5: Mechanical propeties of thermosets resins (Lee et al., 2021)

Type of resin	**Density (g/cm^3)**	**Tensile strength (MPa)**	**Tensile modulus (MPa)**
Phenolic	1.19–1.2	10	375
Unsaturated polyester	1.025–1.5	40–90	2000–4500
Vinyl ester	1.2–1.4	69–83	3100–3800
Epoxy	1.1–1.4	35–100	3000–6000

2.4.1.3 Elastomers

A resting elastomer is made up of long molecular chains that have been folded back on themselves (Hsissou et al., 2021). Normally known as rubber composites (due to rubber being the most well-known elastomeric material), elastomers achieve crosslinking through the vulcanization process (Erden & Ho, 2017). The vulcanization process is a hardening process whereby the flexibility of the molecular chains is retained while creating an approximately rigid three–dimensional network. During the process, carbon, sulfur, and various chemical agents are put into the elastomer, and depending on the formulations, each synthetic rubber produced caters to its own individual uses. Shoe soles, tires, and cushions are among the products that uses elastomers in their manufacturing (Hsissou et al., 2021).

2.4.2 Processing methods of polymer composites

The production process of composites has become a key factor as the demand for composite products keeps on increasing. There are two main categories of composites manufacturing methods, which are open and closed molding (Lee et al., 2021). Meanwhile, there are three primary basic phases that are involved in the fabrication of composites, namely the flowing, shaping and hardening of resin (Awais et al., 2021). **Figure 2.9** showed the comparison between open and closed molding.

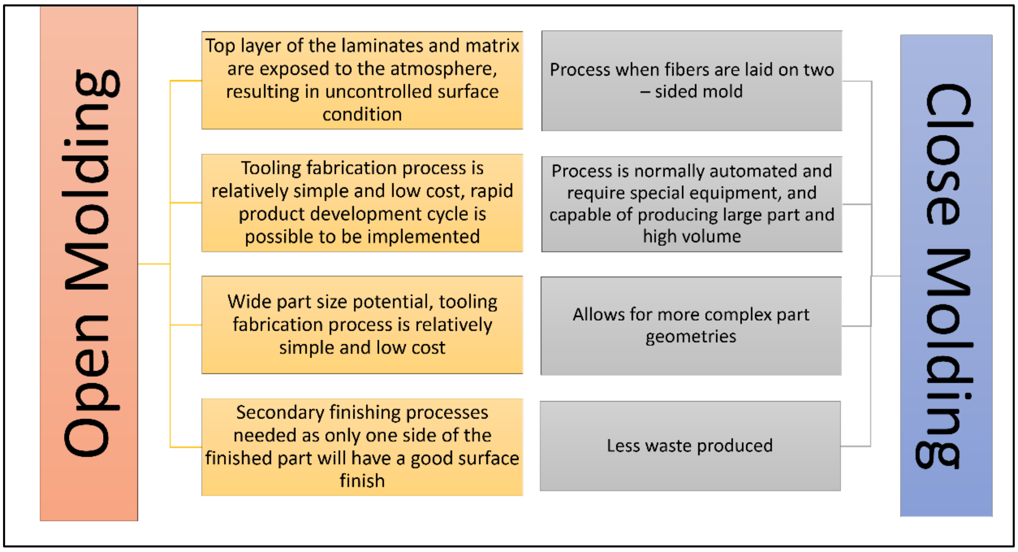

Figure 2.9: Comparison between open and closed molding processes (Lee et al., 2021)

2.4.3 Tensile performance of CNT–CF hybrid reinforced polymer composites

The properties of the fiber reinforcement and matrix, the fiber–matrix ratio in a composite and fiber matrix adhesion in the composite are among the factors that determine the mechanical properties of the manufactured polymer composites (Awais et al., 2021). **Table 2.6** shows the properties of CF and various types of CNT. The performance of the interface bonding of the polymer composites with hybrid CF–CNT directly influenced the composites' mechanical properties since the interface acted as a bridge between the polymer matrix and the CF–CNT hybrid reinforcement. For the load transfer from the polymer matrix to the reinforcement (hybrid CF–CNT) to be sufficient, a good interfacial bonding is necessary. When load transfer is done well, the stress concentration are reduced and composites' mechanical properties are improved (Zakaria et al., 2019).

For composites' structural design, tensile properties are among the utmost crucial mechanical properties to be investigated. The composite's behavior when there is load applied in tension is shown by the tensile properties. The capability of materials to deform or withstand when there are tensile loads applied is checked using tensile tests. Tensile tests are conducted on the materials to obtain several key tensile properties, namely the tensile modulus (young's modulus), tensile strength, breaking point and the elongation at yield. The data obtained is then being used as an assessment to determine whether the tested material is fit to be used in the predetermined application. Typically, the properties of the polymer matrices are improved when fibers are added into the matrix as reinforcement (Awais et al., 2021). **Figure 2.10** demonstrates the benefits of reinforcements in composites. Cracks are able to be prevented when the fibers are present in the composites (Akca & Gursel, 2015).

Additionally, there has been evidence that proves that the mechanical properties of the composites improve significantly when the hybrid CF–CNT are used as reinforcement, owing to their distinctive three dimensional (3D) network structure (Zakaria et al., 2019). It is because multiwalled carbon nanotubes (MWCNTs) or single–walled carbon nanotubes (SWCNTs) are able to form a rigid and strong network with the matrix since they had high aspect ratio. Subsequently, the tensile load resistance of the composites is improved. However, in order to gain improvement in the tensile properties, it is important to know or calculate the optimum weight percentage of CNTs to be added or deposited into. That is because after a certain amount of CNTs added in the matrix, it would be difficult for the CNTs to be mixed and dispersed uniformly. When that occurred, the CNTs would agglomerates, causing the interfacial strength to be reduced. Tariq et al. found that when MWCNTs are added to a composite, the tensile properties improve, but only up to 0.25 wt% addition. After that amount, the tensile properties of the composites decrease. The tensile properties of the CFRPs would be improved if the dispersion of the CNTs was uniform and the reinforcement materials and polymer matrix had strong interfacial bonding. **Table 2.7** presents the list of the studies investigating the tensile properties of composite when MWCNTs are used as reinforcement materials (Bilisik & Syduzzaman, 2021).

From the list, a study done by Maoseri et al. showed the most enhancement for the tensile strength and modulus, where the improvement is 126% and 233%, respectively. In the study, EPD was used to fabricate the hybrid CF–CNT, and epoxy was used as the matrix material. As the CNT coats the CF, the surface roughness of the CF increases, hence improving the tensile strength. Meanwhile, the interlocking between the epoxy matrix and CF surface is due to the stiffening effect of the CNT, which would then enhance the composite's tensile modulus. Apart from that, the wettability of the hybrid CF–CNT is improving as a result of the functionalization that has been done on the CNT during the EPD process. Thus, the epoxy and the hybrid had better molecular contact (Zakaria et al., 2019). In addition, the pre–treatment done on the fibers also had influence on the properties of composites. For instance, the tensile properties for readily available unsized and sized CF vary significantly. The following equations (**Equations 2.1–2.4**) are used to determine the tensile properties of the composites, where F^{tu} is the ultimate tensile strength (MPa), P_{max} is the maximum force before failure (N), A is the average cross–sectional area of the composite (mm^2), σ_i is the tensile stress at *i*th data point (MPa), P_i is the force at *i*th data point (N), ε_i is the tensile strain *i*th data point ($\mu\varepsilon$), δ_i is the extensometer displacement *i*th data point (mm) and L_g is the extensometer gage length (mm), E^{chord} is the tensile modulus of elasticity (GPa), $\Delta\sigma$ is the difference in applied tensile stress between two strain points (MPa) and $\Delta\varepsilon$ is the difference between the two strain points (Bilisik & Syduzzaman, 2021):

$$F^{tu} = \frac{P_{max}}{A} \qquad \text{Equation 2.1}$$

$$\sigma_i = \frac{P_i}{A} \qquad \text{Equation 2.2}$$

$$\varepsilon_i = \frac{\delta_i}{L_g} \qquad \text{Equation 2.3}$$

$$E^{chord} = \frac{\Delta\sigma}{\Delta\varepsilon} \qquad \text{Equation 2.4}$$

Table 2.6: Properties of CF and various types of CNT (Kumar et al., 2020)

Property	Carbon nanotubes (CNT)			Carbon fiber (CF)
	Single walled (SW)	Double walled (DW)	Multi walled (MW)	
Young's modulus (TPa)	0.97 ± (0.16)	0.73 ± 0.07	0.018–0.068	0.965
Tensile strength (GPa)	13–52	31 ± 4	1.4–2.9	3.0
Fracture toughness (MPa $\sqrt{m}$)	2.7	-	-	-
Room temperature mobility (cm^2 V^{-1} s^{-1})	>105	-	104–105	-
Thermal conductivity (W m^{-1} K^{-1})	6000	-	2000	-
Electrical conductivity (S cm^{-1})	250–400	-	-	-
Surface area (m^2 g^{-1})	~ 400–900	-	~ 200–400	0.029–0.7

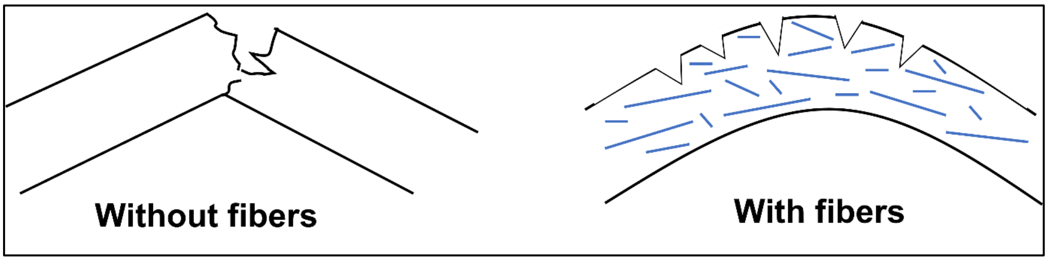

Figure 2.10: The benefits of reinforcements in composites (Akca & Gursel, 2015)

Table 2.7: Tensile properties of MWCNTs reinforced CFRP from various studies (Bilisik & Syduzzaman, 2021)

Textile material	Nanomaterials	Integration technique	Tensile properties	Study by
Sized carbon fiber	MWCNTs	Electrophoretic deposition, EPD method	120% increase in tensile strength	Moaseri et al.
Sized carbon fiber	MWCNTs	Electrophoretic deposition, EPD method	126% and 233% increase in tensile strength and modulus, respectively	Moaseri et al.
Unsized carbon fiber	MWCNTs	Chemical vapor deposition, CVD method	10% decrease in tensile strength	An et al.
Carbon fiber	MWCNTs	Electrophoretic deposition, EPD method	24.42% increase in tensile strength	Zhao et al.
Carbon fiber	MWCNTs	Electrophoretic deposition, EPD method	9.86% and 12.4% and 44.01% increase in tensile strength, modulus, and failure strain, respectively	Mei et al.
Carbon fiber	MWCNTs (0.35 wt%)	Mixing with epoxy	10.41% increase in tensile strength	Zhao et al.

Table 2.7 continued

Carbon fiber nitrate oxidized	MWCNTs	Electrophoretic deposition, EPD method	35.7% and 21.7% and 70% increase in tensile strength, modulus, and failure strain, respectively	Mei et al.
2D biaxial carbon fiber fabric	MWCNTs (0.25 wt%)	Mixing with epoxy	60% increase in tensile strength	Tariq et al.
2D biaxial carbon fiber fabric	MWCNTs	Chemical vapor deposition, CVD method	69% increase in tensile strength	Sharma and Lakkad
2D biaxial carbon fiber fabric	MWCNTs	Electrospray method	21% and 37% increase in tensile strength and modulus, respectively	Zakaria et al.
Monodirectional carbon fiber fabric	MWCNTs (0.1 wt%)	Aqueous suspension deposition	17.6% increase in tensile strength	Xiao et al.

2.4.4 Application of CFRP and CNT–reinforced CFRP composites

Owing to their outstanding properties, carbon–based nanofillers reinforced polymer composites (CFRP and CNT–reinforced CFRP composite) have earned massive recognition in various applications (Nurazzi et al., 2021b). This is because, compared to the traditional metal alloys, these composites had better thermomechanical properties and a higher strength–to–weight ratio. Hence, structural applications such as aerospace and automobiles are in favor of these composites (Kumar et al., 2020).

Generally, this fiber reinforced composite materials are used to replace metallic components in those structural applications as they offer substantial weight reduction in addition to high strength and stiffness. Apart from that, by substituting these FRP composites, the production cost can be reduced due to the decrement in the components needed in a part, and also the manufacturing of complex shapes are achievable (Yassin & Hojjati, 2018).

2.4.4.1 Automotive and automobile

The regulations for carbon dioxide (CO_2) emission reduction and the progress of energy–efficient strategies had made the interest in light weighted automobiles grow steadily. Thus, it is important for the auto industry to develop energy–efficient transportation. Conventional automobiles are made of metal, around 63% by weight. By reducing the weight of those conventional vehicles by merely 10%, it had made internal combustion engines have an increment in fuel economy by 6–8%, while for electric vehicle, the increment is around 10%. Theoretically, carbon fiber composites can offer around 40–70% mass reduction (Sarfraz et al., 2021).

When CFRP composites are used to manufacture automobile parts, the finished product will be 30% lighter than aluminum and 50% lighter than steel. Meanwhile, when the car body and various parts are made of CFRP materials, the weight of the entire vehicle is estimated to have had more than 100kg reduction. For example, at the 2007 Chicago Auto Show, Toyota presented their concept car, 1/X, which had a major weight reduction compared to their Prius. While maintaining an interior space that is comparable to the hybrid Prius, the 1/X only weighs around 420 kg, which is approximately one–third of the weight of the existing Prius. This is possible because the car skeleton utilized CFRP to make it light weight, hence reducing the engine displacement (Moon et al., 2019).

Bumpers, chassis, hood or bonnet, and tailgate are among the vehicle parts that are manufactured using CFRP composites. Being stronger by twofold compared to steel or aluminum, with lighter weight, had made CFRP a suitable material to be used in producing chassis. Normally, super cars use chassis as they prioritize light weight and strong properties of the CF over the high cost (Ahmad et al., 2020).

As for the hood or bonnet, when CFRP are used, those hoods had the strength and stiffness of steel with only one fifth of the density. A CFRP hood is approximately 60% lighter than a steel hood (Masilamani et al., 2017). Additionally, owing to the reduced density and stiffness of the CFRP, two of the tailgate stabilizer can be removed, thereby reducing the vehicle's weight even further. Also, the interior trim components can be removed and can be directly painted instead. The number of assembled parts is reducing too due to CFRP usage (Ahmad et al., 2020). **Table 2.8** shows the mass comparison between produced SMC with the CFRP prototype for tailgate.

Table 2.8: Mass comparison of tailgate produced SMC with CFRP prototype (Masilamani et al., 2017)

	Production SMC mass (kg)	**Prototype of CFRP mass (kg)**
Tailgate inner	5.7	2.3
Tailgate outer	3.2	0.9
Spoiler mechanism carrier	1.1	0.2
Total weight	10	3.4

2.4.4.2 Space and aerospace industry

In the space and aviation industries, CFRP composites are preferred, and the number of aircraft components made up from CFRP composites has been increasing progressively. Both small and large components, such as doors, clips, wing flaps, and the main body, utilized CFRP composites in their production. This is due to the excellent characteristics of the composites such as light weight, high fatigue resistance, as well as strength and stiffness

(Altin Karataş & Gökkaya, 2018). CFRPs are also highly durable and resistant to corrosion (Ozkan et al., 2020).

By reducing the weight of the aircraft structural components, the fuel efficiency and the load bearing capacity of the airplanes are enhanced, and at the same time, CO_2 emissions are reduced (Altin Karataş & Gökkaya, 2018). By reducing the airplane's total weight by just 1 kg, 120 L of fuels is able to be saved. CFRPs also exhibit high thermal resistance as they do not soften and melt easily unless the temperature is really high. Hence, parts that are subjected to high temperatures such as airplane brakes and rocket nozzle, can be produced using CFRP composites (Ozkan et al., 2020). Carbon–carbon materials such as the CFRPs exhibit many remarkable characteristics that make them broadly used in this industry. However, there are a few drawbacks related to this carbon–carbon materials, such as high costs and limitation in terms of the fabrication processes' efficiency (Harussani et al., 2022).

2.4.4.3 Defense technology

Since 2000, CFRP composites have been used in military aircrafts. Not only are CFRP composites are light in weight, but they concurrently exhibit an improved strength–to–weight ratio, which is useful is reducing CO_2 emissions and fuel use. The aerodynamics efficiencies are improved, and the manufacturing costs are lowered as the composites require lesser riveted joints. Those attractive properties had made the manufacture of military aircraft use composites to further increase the speed and mobility of the aircraft (Harussani et al., 2022). The CFRP composite material made up nearly the whole outer surface of the stealth airplane (military aircraft B–2). This airplane uses CF to increase its invisibility, radar reflection and heat dissipation properties. Additionally, Turkish Aerospace Industries (TAI) manufactured their unmanned air vehicle using mostly CFRP composites materials (Ozkan et al., 2020).

CFRP had also been used in the defence structures' enhancement and reinforcement. In vulnerable public buildings, CFRP is incorporated to reinforce the current structure and improve the blast protection properties. Retrofitting and strengthening of civil infrastructure commonly make use of CFRP composites. Adding CFRP to a structure can make it more resistant to blasts because it makes the structure stronger and more flexible and makes it less likely to break apart (Harussani et al., 2022).

2.5 Response Surface Methodology (RSM)

RSM was first developed in 1951 by Box and Wilson, and its initial application was aimed at enhancing the process yield of various industries. RSM has gained extensive application in diverse fields such as biotechnology, agriculture, and automotive (Nair et al., 2014). The implementation of RSM is followed by several steps, starting with selecting the independent variables that substantially effected the chosen responses. After that, before conducting the experiments, an experimental design is selected. The next step is analysing acquired data statistically and fitting it into a polynomial function. The model's fit is evaluated, and the optimum values are determined. By using RSM, the number of tests required to obtain ideal conditions can be reduced (Isam et al., 2019).

This mathematical and statistical technique, previously known as Box-Wilson methodology, is utilized to design experimental sets (Kaur & Kaur, 2013; Veza et al., 2023). The relationship between a set of factors (input or independent variables) and observed responses (output) is evaluated through this technique (Kaur & Kaur, 2013). Furthermore, RSM is also used to optimize the responses that are impacted by the independent variables. Therefore, it is essential to meticulously select appropriate ranges of selected factors and desired responses prior to applying the RSM method to ensure the precision and significance of the obtained findings (Veza et al., 2023).

Using mathematical models to optimize parameters is a highly favoured method for analysing response variables due to its efficiency, time-saving capabilities, and cost-effectiveness. The present approach formulates a suitable experimental design encompassesing all the independent variables and leverages the pertinent data obtained from the experiment to derive a series of equations capable of computing the theoretical outcome (Zulkifle et al., 2022). **Equation 2.5** shows the model structure that is used for the prediction of ideal conditions:

$$y = \beta_0 + \sum_{j=1}^{k} \beta_j x_j + \sum_{j=1}^{k} \beta_{jj} x_{j^2} + \sum_{i} \sum_{<j=2}^{k} \beta_{ij} x_i x_j + \epsilon_i \qquad \text{Equation 2.5}$$

Where y is the response; x_i and x_j are the factors; β_0 is a constant coefficient; the interaction coefficients of the linear, quadratic, and second–order terms are denoted by β_j, β_{jj}, and β_{ij}, respectively; k is the number of studied factors; and ϵ_i is the error. To illustrate the relationship between responses and experimental levels of each factor, the fit polynomial equation is expressed as the surface and contour plots. This is also done to derive ideal conditions (Ahmad et al., 2020). The variables in the second-order model are amendable to easy approximation since it is very pliable. The second-order models are mathematical representations of surfaces that exhibit quadratic behaviour, including the presence of maximum and minimum points, saddle points, ridges, and stationary points (Reji & Kumar, 2022).

The experimental data can be processed using computer software applications such as Minitab (Minitab Inc.) and Design-Expert (State-Ease Inc.). These two are the most commonly used software to perform RSM and help decrease the period required for experiment design and improve the design analysis accuracy (Kassem et al., 2019; Veza et al., 2023). The relationship between the parameters and output is determined using the design of experiments (DoE) (Reji & Kumar, 2022). Three second-order primary categories that are commonly used for the response surface design are full factorial design (FFD), Box-Behnken design (BBD), and central composite design (CCD) (Veza et al., 2023).

2.5.1 Central Composite Design (CCD)

The most used second-order design for experimental studies is the CCD, developed in 1951 by Box and Wilson. There are three types of experimental points involved in this design: (i) factorial (points that allow data generation for 2-sample *t*-hypothesis tests), (ii) centre points (element of design which curvature are assessed in the region of interest), and (iii) axial points (components capable of assessing quadratic effects seen in given region) (de Oliveira et al., 2019).

Both first- and second-order terms can be efficiently approximated using CCD. Additionally, modelling of a response variable is possible via CCD, where curvature with additional centre and axial points to the factorial design are used. Estimating the response surface curvature in the experiment domain is possible because of the points at the domain's midpoint and the "star" outside the domain. ± 1 referring to the points levels of factorial design, while $\pm\alpha$ are those on a "star" design, where $|\alpha| \geq 1$ (Veza et al., 2023). After the identification of the curvature and the addition of axial points are done, the calculation of total number of experiments for this design is indicated by **Equation 2.6**:

$$N = 2^k + 2k + n_c \qquad \textit{Equation 2.6}$$

Where N refers to the total number of experiments, k refers to the number of factors, 2^k are referring to the factorial points, $2k$ denotes the number of axial points, and the centre point runs are denoted by n_c (de Oliveira et al., 2019). It is necessary to correctly assign each variables to its attributed values with these five levels (-α. -1, 0, +1, +α) (Nazeri Abdul Rahman et al., 2023). The flow diagram for CCD is illustrated in **Figure 2.11**.

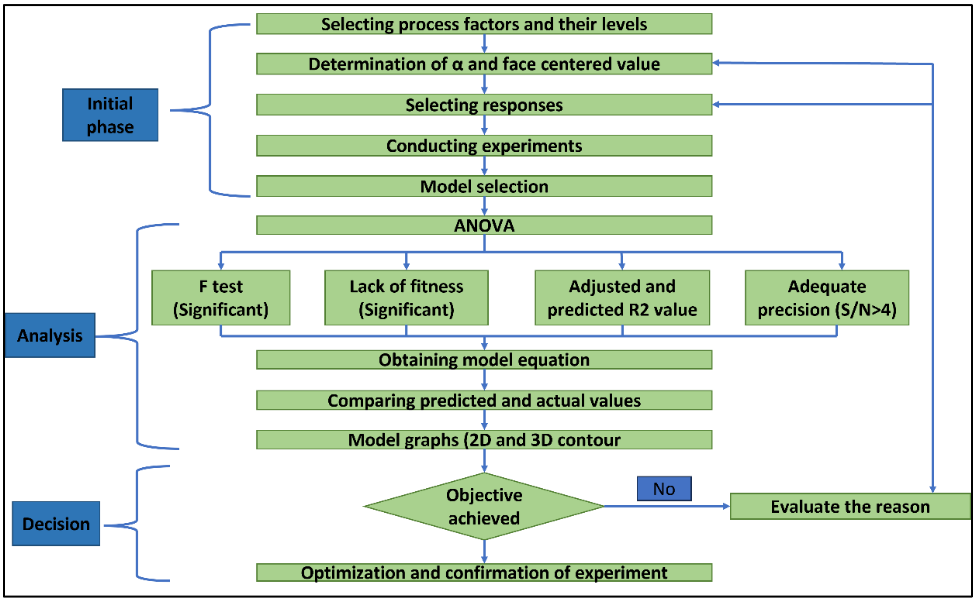

Figure 2.11: CCD flow diagram (Bhattacharya, 2021)

2.5.1.1 Types of CCD

Figure 2.12 demonstrates the schematic illustration of CCD, where the stars represent the axial points and the distance from the stars to the cube's edge is the alpha (Njoku & Otisi, 2023). The response surface plot is determined by the star point outside the domine and the centre point, corresponding to the experimental domine. Meanwhile, the location of the α value determines the quality of design or estimation. The determination of the points' position would identify the rate of design. Additionally, the number of trials near the centre of the domine influences the estimation precision. There are three categories of CCD, namely Circumscribed Central Composite Design (CCC), Inscribed Central

Composite Design (CCI), and Face-Centred Central Composite Design (CCF) (Bhattacharya, 2021). **Figure 2.13** shows a brief description of the three classifications of CCD. CCC and CCI are rotatable type design with five levels per factor, while CCF are non-rotatable with only three levels per factor (Njoku & Otisi, 2023).

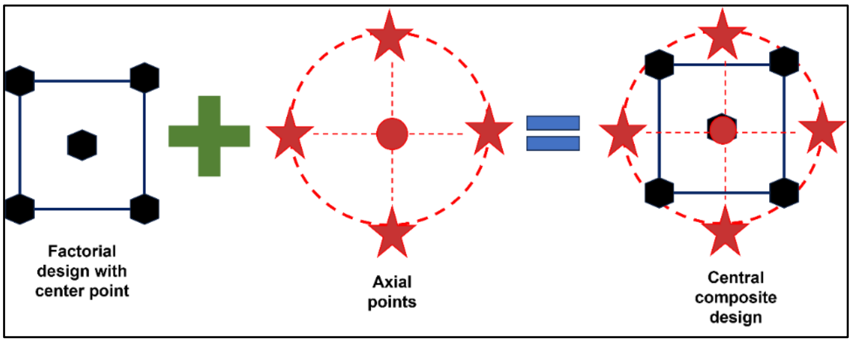

Figure 2.12: CCD schematic illustration (Veza et al., 2023)

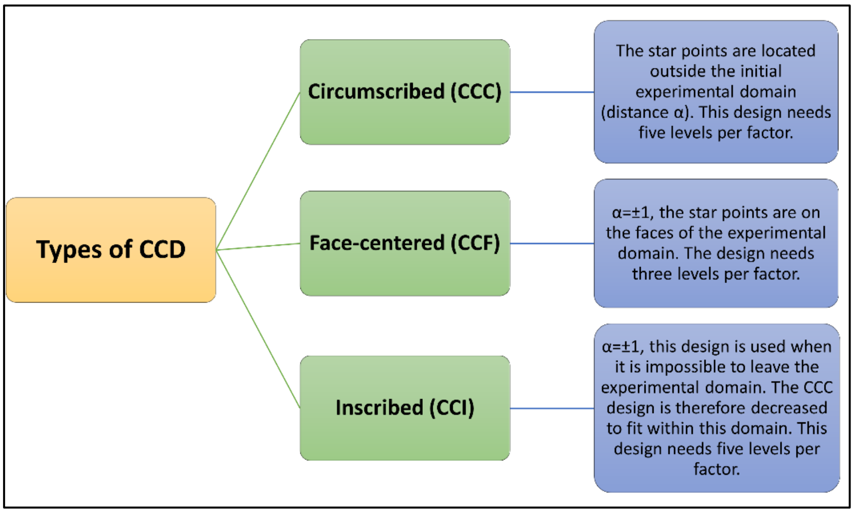

Figure 2.13: Three types of CCD (Veza et al., 2023)

2.5.2 Analysis of Variance (ANOVA)

The model's evaluation and the testing of the model's meaningfulness are done by using the analysis of variance (ANOVA) (Ebrahimi et al., 2021). The comparison of variance caused by the modification in the combination of variable levels due to the random errors caused by the generated responses is known as ANOVA (Nazeri Abdul Rahman et al., 2023).

In ANOVA, the significance of the regression model equation or the model's coefficient terms is determined by the *f*-value and *p*-value (Zhou et al., 2020). The f-value (Fisher's f-value) compares the variance of the model or curvature with the residual errors, and it is another indicator to evaluate the model's adequacy and measure the overall significance. The greater the f-value, the greater the data dispersion. This value is calculated using the mean squares model and the error mean square. A model's F-ratio must be higher than the critical f-value indicated in the F-distribution table to be considered significant. To calculate and compare the two f-values, the degree of freedom and significance level α = 0.05 are considered. ANOVA verified of the predicted model, and the importance of model components was measured using a $p\text{-value} < 0.05$, indicating a 95% confidence level (Beiramzadeh et al., 2019).

An ideal model exhibits statistical adequacy, as demonstrated by its lack of significant lack of fit, with a high R^2 value, high Adjusted and Predicted R^2, and a low predicted residual error sum of squares (PRESS). The models' factors were assessed with a confidence level of 95% (Niazmand et al., 2020). **Table 2.9** lists the expression used for model adequacy verification. R^2 estimates the total variation of predicted or model values from the mean by dividing the regression sum of squares by the total sum of squares. R^2 should be close to 1.0 for a model with good prediction accuracy. However, the model's prediction's effectiveness should not be judged just by R^2 because it rises as the number of terms in the model increases, regardless of its statistical significance. The Adjusted R^2 value, which considers the number of factors in the experiment, should be compared to the R^2 value. When statistically inconsequential factors are included, the Adjusted R^2 value typically reduces (Nair et al., 2014).

Table 2.9: Expression used for model adequacy verification (Nair et al., 2014)

Terms	Expressions	Remarks
Coefficient of determination	$R^2 = \frac{SS_{Res}}{SS_T}$	R^2 should be close to 1.0
$R^2_{Adjusted}$	$R^2_{adjusted} = 1 - \frac{SS_{Res}/(n-p)}{SS_T/(n-1)}$	$R^2_{Adjusted}$ should be close to 1.0
Prediction error sum of square (PRESS)	$PRESS = \sum_{i=1}^{n} [y_i - \hat{y}_i]^2$	PRESS should have a small value
$R^2_{Predicted}$	$R^2_{predicted} = 1 - \frac{PRESS}{SS_T}$	$R^2_{Predicted}$ should not have difference of more than 0.2 with $R^2_{Adjusted}$
Significance of regression	$F_0 = \frac{Mean\ square\ of\ model}{Mean\ square\ of\ residual}$	This ratio should be larger than the tabulated F value for a good model
Lack of Fit (LOF) test	$F_{LOF} = \frac{SS_{LOF}/(f-p)}{SS_{PE}/(n-p)}$	This ratio should be lower than the tabulated F value for a good model

SS_{Res} = sum of square of error; SS_T = total sum of squares; n = number of experiments in the sets; f = number of distinctly different factor combinations; p = number of parameters in the model; y_i = observed value; $\hat{y}_i$ = predicted value

The parameters F-value, R^2, p-value, and lack of fit are used to measure the fitting of the suggested models with the experimental data (Liu et al., 2018). The coefficient of determination, R^2 , is utilised to indicate the quality of model fitting (Niazmand et al., 2020). In addition, R^2 is also known as correlation coefficient, and it was used to analyse the relationship between the experimental data and the predicted model. A correlation coefficient is a value between -1 and +1 used to assess the existence of a statistical correlation between two variables. The residual analysis diagram is another important criterion for determining the predicted model's validity and accuracy. The disparity between the observed and predicted value is residual error. The model fits the data better when the R^2 value is large (Beiramzadeh et al., 2019). A higher R^2 value indicates a good relationship between experimental and predicted model values (Abdul Rahman et al., 2020).

The modified version of the R^2 is Adjusted R^2 (R^2_{Adj}), which considers the degree of freedom in its computation (Beiramzadeh et al., 2019). The Adjusted R^2 is the R^2 value adjusted depending on the number of predictors. Suppose the value of R2 increases with adding a new independent variable. This value indicates that the variables impacted the model and should be addressed during the modelling process to obtain a more varied model. Compared to the Adjusted R^2, the value of R^2 is higher (Abdul Rahman et al., 2020). However, the difference between those two values should be close (R^2 - R^2_{Adj}< 5%) to indicate that undesirable independent variables do not need to be removed from the model (Beiramzadeh et al., 2019). When the differences between those two values varied, significantly, inconsequential factors may have been included in the model (Abdul Rahman et al., 2020).

Additionally, the Predicted R^2 (R^2_{Pred}) demonstrated the ability of the model to predict responses for a new set of observations. The model is more accurate when the predicted R^2 is higher ($R^2 – R^2_{Pred} < 0.2$) (Beiramzadeh et al., 2019). Nevertheless, the value of R^2 should be larger than Predicted R^2 (Abdul Rahman et al., 2020). The R^2_{Pred} is more significant for model comparison than R^2_{Adj} because it is based on observations that are not part of the model (Beiramzadeh et al., 2019).

In addition, ANOVA also assessed the formulated mathematical models by using p-values. The p-values indicate the marginal significance level within a statistical hypothesis test, which must be less than 0.05 to prove that the mathematical models obtained are statistically significant (Nazeri Abdul Rahman et al., 2023). The probability of encountering the measured F-value if the null hypothesis is true is the p-value (probability > F). Small probability values imply that the null hypothesis is rejected and the curvature is unimportant (Sarrai et al., 2016). According to the null hypothesis, there is no correlation between the predictor and outcome variables in the population. The formal framework for the evaluation of statistical significance is the null hypothesis. Meanwhile, the alternative hypothesis is the notion that an association exists. When the statistical significance test rejects the null hypothesis, the alternative hypothesis, which cannot be tested directly, is accepted by exclusion (Banerjee et al., 2009). Through null hypothesis significance testing (NHST), the p-value used as a decision indicator is obtained (Tsushima, 2022). The alternative hypothesis (H_A) is favoured, and the null hypothesis (H_0) is rejected in NHST when the p-value is lower than the pre-specified α-level (McNulty, 2022). The chosen significance level is typically 0.05 (5%) (Du Prel et al., 2009). The corresponding coefficient is more significant when the p-value is smaller, but the F-value is larger (Sarrai et al., 2016). If the 'p > F' value is less than 0.05, the model is significant at a confidence level of 95% (Nair et al., 2014).

By comparing the residual error to the pure error from the replicated experimental design points (often the central points in the experimental design), the lack of fit test determines whether the model fails to describe data points in the experimental domain and should be insignificant (Nair et al., 2014). Lack-of-fit is an error when the analysis removes one or more essential terms or components from the process model (Ighalo et al., 2020). If this ratio is higher than the calculated F-value, it is determined that the model requires improvement because there is evidence of a lack of fit (Nair et al., 2014). The ideal model should have a p-value that is insignificant. A standard criterion for determining an insignificant lack of fit would be a p-value greater than 0.10. A desirable model should have an insignificant lack of fit (Njoku & Otisi, 2023). In addition, the prediction error sum of squares (PRESS) is another statistic used to assess the model's predictive capabilities. It evaluates how accurately the experiment's model is likely to forecast the outcome of a later experiment. Small PRESS values are preferable (Nair et al., 2014).

Adequate precision is the ratio of the predicted value range at design points to the average prediction error (Breig & Luti, 2021). Adequate precision measures the signal-to-noise ratio. It is preferable to have a ratio of a least 4 for a model to navigate the design space (Njoku & Otisi, 2023). The range of values within which factors can be altered or changed is known as the design space (Lamidi et al., 2023).

The ratio of standard deviation to mean is indicated by the coefficient of variation (CV). This value represents the level of accuracy used to compare the experiments. The dependability of the experiment often decreases as the CV value increases. When the CV value is below 10, the model is reproducible. A smaller number of CV indicates that the experiments were more reliable (Isam et al., 2019; Mohan et al., 2014).

Residual is the difference between the actual and predicted values and is essential in evaluating the model adequacy (Nair et al., 2014). Residual error, or the discrepancy between observed and predicted response values, was used to assess the model's validity. 'Normal probability plot of residuals' and 'residual versus fitted/ predicted values' are two crucial graphs that demonstrate the normality of the residuals (Beiramzadeh et al., 2019). The normal probability plot of the residuals is created to test the assumption of normality. The plot of the residuals will follow a straight line with a relatively modest scatter if the residuals are normally distributed, suggesting that the model is well-fitted (Nair et al., 2014). The distribution becomes more normal as the residual values become closer to a straight line (Beiramzadeh et al., 2019). The evaluation of the model is also aided by the plot of experimental/ actual values versus predicted values. The points should be distributed uniformly along the 45° line. Regions of over or under-prediction are shown by the groups of points above or below the lines (Nair et al., 2014). Additionally, for the 'residual versus predicted' graph, the residuals should scatter irregularly on either side of the borderline for the model to be reliable (Beiramzadeh et al., 2019).

The final step in RSM is the statistical model analysis, where three-dimensional (3D) contour plots are produced (Nazeri Abdul Rahman et al., 2023). RSM typically produces contour plots in two dimensions and three-dimensional response surface plots. The latter approach is more advantageous in comprehending the factors' primary impacts and interdependent effects on the responses (Jena et al., 2017).

2.5.3 Optimization

RSM is often used in various optimization studies as it can analyse the effects and interactions between multiple factors on several response variables (Reji & Kumar, 2022). There are three significant steps involved in the optimization process: (i) execution of the statistically design experiments, (ii) estimation of the mathematical model's coefficients, and (iii) response prediction and the adequacy of the model are checked (Sadhukhan et al., 2016).

The main objective of the optimization process is to maximize the preferred outputs or to minimize the disagreeable outputs. The quadratic model shown in **Equation 2.5** is the optimal model to be used for optimization as the model encompasses linear and squared terms for all factors and the products of all pairs of variables. Response surface designs are commonly employed to fit quadratic models. CCD and Box-Behnken designs are widely employed in response surface modelling as they are the most prevalent designs (Njoku & Otisi, 2023). Additionally, the RSM method was utilized to clarify the impact of factors on the responses. This approach is prevalent in the development and optimization of formulations, as it enables the examination of the impacts of factors and their respective levels on a model, thereby facilitating the prediction of responses within the domain (Jena et al., 2017).

Utilizing the desirability function enables the optimization of one or more responses, resulting in the maximization or minimization of the studied matters. This optimization is achieved by converting the obtained response values into desirability function values that fall from 0 to 1. The value of 0 is assigned in cases where the study factors do not elicit a desirable response, while the value of 1 indicates the optimal performance of said factors. The integration of RSM and the desirability function is called the optimization methodology of desirability (DOM). When the optimization of process conditions relies upon multiple responses, the optimization criteria frequently exhibit conflicting objectives. The situation must be valued within an optimal range, resulting in an in-accordance solution (Pereira et al., 2021).

2.6 Chapter Summary

This chapter elaborates on the collection of information related to this study obtained from journals, conferences, book chapters, and reports. There are four main parts of this chapter: (i) electrophoretic deposition (EPD), (ii) carbon nanotubes (CNTs), (iii) carbon fibre reinforced polymer (CFRP) composites and (iv) Response Surface Methodology (RSM). The first part discusses all related information regarding the EPD process, such as the definition, mechanisms, influencing factors, and applications, in detail. Meanwhile, the second parts focus on the study's primary reinforcement material, the CNTs. The types of CNTs and their applications are among the information in this chapter. The third part focuses on the finished product of the study, which is CFRP composites. The raw materials that make up the composites, manufacturing techniques, tensile properties, and the application of composites are described in this part. Lastly, information related to RSM is also explained in detail.

CHAPTER 3

METHODOLOGY

3.1 Overview

In this chapter, the research methodology is discussed. The methodology corresponds to the aim and objectives of the study in **Chapter 1**. The literature review is done next, followed by the research flowchart, the variables in the study, and the experimental study. Both experimental and statistical studies are included in the experimental study, along with the process optimization. The procedures are listed in the production sequence to ensure that all the critical procedures are executed. The procedures are vital as they would affect the samples' final properties and results. **Figure 3.1** illustrates the research flowchart.

3.2 Literature review

The literature review of the research, as elaborated in **Chapter 2**, consists of four main points: (i) electrophoretic deposition (EPD), (ii) carbon nanotubes (CNTs), (iii) carbon fiber–reinforced polymer composites (CFRPs) and (iv) response surface methodology (RSM). The published journal articles, book chapters, conferences, etc., have been reviewed before starting the research.

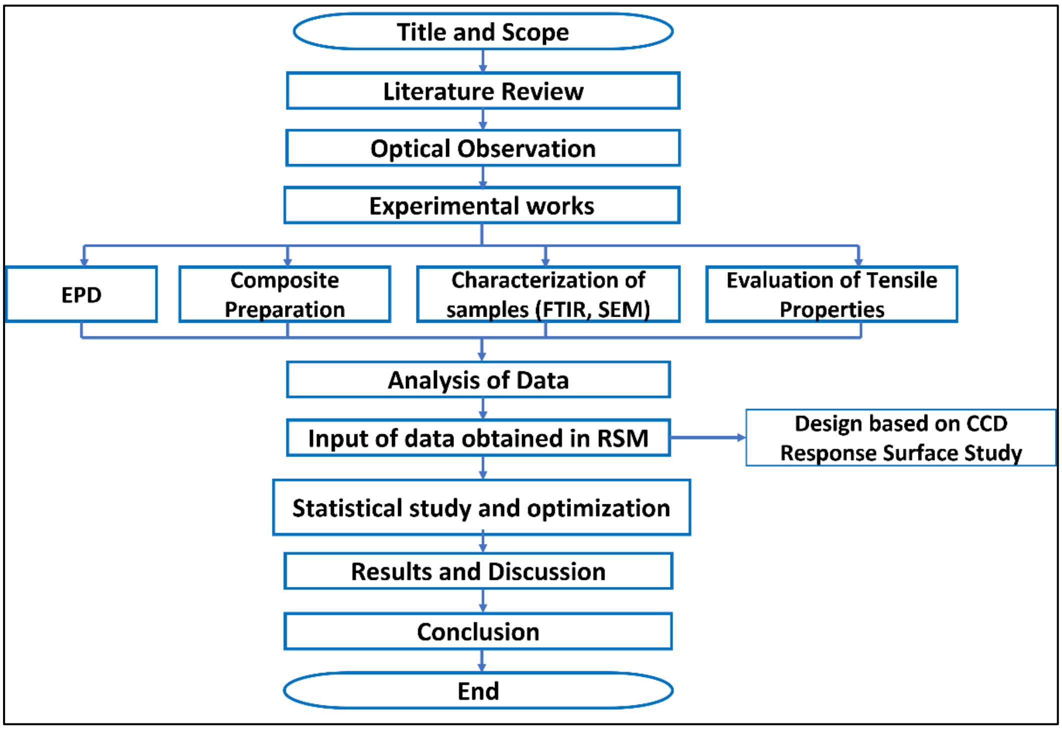

Figure 3.1: The process flow chart for the study

3.3 Experimental study

3.3.1 Experimental study overview

The experimental study is conducted based on three input parameters: the volume ratios of the suspension media, deposition voltage, and deposition time. **Table 3.1** lists the input parameters and their ranges used in the experiment. First, before starting the EPD process, the input parameters are determined based on the research done during the completion of the literature review. After that, the design of the experiment is done using Design Expert software, with a Central Composite Design (CCD) model, where the input parameters are used to design the experimental work. The responses of the experiment are also determined, which are the tensile properties of composites. The EPD process is based on the tabulated experimental design, and the composites are prepared after its completion. The tensile properties of the composites are determined before proceeding to composites' characterization testing. The results obtained are analysed and optimised using Response

Surface Methodology (RSM) to get the ideal input parameters that will produce maximum responses. The complete details of the experimental studies are discussed throughout this chapter.

Table 3.1: The input parameters and their ranges

Input Parameters	Ranges
Volume ratios of the suspension medium, % (w/w)	0% water,100% methanol; 100% water,0% methanol; 20% water,80% methanol; 80% water,20% methanol
Deposition Voltage (V)	10–20 volts
Deposition Time (min)	5–15 minutes

3.3.2 Materials

The solution used for the EPD process consisted of two solvents: methanol (MeOH) and water (W). The methanol (CAS Number: 67-56-1) is supplied by Merck kGaA (Darmstadt, Germany). This clear solvent has a purity of ≥ 99.99%. The chemical formula for methanol is CH_3OH, with a molar mass of 32.04 g/mol. The physicochemical properties of MeOH are as follows: boiling point of 64.5°C, flash point of 9.7°C, melting point of –97.6°C, density of 0.792 g/cm^3 (20°C), and vapor pressure of 128 hPa (20°C). MeOH is highly flammable and toxic in both liquid and vapor form and needs to be stored at +2°C to +30°C (Merck KGaA, 2023). Meanwhile, the water is obtained using an Arium Pro UV Ultrapure water system (Sartorius).

The multi-walled carbon nanotubes (MWCNTs) are from SkySpring Nanomaterials, Inc. (Houston, TX, USA) (Product No. 0552CA). The MWCNTs have a purity of 95% and are produced via catalytic CVD. The length of the MWCNTs is 2-5nm. The nanomaterial's specific surface area (SSA) is >500 m^2/g and has ash content <1.5 wt%. The bulk and true density of the MWCNTs are 0.27 g/cm^3 and ~2.1 g/cm^3, respectively. The MWCNTs' electrical conductivity is >100 s/cm (SkySpring Nanomaterials Inc., 2023).

The carbon fibre (CF) used in the experiment is black plain weave CF supplied by PiCarbon (Malaysia). The CF is a high-quality grade A CF fabric (3K 240 gsm). In addition, both Epocast PT100 (clear type epoxy resin) and Epoharden PT100S (amine-based epoxy hardener) are obtained from Portal Trading (P.T.) (Malaysia) and are used as matrix and curing agents, respectively. The working pot life of this two parts liquid plastic resin is 15 to 20 minutes at room temperature (30°C). The materials must be kept at room temperature (about 30°C), away from direct sunlight or heat source.

3.3.3 Characterization of pristine materials

Pristine CF and MWCNTs are analysed using scanning electron microscopy (SEM) and Fourier Transform Infra-Red (FTIR).

3.3.4 Preparation of the suspension medium

Five suspension mediums are prepared, each with their corresponding volume ratios of water and methanol mixture (water is used as the basis of volume ratio). The ratios of the medium are as follows: (i) 100% water, 0% methanol, (ii) 0% water, 100% methanol, (iii) 20% water, 80% methanol, (iv) 80% water, 20% methanol, and (v) 50% water, 50% methanol (the last medium ratio is prepared in accordance with the CCD model used). The values used for the volume ratios of the suspension medium are obtained from previous studies conducted by Cordero-Arias et al. (2013), Ervina et al. (2019), and Moaseri et al. (2016). Meanwhile, the concentration of the suspension medium of 0.05 mg/mL is referred from previous studies conducted by Ervina et al. (2019), Guo et al. (2012), and Moaseri et al. (2016). 0.004 g of MWCNTs are dispersed in 80 mL solvents of respective volume ratios listed before inside the laboratory glass sample bottles.

The MWCNTs are then dispersed uniformly using ultrasonic cleaner (sonicator) (KUDOS SK2200HP) for 15 min to ensure uniform dispersion of the MWCNTs in the suspension medium.

3.3.5 Optical observation of MWCNTs' stability in the suspension medium

Optical dispersion and stability of the MWCNTs over specific periods are observed before starting the EPD process, and this methodology corresponds to the study's first objective. This stability test is done without the presence of voltage. The periods range from after sonication (minute 0) until two months (Day 60) (Ervina et al., 2019; Zakaria, Omar, et al., 2020). In this test, the volume ratio of the suspension medium used is described in 3.3.4. The dispersion of MWCNTs in the mediums was done for 15 minutes using an ultrasonicator. After the sonication process was completed, the suspension medium was left undisturbed. The progress of the MWCNTs in the medium, starting from its stable conditions (well-dispersed in the medium) until it has completely sedimented at the bottom of the sample bottle, is recorded and photographed at selected time intervals to demonstrate the differences in the MWCNTs' stability in different mediums.

3.3.6 Electrophoretic deposition (EPD) process

3.3.6.1 Design of Experiment (DoE)

The effects of various combinations of input factors, i.e., volume (% w/w/), voltage (V) and time (min) on the tensile properties of the hybrid CNT-CF/epoxy composites were investigated using the central composite design (CCD) response surface study. The values of the input factors were indicated in **Table 3.2** and **Table 3.3** as two pairs of different volume ratios were used for each DoE. The volume ratios used are listed at **3.3.4**. Meanwhile, the variations of deposition voltage and time were referred from various previous studies conducted by Ervina et al. (2019), Guo et al. (2012), M. Li et al. (2013), Moaseri et al. (2016), Wu et al. (2020), Xiao et al. (2018).

The design generated 18 runs with different factor conditions for each volume ratio pair. The tabulated experimental design is shown in **Table 3.4** and **Table 3.5.** The medium percentage used in the experiment is shown in terms of the percentage of water since it is used as the basis of the suspension medium. For instance, in **Table 3.4**, the condition for experimental run 1 is 100% water, and 0% methanol with deposition voltage and time of 20V and 15 minutes, respectively. Meanwhile, experimental run 4 (**Table 3.4**) indicated the observed condition of 0% water and 100% methanol with a deposition voltage of 10V and time of 15 minutes.

For both **Table 3.2** and **Table 3.3**, the "Coded Low" and "Coded High" indicate the lowest and highest value designed for each input parameter in the experiment in terms of coded value, where -1 is the lowest designed value. At the same time, +1 is the highest designed value. Additionally, the "Mean" and "Std. Dev." refer to the setting's average and standard deviation in each of the numeric factor columns (Stat-Ease Inc., 2023). "Min." and "Max." refer to the minimum and maximum range of the input parameters.

Table 3.2: Chosen variables levels and coded values for first DoE (volume ratio of 0% water, 100% methanol and 100% water, 0% methanol)

Factor	Name	Units	Type	Min.	Max.	Coded Low	Coded High	Mean	Std. Dev.
A	Volume	% (w/w)	Numeric	0.0000	100.00	-1 ↔ 0.00	+1 ↔ 100.00	50.00	38.35
B	Voltage	V	Numeric	10.00	20.00	-1 ↔ 10.00	+1 ↔ 20.00	15.00	3.83
C	Time	min	Numeric	5.00	15.00	-1 ↔ 5.00	+1 ↔ 15.00	10.00	3.83

Table 3.3: Chosen variables levels and coded values for second DoE (volume ratio of 20% water, 80% methanol and 80% water, 20% methanol)

Factor	Name	Units	Type	Min.	Max.	Coded Low	Coded High	Mean	Std. Dev.
A	Volume	% (w/w)	Numeric	20.00	80.00	-1 ↔ 20.00	+1 ↔ 80.00	50.00	23.01
B	Voltage	V	Numeric	10.00	20.00	-1 ↔ 10.00	+1 ↔ 20.00	15.00	3.83
C	Time	min	Numeric	5.00	15.00	-1 ↔ 5.00	+1 ↔ 15.00	10.00	3.83

Table 3.4: Experimental design for the ratio of 0% water, 100% methanol and 100% water, 0% methanol with designated voltage and time range

Run	Factor 1 A: Volume %(w/w)	Factor 2 B: Voltage V	Factor 3 C: Time min
1	0	20	15
2	100	20	5
3	0	10	15
4	50	10	10
5	50	20	10
6	0	10	5
7	100	10	5
8	100	15	10
9	50	15	10
10	0	20	5
11	50	15	15
12	0	15	10
13	50	15	5
14	50	15	10
15	100	10	15
16	50	15	10
17	100	20	15
18	50	15	10

Table 3.5: Experimental design for the ratio of 20% water, 80% methanol and 80% water, 20% methanol with designated voltage and time range

Run	Factor 1 A: Volume %(w/w)	Factor 2 B: Voltage V	Factor 3 C: Time min
1	50	10	10
2	20	20	5
3	50	15	10
4	20	15	10
5	20	10	15
6	80	10	5
7	20	20	15
8	50	15	5
9	50	15	10
10	50	20	10
11	80	10	15
12	20	10	5
13	50	15	10
14	80	20	15
15	80	15	10
16	80	20	5
17	50	15	15
18	50	15	10

3.3.6.2 Fabrication of the hybrid MWCNT – CF strips via EPD

After the suspension medium with the MWCNTs had fully dispersed, as elaborated in sub–unit **3.3.4**, the medium was placed in a glass deposition bath. The experimental setup of the EPD process is illustrated in **Figure 3.2**. It consisted of a direct current (DC) power supply (Model 1672, B&K Precision, California), two multimeters (Fluke 115, USA; and UNI-T UT61C, China), copper plate electrode, mini LED, and glass deposition bath. After cutting the CF strip into approximately 7.7 cm × 1.8 cm, duct masking tape is used to tape up all sides of the CF strip to avoid frayed edges during the EPD process. The CF and copper plate were attached to the non-insulator electrode holder using alligator clips hung up using a retort stand. This study used the CF as the cathode while a copper plate was positioned as the anode (counter electrode). The gap between the two electrodes was fixed at 1.5 cm, and both electrodes were then immersed in the MWCNT suspension medium (Ervina et al., 2019). The EPD was conducted per the experimental design listed in **Table 3.4** and **Table 3.5**. Throughout the process, the mini LED indicated that currents are flowing into the EPD set-up, as the mini LED will light up as long as the current continuously flows. Meanwhile, each multimeter had its respective function, one to check for current flowing, and another to check the voltage of the EPD process. After the deposition process had been completed, the deposited CF strip was dried in the oven at 70 °C for 12 hours (Wu et al., 2020).

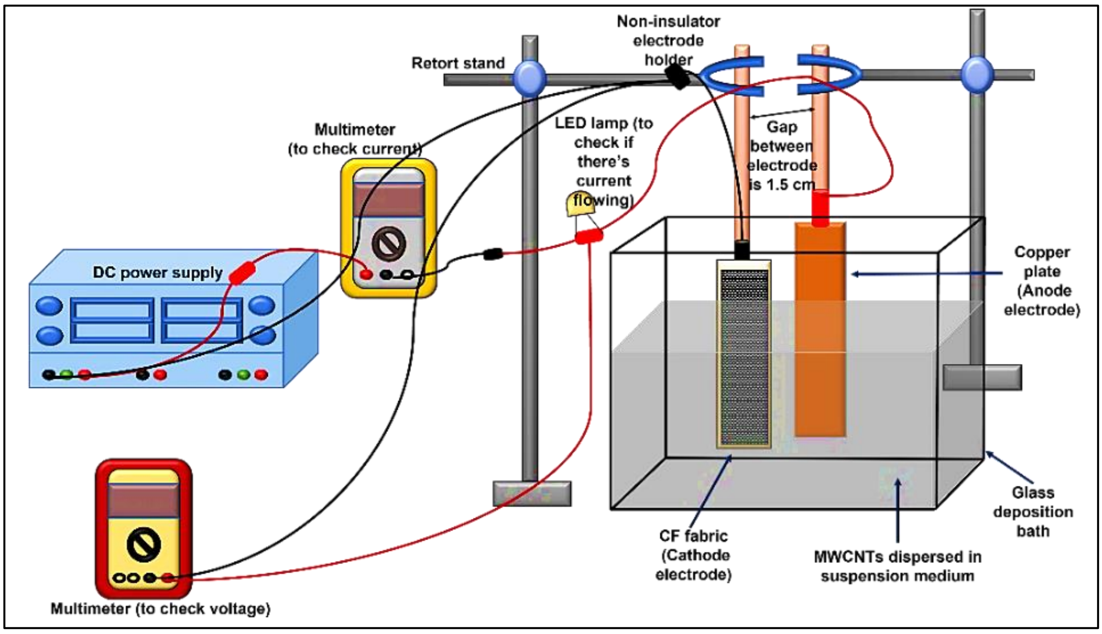

Figure 3.2: Schematic diagram of the EPD process for the fabrication of hybrid MWCNT-CF materials

3.3.7 Composites preparation

The fabrication of the 3-ply MWCNT-CF/Epoxy laminated composites was done using the open molding method, and the selection of the method is with reference from previous studies carried out by Moaseri et al. (2016) and Ervina et al. (2019). Each laminated composite consisted of three pieces of MWCNT-deposited CF strip with dimension as aforementioned in **3.3.6.2**. The mixture of matrix resin-hardener was prepared by combining the Epocast PT100(matrix) and Epoharden PT100S (curing agent) in a ratio of 2:1 by weight as per the manufacturer's manual before the molding process. Silicon molds are used to fabricate the composite, and alternate layers of matrix resin-hardener mixture and MWCNT-deposited CF strips are placed in the mold. After the last layer of the MWCNT-deposited CF strip, the remaining resin was poured until it filled the mold. Afterwards, after about 1 to 2 minutes, any air bubbles presented in the resin would be removed using utility lighter. The heat exposure is limited up to 3 seconds per removal process and it was repeated until all the air bubbles are thoroughly removed. Finally, the samples were left in room temperature for 24 hours to solidified and cured as per manufacturer manual. **Figure 3.3** showed the schematic illustration of the composites with its dimensions, and **Table 3.6** showed the description of the produced composites.

Table 3.6: Description of the samples

Sample	**Composite description**
Pure CF/epoxy composite	Epoxy laminated composite with three layers of woven CF
MWCNT-CF/epoxy composite	Epoxy laminated composite with three layers of woven CF reinforced with CNT

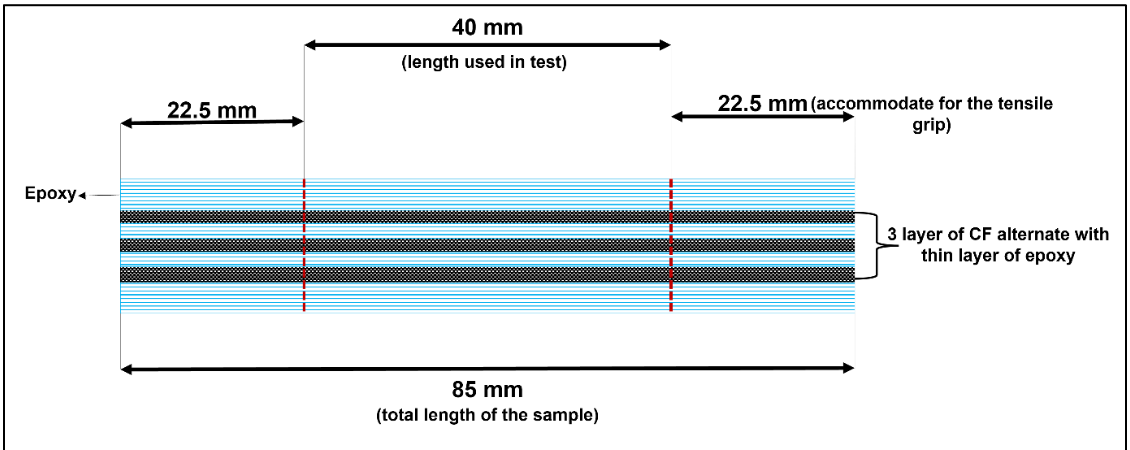

Figure 3.3: Schematic illustration of composites and their dimension

3.3.8 Evaluation of the composites' tensile properties

The testing of tensile properties corresponds to the study's second objective, and the methodology in **3.3.6** and **3.3.7** are the prerequisites to obtain the composites to be tested. A tensile test was conducted to evaluate the composites' tensile properties (tensile strength and Young's modulus) using universal testing instruments (Shimadzu Autograph AGS–50kNX, Japan) per ASTM D638. The cross-head speed used was 0.5 mm/min, and excluding the length required for the test grip, the samples' length taken into calculation was 40 mm. Additionally, the width and thickness of the samples were 27 mm and 2 mm, respectively.

The tensile strength, TS (unit: N/mm^2), was calculated using the following **Equation 3.1**:

$$TS\left(\frac{N}{mm^2}\right) = \frac{maximum\ force\ to\ rupture}{cross\ section} = \frac{F_{max}}{A} \qquad \text{Equation 3.1}$$

where F_{max} (N) is the maximum force needed to break the sample during the test, and A (mm^2) is the sample's cross-section, which can be obtained by multiplying the length by the width. Meanwhile, the stress-strain graph was plotted using the raw data obtained. The graph's slope helps determine Young's modulus of composite (E).

3.3.9 Characterization of the MWCNT–CF/ epoxy composites

3.3.9.1 Fourier Transform Infra-Red (FTIR)

The FTIR analysis used Shimadzu IRAffinity -1 to study the difference in the functional groups of the carbon fibers' surface when the EPD factors were varied. Each sample was analysed in the 4000–400 cm^{-1} regions with the resolution of 1 cm^{-1}.

3.3.9.2 Scanning electron microscopy (SEM)

The surface morphology of the MWCNT-CF/epoxy laminated composites was performed with SEM Hitachi TM4000Plus Tabletop Microscope.

3.3.10 Statistical study and optimization

The Response Surface Methodology (RSM) using Design Expert (DE) software (version 11, Stat–Ease, Inc.) was used for the data evaluation and optimization, and this method corresponds to the third objective of the study.

Physical and chemical experiment designs and optimization often utilize RSM to reduce the cost of experimental study. This selection is because RSM is an effective statistical method used in complex processes' evaluation and optimization via controllable forward model computations (Liu et al., 2018). The design of the experiment using RSM depends on using quantitative experimental data from earlier screening experiments to fit regression model equations and determine the ideal operating parameters (Kassem et al., 2019). This study used RSM to design the three-factorial central composite design (CCD) optimization study. For this study, the development of mathematical models to calculate the correlation between the variables and responses is using the face-centred CCD with α=1, where the axial points for this experimental design are concentrated more on the cubic surface rather than the sphere (Rahman & Dzulkarnain, 2021; Uche et al., 2022). The three selected manipulated variables are the volume ratios of suspension medium (%), deposition voltage (V), and deposition time (min). The responses are tensile strength and Young's modulus.

The study of the experimental data involved fitting to a second-order polynomial model, which was then statistically confirmed by running the analysis of variance (ANOVA) and lack-of-fit test to determine the model significance (Sadhukhan et al., 2016).

Additionally, the evaluation of the reliability of the regression equation can be done using the coefficient of determination (R^2) and the standard deviation (SD) of the regression model equation (Zhou et al., 2020). Other vital data required for ANOVA analysis were elaborated in detail in **Chapter 2**, **sub-unit 2.5.2**. Graphical analyses are also done, as RSM had this advantage compared to other methods. Since RSM can determine the interaction effect between two parameters onto the model response, 2D contour and 3D response level diagrams will be plotted. A constant is then assumed when plotting the curves to obtain the concurrent changes in the two other variables (Ebrahimi et al., 2021).

The determination of the optimum input parameters to obtain the maximum tensile properties of composites was possible by using CCD. A second order which requires the least amount of experiments for modelling, was fitted using CCD (Sadhukhan et al., 2016). Using the following formula, CCD was able to discern the effect of each variable on the selected responses:

$$Y = b_0 + b_1 X_1 + b_2 X_2 + b_3 X_3 + b_{12} X_1 X_2 + b_{23} X_2 X_3 + b_{13} X_1 X_3 + b_{11} X_1^2 + b_{22} X_2^2 + b_{33} X_3^2 \qquad \text{Equation 3.2}$$

where Y is the measured response, b_0 is the intercept, ($b_1 - b_{33}$) denoted the linear regression coefficients of the factors, (X_1, X_2, X_3) is the independent variables, (X_1X_2, X_2X_3, X_1X_3) is the effects of the interactions, and (X_1^2, X_2^2, X_3^2) denotes the quadratic effects (Kassem et al., 2019). A numerical approach was chosen for the optimization study. The input parameters are kept within the range while the responses are maximized. The predicted data from the DE software was compared to the actual data obtained from the experimental results (Mohmad Noor et al., 2020).

3.4 Chapter Summary

This chapter discussed the research flow to achieve the objectives mentioned in **Chapter 1**. After obtaining the title and scope of the study, the literature review is written to understand more about the study. After that, the experimental study is conducted. The experiment consisted of a few stages: characterization, preparation of mediums, optical observation testing, EPD process, preparation of composites, and evaluation of the composites' tensile properties. Composites are characterised after the tensile testing, and lastly, statistical study and optimization are done afterwards.

CHAPTER 4

RESULTS AND DISCUSSION

4.1 Overview

All the findings from the experimental, statistical and optimization study are discussed in detail in this chapter. There are several parts in which the data is discussed. Firstly, the characteristics of the pristine materials used in the study are discussed. Secondly, before the EPD process is conducted, optical observation is done on the suspension mediums that are to be used for the experimental work. The third part is the composites' characterization. After completing all the experimental work (EPD, composite production, and tensile testing), the selected composites' characteristics were evaluated. Fourth, the data obtained from the tensile testing and the composites' statistical analysis are studied. Graphical analysis is also done. Design Expert 11 software is used to conduct those analyses. The optimum input parameters required to obtain maximum responses are calculated through the analysis.

4.2 Characterization of Pristine Materials

This study has two main materials: multi-walled carbon nanotubes (MWCNTs) powder and carbon fiber (CF) fabric. Several characterizations were done on the pristine materials. The details of the analysis were discussed further in the chapter.

4.2.1 Characterization of MWCNTs

The pristine MWCNTs powder is characterized by using Fourier Transform Infra-Red (FTIR) and scanning electron microscopy (SEM). **Figure 4.1** shows the FTIR analysis of the MWCNTs. The peak at 1224.80 cm^{-1} was ascribed to **C–N** stretching bond. This peak showed that at the interior part of the nanotube walls, intercalated N atoms existed between the graphite layer (Misra et al., 2007). Additionally, the 1485.19 cm^{-1} peak showed the presence of the **C=C** groups in aromatic rings. The group was attributed to the bands that existed in the range of 1640–1400 cm^{-1} for the case of pristine MWCNTs (Wang et al., 2013). Meanwhile, the peak at 2339.65 cm^{-1} might be referring to the pristine MWCNTs' backbone (Wulan et al., 2018).

The presence of peaks at 2974.23 and 2887.44 cm^{-1} were assigned to the asymmetric methyl **C–H** stretching band and symmetric methylene **C–H** stretching band, respectively. These groups were generally assumed to have existed at the defect sites on the surface of the sidewall (Do Amaral Montanheiroa et al., 2015). In addition, the peak at 3589.53 cm^{-1} was attributed to the **O–H** stretch of the nonbonded hydroxy group, which is also known as the free hydroxyl group (Azri et al., 2017; Nandiyanto et al., 2019).

Meanwhile, the SEM analysis of the pristine MWCNTs is shown in **Figure 4.2**. The nanotubes are displayed on a micron scale, and it is clear that the clustered MWCNTs powder shown had different sizes (Ervina et al., 2017).

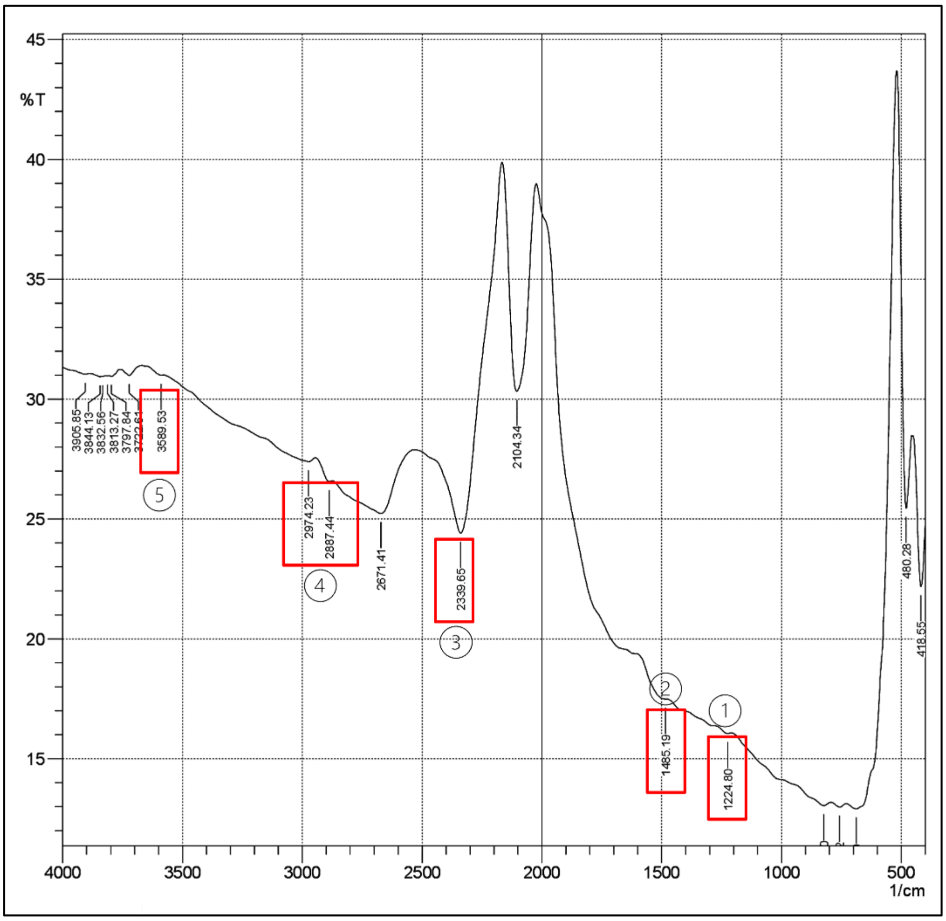

Figure 4.1: The FTIR analysis of pristine MWCNTs powder

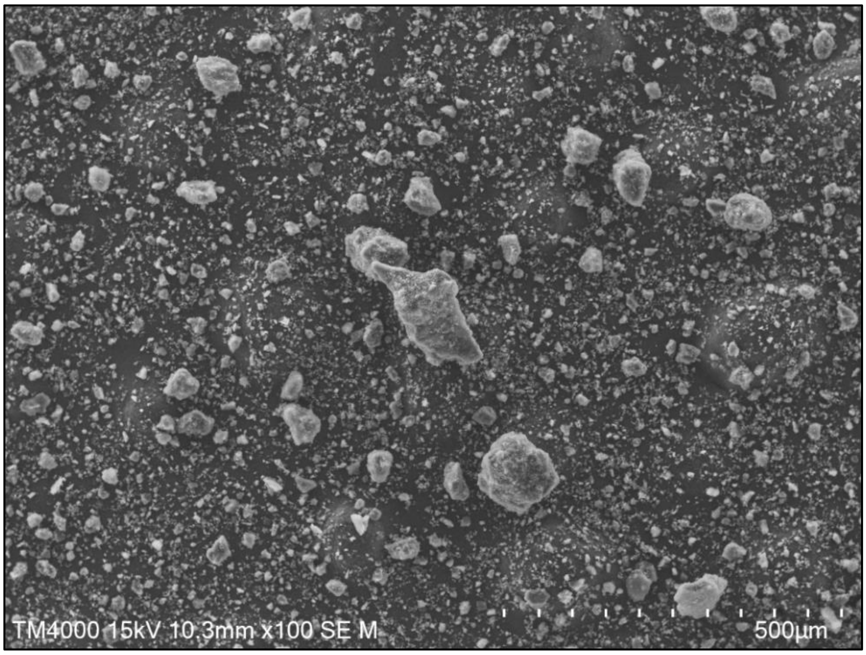

Figure 4.2: SEM of pristine MWCNTs powder at a magnfication of x100

4.2.2 Characterization of CF

The study used CF as the deposition fabric for the CNTs. Two characterisations are done onto the CF: the FTIR and SEM analysis. **Figure 4.3** illustrates the FTIR analysis of the CF, where from 4000 to 700 cm^{-1}, the pristine CF showed rapid decrement of the line (Kim et al., 2022). The peaks 2893.22 and 2831.50 cm^{-1}, found at 2800–3000 cm^{-1}, were ascribed to the **C–H** bond (Kim et al., 2016). The peaks existed at wavenumbers ranging from 500 to 1200 cm^{-1} were assigned to the fingerprint **C–H** band (Gravis et al., 2021). Overall, the CF does not show many functional groups as it is in pristine condition. **Figure 4.4** shows the SEM analysis for the CF. There was no significant groove observed on the surface of the CF. It had a smooth and clean surface (Kim et al., 2016).

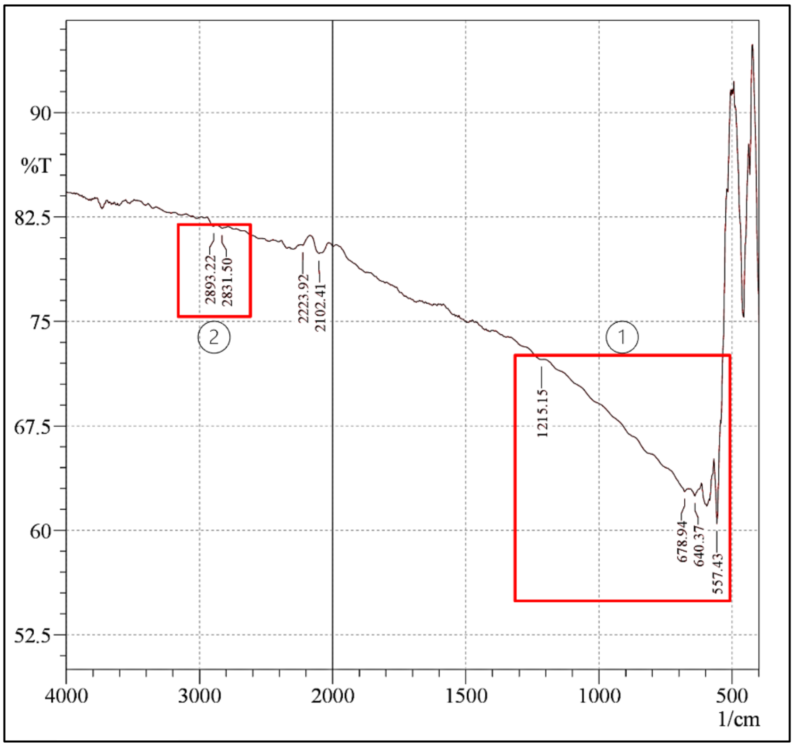

Figure 4.3: The FTIR analysis of pristine CF fabric

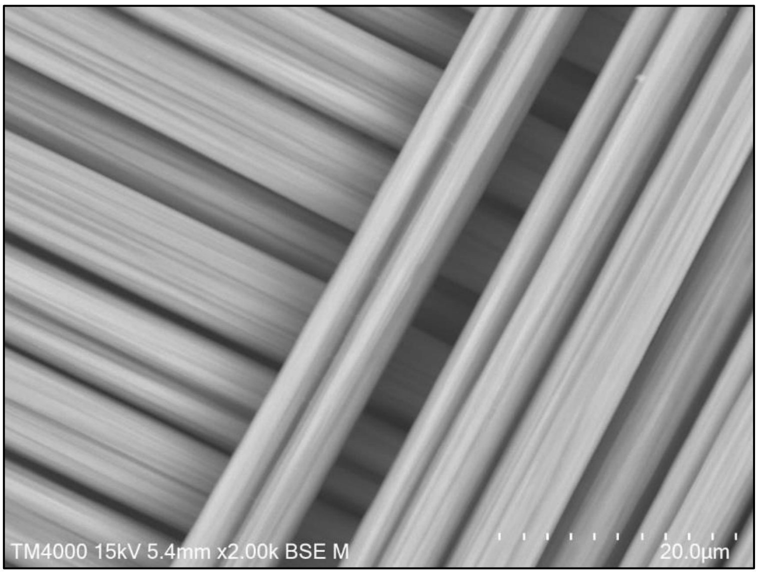

Figure 4.4: SEM of pristine CF fabric at a magnification of x2000

4.3 Optical Observation of the MWCNTs' dispersion in media

The stability of the MWCNTs in the suspension mediums was investigated, and as aforementioned in **Chapter 3**, this observation corresponded to the study's first objective. The observation was a helpful indicator of the quality of MWCNTs' dispersion in the solvent. When an unstable solvent was used, the CNTs tended to re–agglomerate into bundles and formed sedimentation. There would be less agglomeration and longer duration before sedimentation started to occur when the CNTs had high dispersion quality (Zakaria et al., 2020b). Fewer or smaller occurrences of the CNT bundles and longer dispersion time indicate higher quality of dispersion. The dispersion quality was evaluated through simple optical observation of the CNT bundles. However, this observation cannot deduce the dispersion's absolute quality. This approach was only helpful for comparative studies when identical conditions were used to prepare the samples (Do Amaral Montanheiroa et al., 2015). Additionally, qualitative information was obtained from this cheap and fast observation method (Wulan et al., 2018).

Figure 4.5 demonstrates the suspension stability of the MWCNTs in the suspension medium with respective ratios of water and methanol without the presence of applied voltage. Digital pictures of the sample bottles with dispersed MWCNTs were taken for two months, starting from before the dispersion process (Label: “Before”) until 60 days (Label: “Day 60”).

From the observation, several deductions can be made. Firstly, the hydrophobic nature of the pristine MWCNTs was proved as the MWCNTs directly agglomerated at the bottom of the sample bottle when placed in the medium before the sonication process (Ervina et al., 2019). CNTs were created as intractable black powder made of CNTs with a strong propensity to agglomerate and form bundles, ropes, or aggregates (Gharib et al., 2018). CNTs were materials that were hydrophobic with a small amount of hydrophilicity due to the oxygen-based functional groups that were dispersed randomly on their surface (e.g., hydroxyl, lactone, carboxylic, phenolic, etc.) (Youssry et al., 2020).

Secondly, at time zero (right after sonication; label in the figure: “After”), the MWCNTs were well dispersed in all the mediums. At a particular time and energy, the ultrasonicator process helped de-bundle the MWCNTs agglomeration due to the van der Waals reaction. The energy and sonication period greatly influenced the dispersion of MWCNTs because the sonication process could destroy the structure of the MWCNTs if the duration of the process were not optimized (Sabri et al., 2020). The bath sonication was a moderate technique that helped the MWCNTs dispersion without significantly reducing the nanotubes’ length (Youssry et al., 2020).

Thirdly, the observation also showed that in all the mediums, the MWCNTs were almost completely sedimented at the bottom of the sample bottles after 24 hours. This was caused by a lack of affinity (de León-Martínez et al., 2021). When CNTs were dispersed in solvents, it has a strong affinity to agglomerate. CNTs acted to reduce their surface energy by reducing interfacial contact with the solvent, which caused CNTs to form bundles and agglomerate. This was related to the affinity to agglomerate (Dumée et al., 2013). Additionally, the aggregation (bundling) of nanotubes and the buildup of bigger agglomerates were caused by the van der Waals attraction forces, which causes sedimentation to occur (Youssry et al., 2020).

Lastly, **Figure 4.5** also demonstrated that after thirty days, the sedimentation process had completed as the MWCNTs had fully sedimented at the bottom of the sample bottles for all the mediums. The lack of changes in the observation in Day 60 further verified this. This finding was consistent with the findings from another previous study (Ervina et al., 2019).

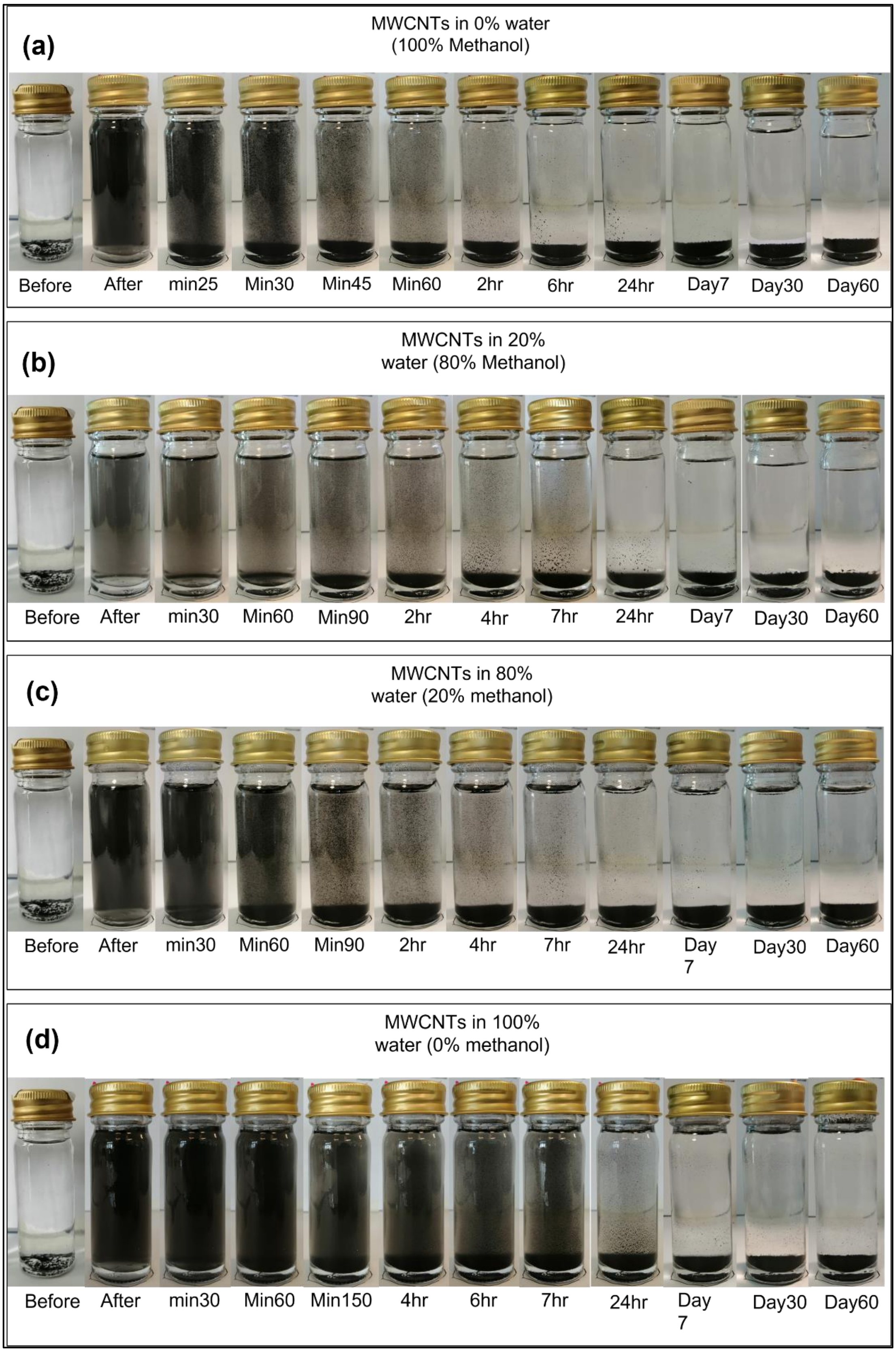

Figure 4.5: Optical observations of MWCNTs dispersed in suspension medium with different ratios of water-methanol

4.4 Characterization of samples

4.4.1 Functional group analysis

The composites' chemical functional groups were investigated using FTIR; the results are shown in **Figure 4.6**. FTIR is a structural spectroscopic method that uses the interaction of infra-red (IR) light with matter to define and identify the bonding structure of atoms. It determines the radiation frequencies a substance absorbs and causes vibrations in the molecules (Zakaria, Akil, et al., 2020). The chemical compositions and functional groups were examined using this analysis. Different bonds were stretched and bent by the IR radiation. The wavenumber and the variation in absorption intensity (abs) were two parameters that influenced the FTIR results (Bassiouny et al., 2021).

There are three wavenumber regions in which the infrared (IR) spectrums were divided, i.e., the far–IR spectrum (<400 cm^{-1}), the mid–IR spectrum (400–4000 cm^{-1}) and the near–IR spectrum region (4000–13000 cm^{-1}). However, the mid–IR spectrum is the most commonly used in conducting sample analysis. The spectra are further divided into four regions, namely the fingerprint region (600–1500 cm^{-1}), the double bond region (1500–2000 cm^{-1}), the triple bond region (2000–2500 cm^{-1}) and the single bond region (2500–4000 cm^{-1}) (Nandiyanto et al., 2019).

It showed in the figure that due to the graphitic carbon base structure of CNT and CF, all samples gave almost identical spectra. The hexagonal aromatic rings of sp2 hybridized carbon atoms made up the CNT and CF. The only aspect of each sample's FTIR spectra that varied was how broad and sharp the peaks were, which revealed the concentration or quantity of functional groups in the samples (Zakaria, Akil, et al., 2020).

Peaks from 900–670 cm^{-1} were attributed to aromatic **C–H** out–of–plane bend in pure CF/epoxy composite (Nandiyanto et al., 2019). This peak was further verified by the study of Cecen et al. (2008), where they ascribed the 828 cm^{-1} band to an aromatic ring bend out of plane. In addition, apart from pure CF/epoxy composite, the other samples exhibited peaks at around 2800 and continued till 2999 cm^{-1}. This peak corresponded to **C–H** stretching, indicating the presence of methanol impurity (Zhuang et al., 2020). The study used methanol as the organic solvent for the EPD process. Thus, it explained why methanol was present. Furthermore, the peaks in the 900-670 cm^{-1} and 2800-2999 cm^{-1} range demonstrated the presence of the epoxy functional group (Sarath Kumar et al., 2020).

The peak at around 2312 cm^{-1} in all the composites showed that carbon fiber and epoxy resin reacted strongly with one another. So bonding occurred between the OH (hydroxyl) groups and carbon fiber as epoxy molecules only had two reaction groups, namely the epoxide and the hydroxyl group (Cecen et al., 2008). It was essential that throughout composite processing, the CF and matrix had a sufficient amount of hydrogen bond and van der Waals forces in order to have strong interfacial adhesion (Salahuddin et al., 2021). Additionally, when MWCNTs were introduced in the CF/epoxy composite, a shift in peaks was observed from 3288 to 3313 cm^{-1}, which indicated **O–H** strong stretch. Therefore, the matrix and reinforcement have formed good interaction and dispersion (Sarath Kumar et al., 2020).

The finding also implied that the chemistry of the epoxy, which can affect the epoxy's curing, was not significantly altered by the presence of CNTs. The sample spectra exhibited a broad band at 3100-3700 cm^{-1} attributed to **O-H** stretching vibration. The existence of the OH group was proof that the epoxy had cured. The peak 1114.86 cm^{-1}

demonstrated the epoxy-derived aromatic ring **C-O** stretching. Since the aromatic ring does not change as the epoxy cures, this peak served as a reference peak.

Meanwhile, as mentioned above, the peak presented in the 900-670 cm^{-1} range showed the epoxide group. The extent of the epoxy curing reaction was directly related to the ratio of the area under the epoxide group peak to the area under the reference peak. This ratio was relatively small in all spectra, indicating that the epoxy curing occurred with a similar curing degree. If the epoxy were not cured, the sudden decrease in the force after the fracture in the bending test would not be feasible, thus affecting the outcomes of the tensile properties (Zhang et al., 2017).

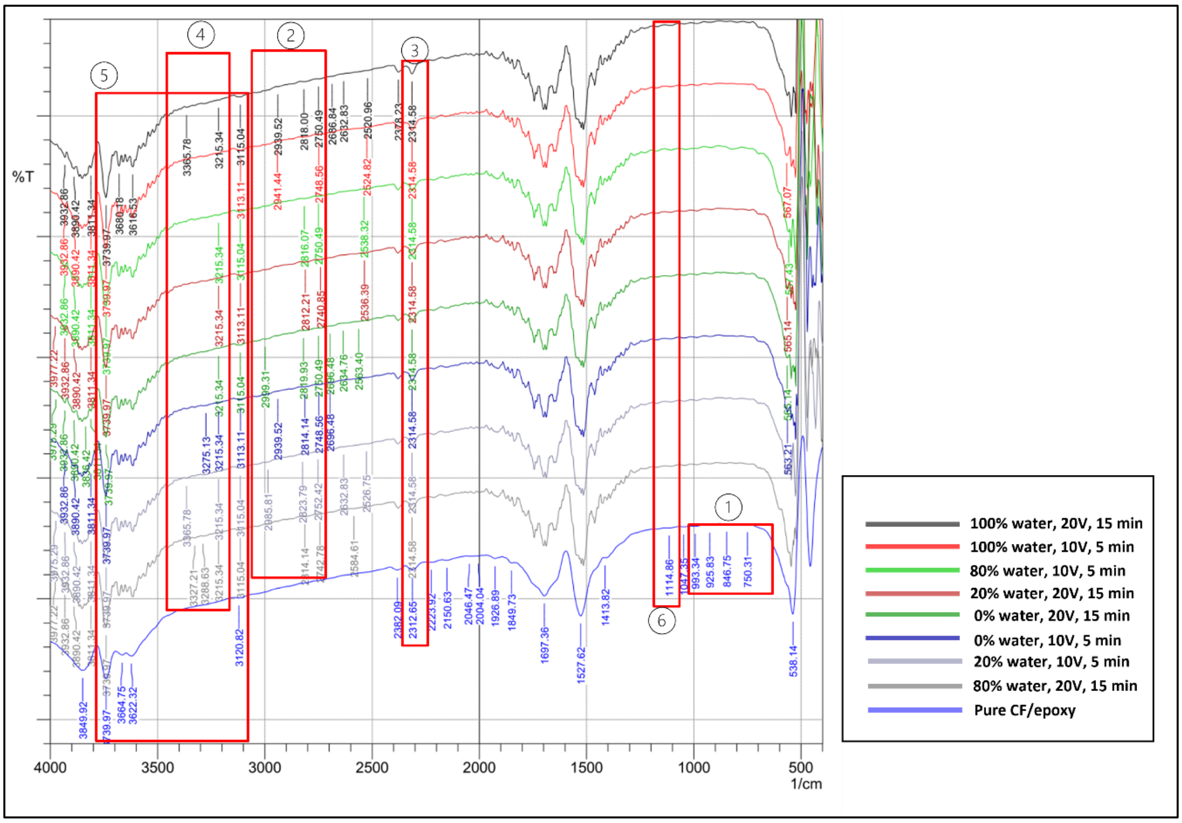

Figure 4.6: The FTIR analysis of composites

4.4.2 Surface morphological analysis

The interfacial bonding of the CF and hybrid MWCNT-CF with the epoxy matrix significantly determined their success as reinforcement in epoxy composite laminates. Due to this, morphological characterization was essential for determining the CF and hybrid MWCNT-CF's interfacial condition in the epoxy matrix (Zakaria, Akil, et al., 2020). The SEM analysis can deduce information regarding the level of fiber-matrix interactions. The analysis can also reveal extensive interfacial failure or interfacial adhesion. SEM can also demonstrate adhesive failure at the interface between CF and matrix (Cecen et al., 2008). Apart from that, the SEM images of the tensile tests fractured composites were taken to examine the behaviour of the reinforcement and matrix adhesion (bonding) and the existence of voids and fractures (Atmakuri et al., 2021). The surface morphology of neat CF/epoxy composite was shown in **Figure 4.7,** while **Figure 4.8** and **Figure 4.9** showed the surface of MWCNT-CF/epoxy composites in various ratios of suspension medium, with the conditions of deposition voltage and time at the highest values (**Figure 4.8**) and lowest values (**Figure 4.9**) of parameters.

All figures showed that the CFs remained attached to the epoxy matrix, indicating interfacial adhesion between the CF and epoxy. Though some voids could be seen in those images since no CFs were pulled out from the composites, the adhesion was deemed sufficient (dos Santos et al., 2021). The findings revealed a brittle fracture of the reinforcement and matrix materials. Strong interfacial bonds between the fiber and epoxy resin were to be held accountable for this (Atmakuri et al., 2021). It was asserted that there was a significant interaction between the CF and epoxy resin based on the findings of FTIR analysis (Cecen et al., 2008)

Figure 4.8 and **Figure 4.9** demonstrated that the EPD process successfully deposited the MWCNTs as the CFs were seen to be closely packed in the composite. However, the orientation of deposited MWCNTs was randomly distributed along the CF strips. The SEM images of the fracture surface proved that the MWCNTs deposition to epoxy laminated composites helped to improve the fiber-matrix delamination strength by enhancing the surrounding matrix's toughness. After the fracture, the CNT remained securely on the CF surface. This demonstrated that the interlocking between the CF and epoxy matrix was facilitated by the deposition of CNT on the CF surface. The neat CF/epoxy composite exhibited greater fiber breakage and fiber-matrix delamination than the CNT-based laminates. The presence of CNT reduced fiber degradation and damage to the fiber-matrix interphase. Additionally, CNT helped to boost the interfacial friction and limit the epoxy matrix's motion at the interface area (Bhowmik et al., 2022; Zakaria, Akil, et al., 2020).

The input parameters, i.e., the deposition voltage and time of the EPD process, also helped to improve adhesion between the matrix and reinforcement. Both **Figure 4.8** and **Figure 4.9** showed accumulations of MWCNTs, with composites in **Figure 4.8** demonstrating more accumulation owing to the high deposition voltage used during the EPD process. Excessive collection of similar charged electrons would occur when the direct electric field applied was high. This caused the MWCNTs to strongly repel one another due to the exact electrical charges, forcing them to relocate to the most stable position at the CF strips (Moaseri et al., 2016). In addition, the interfacial adhesion between the CF and epoxy was increased with the increment of the deposition time. The quantity of MWCNTs in the vertical fiber slowly increased, making it harder to pull out from the epoxy resin (Zhang et al., 2018). Thus, it can be deduced that the deposition voltage and time influenced the quantity of MWCNTs' deposition onto the CF, which helped improve the bonding of the matrix and reinforcements.

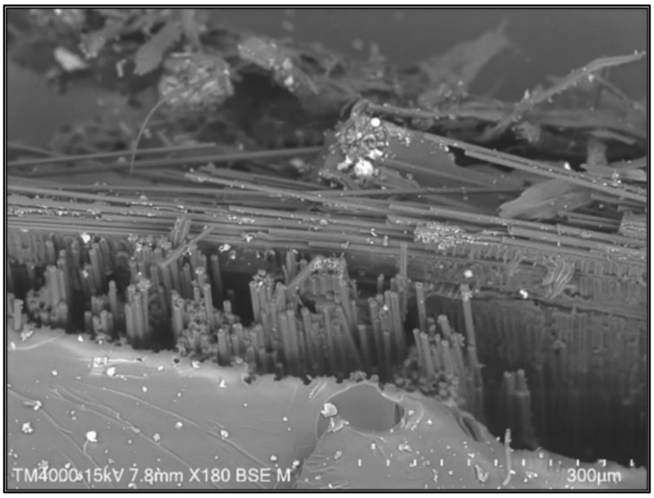

Figure 4.7: Surface morphology of pure CF/ epoxy composite

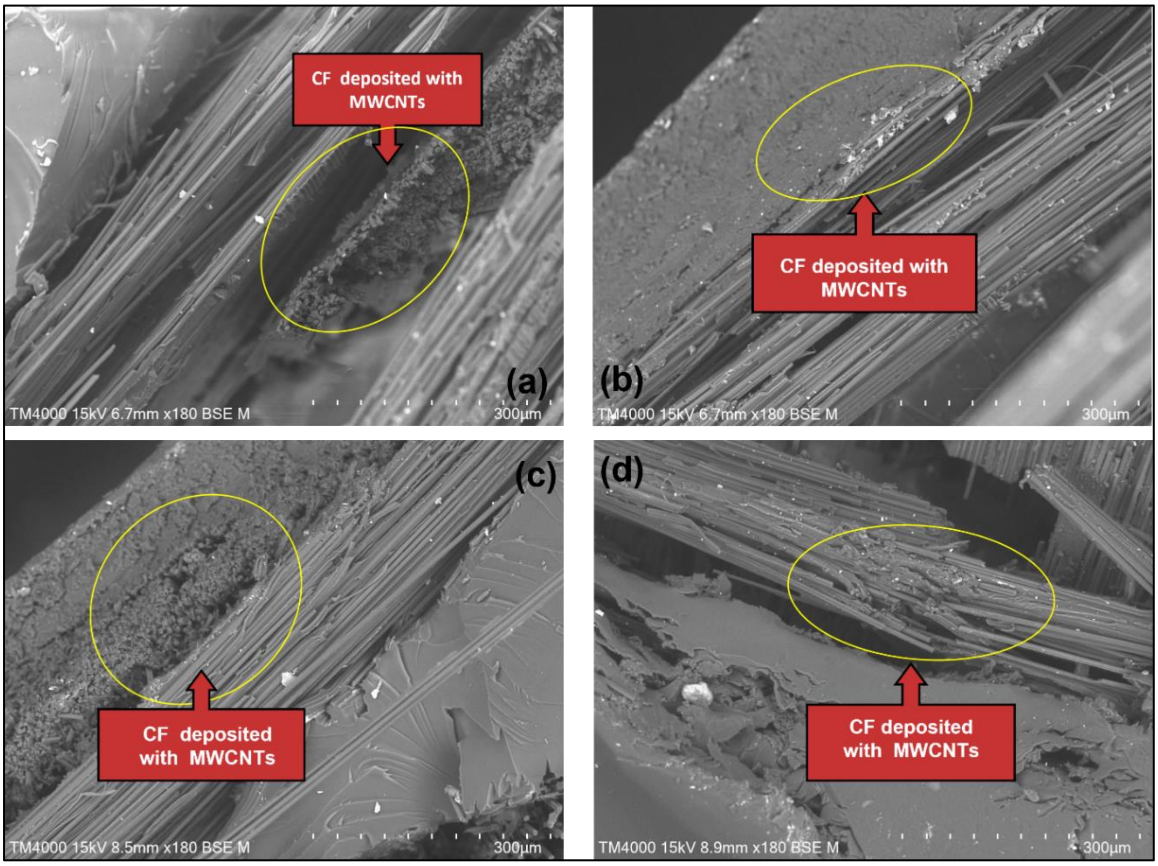

Figure 4.8: SEM images of CNT-CF/epoxy composites when deposition voltage: 20V, deposition time: 15 minutes: (a) 0% water, (b) 20% water, (c) 80% water, (d) 100% water

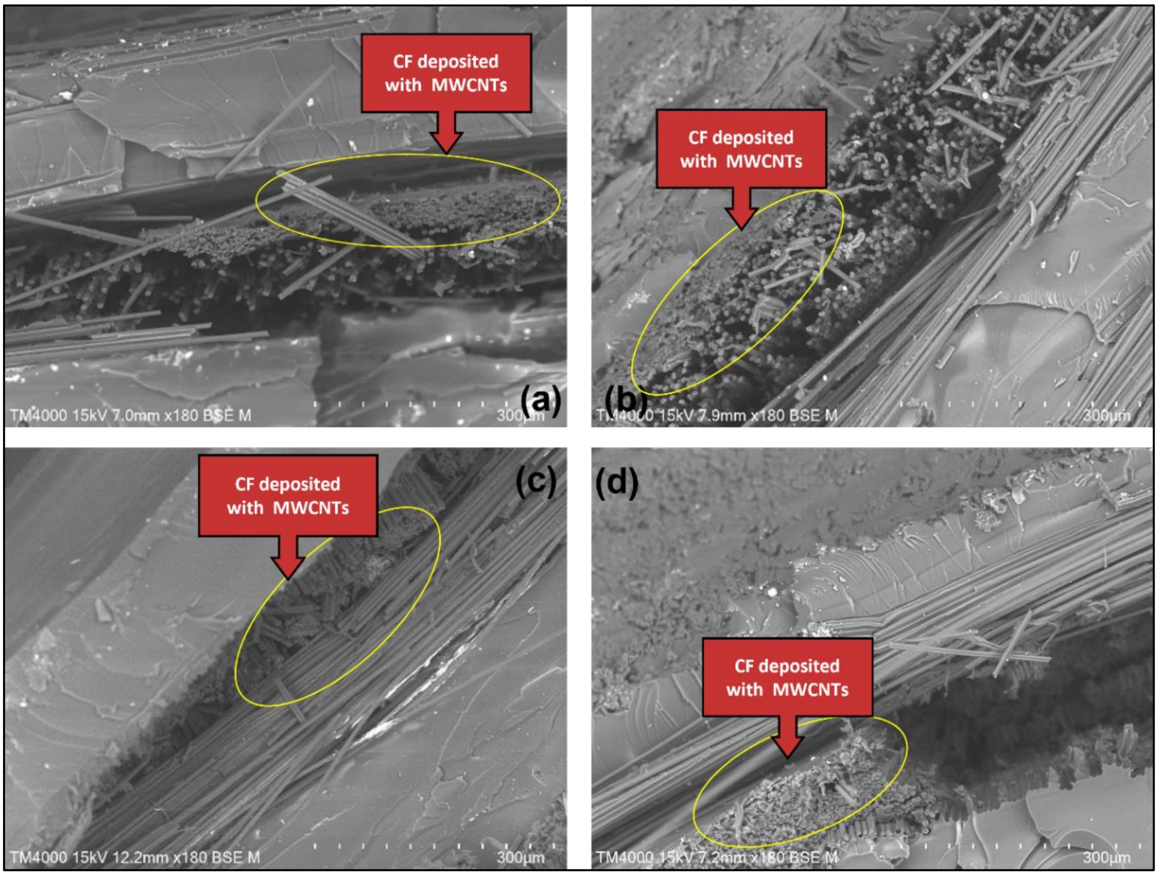

Figure 4.9: SEM images of CNT-CF/epoxy composites when deposition voltage: 10V, deposition time: 5 minutes: (a) 0% water, (b) 20% water, (c) 80% water, (d) 100% water

4.5 Tensile and statistical analysis of composites' properties

4.5.1 Tensile properties of MWCNT-CF/epoxy composites

The hybrids' applicability as polymeric matrices reinforcements was evaluated by studying the composites' mechanical properties. For example, the reinforcing effect of CF could be significantly improved when there was high compatibility and interaction between CF and the matrix. Furthermore, the interaction could be further enhanced with the addition of active nanomaterials such as MWCNT (Moaseri et al., 2016). The neat CF/Epoxy and MWCNT-CF/Epoxy laminated composites were tensile tested to determine the effect of the reinforcements on the tensile properties of the laminated composites, corresponding to the second objective of the study. **Table 4.1** shows the tensile properties of the neat CF/Epoxy laminated composite.

Meanwhile, **Table 4.2**, **Table 4.3**, **Table 4.4,** and **Table 4.5** showed the results of the tensile testing of the laminated composites, categorized according to their respective volume ratios used in the EPD process. For each table for the hybrid composites, variations in tensile properties were observed as the deposition voltage and time were varied under a constant volume ratio. The values of the tensile properties of the neat CF/Epoxy laminated composite were used to compare with the values of the tensile properties of the MWCNT-incorporated composites.

Table 4.2 (volume ratio of 100% water,0% methanol) and **Table 4.3** (volume ratio of 80% water, 20% methanol) demonstrated that when the composition of the suspension medium was made up of mostly water, the tensile strength of the composites showed enhancement as the deposition voltage increased. For instance, in **Table 4.2** and **Table 4.3**, composites with maximum voltage (20V) showed maximum improvement by 52.59% (**Table 4.2**, sample number 5) and 41.39% (**Table 4.3,** sample number 3), respectively. These results indicated that at 20V, the MWCNTs still had high solubility in water, which helped improve the dispersion of MWCNTs onto the CF. This finding was consistent with the previous study by Ervina et al (2019), which demonstrated that the MWCNTs' showed no agglomeration and precipitation at applied voltage 20V at various times (3,5,15, and 30 minutes). This would increase MWCNTs' deposition on the CF surface (Ervina et al., 2019).

Meanwhile, **Table 4.4** (volume ratio of 20% water, 80% methanol) and **Table 4.5** (volume ratio of 0% water, 100% methanol) demonstrated that when the composition of the medium mainly was methanol, low deposition time would produce composites with improved tensile strength. For example, from **Table 4.4** and **Table 4.5**, the composites with low deposition time showed improvement by 20.68% (**Table 4.4**, sample number 1) and 46.53% (**Table 4.5**, sample number 2), respectively. The suspension prepared using alcohol with low molecular weight, such as methanol, had a fast deposition rate due to its high dielectric constant and low viscosity. Thus, the nanoparticles would have higher mobility. The rate of EPD would decrease at longer EPD duration (Farrokhi-Rad, 2016).

Overall, most of the composites showed improvement in tensile strength with the introduction of MWCNTs as reinforcement. The matrix elongates as the tensile load increases, but the nanofiller (MWCNTs) resist the deformation. As a result, lower deformation occurs in the composite than in the neat polymer. Thus, higher tensile modulus and strength were obtained compared to the composite without any nanofiller, as the composites could sustain more loads (Tzetzis et al., 2017). The presence of MWCNTs helped the interface between the layers to have a good bond with one another, as illustrated in the SEM analysis (**Figure 4.8** and **Figure 4.9)** (Li et al., 2015). The interfacial behaviour of CF/epoxy was changed by introducing MWCNTs into the composite. The CF's non-polar and inert surface properties had caused weak interfacial adhesion between the woven CF and epoxy matrix. So, the total CF/matrix interfacial area was decreased with the deposition of the MWCNTs on the woven CF surface, and CNT/matrix interfacial area was increased instead. In addition, the stress transfer between CF and epoxy was improved due to the load-carrying capacity of CF with increased surface roughness. The twists and kinks created mechanical interlocks between the MWCNTs and the epoxy matrix in the CNTs structure. As a result, the tensile strength of the MWCNT-CF/epoxy was improved as MWCNTs had excellent mechanical properties (Zakaria et al., 2020a). However, since the improvement in Young's modulus was insufficient, it was indicated that the agglomeration and orientation of MWCNTs formed on the CF surface were not enough to raise the interfacial interaction

(Moaseri et al., 2016). Therefore, it was implied that the overall composite's Young's modulus was not affected by adding nanostructure onto the epoxy system, though it increased the tensile strength of composites (Leão et al., 2017).

Table 4.1: Tensile strength and Young's modulus of pure CF/epoxy composite

Sample	Tensile strength (N/mm^2)	Young Modulus (N/mm^2)
Pure CF/epoxy composite	5.062215	255.52

Table 4.2: Tensile strength and Young's modulus of MWCNT – CF/epoxy composites with different deposition voltage and time for 100% water,0% methanol (water is used as the basis of medium)

Sample	Factor 1 A: Volume %(w/w)	Factor 2 B: Voltage (V)	Factor 3 C: Time (min)	Response 1 Tensile strength (N/mm^2)	Response 2 Young Modulus (N/mm^2)
1	100% water, 0% methanol	20	15	7.61305	243.22
2		10	5	4.91122	226.02
3		15	10	6.99095	250.91
4		10	15	6.62504	279.9
5		20	5	7.72467	260.16

Table 4.3: Tensile strength and Young's modulus of MWCNT – CF/epoxy composites with different factors' values for 80% water, 20% methanol (water is used as the basis of medium)

Sample	Factor 1 A: Volume %(w/w)	Factor 2 B: Voltage (V)	Factor 3 C: Time (min)	Response 1 Tensile strength (N/mm^2)	Response 2 Young Modulus (N/mm^2)
1	80% water, 20% methanol	10	5	5.13248	271.98
2		10	15	2.15553	218.42
3		20	15	7.1577	229.22
4		15	10	7.00801	251.08
5		20	5	6.94222	266.59

Table 4.4: Tensile strength and Young's modulus of MWCNT – CF/epoxy composites with different factors' values for 20% water, 80% methanol (water is used as the basis of medium)

Sample	Factor 1 A: Volume %(w/w)	Factor 2 B: Voltage (V)	Factor 3 C: Time (min)	Response 1 Tensile strength (N/mm^2)	Response 2 Young Modulus (N/mm^2)
1	20% water, 80% methanol	20	5	6.10913	240.39
2		15	10	4.04905	273.44
3		10	15	4.72418	223.92
4		20	15	3.96751	216.10
5		10	5	4.19924	263.34

Table 4.5: Tensile strength and Young's modulus of MWCNT – CF/epoxy composites with different factors' values for 0% water, 100% methanol (water is used as the basis of medium)

Sample	Factor 1 A: Volume %(w/w)	Factor 2 B: Voltage (V)	Factor 3 C: Time (min)	Response 1 Tensile strength (N/mm^2)	Response 2 Young Modulus (N/mm^2)
1	0% water, 100% methanol	10	15	5.19014	229.48
2		15	10	7.41783	241.61
3		10	5	4.07182	265.58
4		20	5	4.47299	249.36

4.5.2 The Analysis of Variance (ANOVA)

The analysis of variance (ANOVA), which was in full cubic model, for the tensile properties of the experimental design, i.e., first DoE (0% water, 100% methanol and 100% water,0% methanol) and second DoE (20% water, 80% methanol and 80% water, 20% methanol) were given in **Table 4.6, 4.8, 4.10** and **4.12**. However, since CCD does not contain enough run to support the full cubic model, the model would always be aliased even though it had better performance (Hashim et al., 2015; Ocholi et al., 2018). Hence, modifications were to be done to the cubic model, where non-influential interaction terms were removed (Bahmani et al., 2021). Step-by-step methods were used for the model reduction, starting from the most insignificant term (Rajewski & Dobrzyńska-Inger, 2021). The modified or reduced models were given in **Tables 4.7, 4.9, 4.11** and **4.13**.

For the tensile strength of the first DoE (0% water, 100% methanol and 100% water,0% methanol), the full cubic model (**Table 4.6**) demonstrated an insignificant model, with a p-value of 0.1078 and an F-value of 3.71. The regression model was statistically significant when the F-value was large, and the p-value was small ($p < 0.05$) (Zhou et al., 2020). There was also a low amount of significant model terms obtained in the analysis. However, the reduced cubic model (**Table 4.7**) was significant because of its p-value of 0.0155, less than the chosen significant level of α=0.05. This value indicates that the null hypothesis was rejected as the p-value was below the alpha value. The model terms B, A^2, C^2, A^2B and A^2C were identified as significant model terms with values of p lower than 0.05, implying that adding these terms to the model would cause a significant effect (Madondo et al., 2022). The model term B (voltage) was more significant compared to the other input variables (A: volume ratio and C: time)., indicating that it has a more significant influence on the tensile strength of the composite for this DoE. However, for the interaction effects, the combination of model terms A and C with others was shown to be significant (Qiu et al., 2014). The lack-of-fit of 0.843 showed by the reduced model indicated that relative to the pure error, the lack-of-fit was insignificant. As model fitting was desired, the non-significant lack-of-fit was good (Konneh et al., 2014).

Table 4.8 and **Table 4.9** showed the full and reduced cubic ANOVA models, respectively, for Young's modulus of the first DoE. Both models showed insignificant p-value. However, compared to the full cubic model (p-value 0.5471), the reduced model showed improvement with a p-value of 0.1363. Thus, compared to the full cubic model, there was only a 13.63% possibility that the reduced model did not significantly affect the response. Additionally, the number of significant model terms also increased. B^2, C^2 and ABC were the significant model terms for the reduced analysis. These model terms showed that the interaction between the variables would affect Young's modulus of composites for this DoE. The interaction was proved by the large F-values of those model terms indicating influences of the variables on the response (Bahmani et al., 2021). Despite being insignificant, the lack-of-fit showed that the model was fitted well as it was non-significant with a value of 0.9559 (Uche et al., 2022).

Meanwhile, the full and reduced cubic ANOVA model of tensile strength for the second DoE (20% water, 80% methanol and 80% water, 20% methanol) were shown in **Table 4.10** and **Table 4.11**, respectively. Even though both the full and reduced model showed significant p-value, the reduced model demonstrated a smaller p-value (0.0087) than the full cubic model, implying this model was more significant (Talib et al., 2017). The null hypothesis can be rejected because the p-value was lower than the alpha value of 0.05. The model terms A, C, AB, B^2, C^2 and ABC were significant as they were less than 0.05. For the tensile strength of this DoE, model terms A and C influences the response more than B. However, the interaction between the three variables (model terms ABC) affected the response as it has a significant p-value of 0.0225. This implied that both linear coefficients (A and C) and quadratic terms (B^2 and C^2) influenced the tensile strength (Isopencu et al., 2019). Moreover, the insignificant lack-of-fit value of 0.1553 verified a good fit of the model (Rahman & Dzulkarnain, 2021).

Apart from that, **Table 4.12** and **Table 4.13** demonstrated the full cubic and reduced linear ANOVA model of Young's modulus for the second DoE, respectively. Initially, the full cubic model was insignificant, with a p-value of 0.5098. However, after the modification, the model was reduced to a highly significant linear model with a p-value of

0.0013. This value indicated that the null hypothesis could be rejected. Only one significant term was retained after the reduction: C (time). This reduction of the model term occurred as the initial statistically non-significant terms were removed from the analysis (Rajewski & Dobrzyńska-Inger, 2021). The reduced linear model showed an insignificant lack-of-fit value of 0.9277, implying that the model fit well (Madondo et al., 2022).

Typically, insignificant terms were removed from the model. However, apart from the reduced linear ANOVA model of Young's modulus from the second DoE, the other reduced cubic models retained some insignificant terms to support the hierarchy. Depending on the suitability, non-significant terms can either be removed from or remain in the model. Nonetheless, retaining the non-significant terms has become usual practice; thus, insignificant terms are not necessarily removed from the model (Talib et al., 2017).

Table 4.6: ANOVA for tensile strength analysis for the full cubic model of first DoE (0% water, 100% methanol and 100% water,0% methanol)

Source	**Sum of Squares**	**df**	**Mean Square**	**F-value**	**p-value**	
Model	33.83	13	2.60	3.71	0.1078	not significant
A-Volume	0.0911	1	0.0911	0.1298	0.7369	
B-Voltage	4.78	1	4.78	6.81	0.0595	
C-Time	1.69	1	1.69	2.40	0.1962	
AB	0.4970	1	0.4970	0.7079	0.4475	
AC	0.3361	1	0.3361	0.4787	0.5271	
BC	0.0841	1	0.0841	0.1198	0.7467	
A^2	9.93	1	9.93	14.14	0.0198	
B^2	0.1287	1	0.1287	0.1834	0.6905	
C^2	6.72	1	6.72	9.57	0.0365	
ABC	1.00	1	1.00	1.43	0.2983	
A^2B	8.08	1	8.08	11.50	0.0275	
A^2C	3.71	1	3.71	5.29	0.0829	
AB^2	1.70	1	1.70	2.42	0.1945	
AC^2	0.0000	0				
B^2C	0.0000	0				
BC^2	0.0000	0				

Table 4.6 continued

A^3	0.0000	0				
B^3	0.0000	0				
C^3	0.0000	0				
Residual	2.81	4	0.7021			
Lack of Fit	0.0187	1	0.0187	0.0201	0.8962	not significant
Pure Error	2.79	3	0.9298			
Cor Total	36.64	17				

Table 4.7: ANOVA for tensile strength for the reduced cubic model of first DoE (0% water, 100% methanol and 100% water,0% methanol)

Source	**Sum of Squares**	**df**	**Mean Square**	**F-value**	**p-value**	
Model	32.62	10	3.26	5.68	0.0155	significant
A-volume	0.0911	1	0.0911	0.1586	0.7024	
B-voltage	4.78	1	4.78	8.31	0.0235	
C-time	1.69	1	1.69	2.93	0.1305	
AB	0.4970	1	0.4970	0.8648	0.3833	
AC	0.3361	1	0.3361	0.5848	0.4694	
A^2	12.30	1	12.30	21.40	0.0024	
C^2	6.95	1	6.95	12.09	0.0103	
A^2B	8.08	1	8.08	14.05	0.0072	
A^2C	3.71	1	3.71	6.46	0.0385	
AC^2	1.70	1	1.70	2.96	0.1290	
Residual	4.02	7	0.5747			
Lack of Fit	1.23	4	0.3083	0.3315	0.8430	not significant
Pure Error	2.79	3	0.9298			
Cor Total	36.64	17				

Table 4.8: ANOVA for Young's modulus analysis for the full cubic model of first DoE (0% water, 100% methanol and 100% water,0% methanol)

Source	**Sum of Squares**	**df**	**Mean Square**	**F-value**	**p-value**	
Model	4358.41	13	335.26	1.02	0.5471	not significant
A-Volume	27.49	1	27.49	0.0838	0.7866	
B-Voltage	726.23	1	726.23	2.22	0.2109	
C-Time	195.73	1	195.73	0.5970	0.4828	
AB	13.86	1	13.86	0.0423	0.8471	

Table 4.8 continued

AC	694.01	1	694.01	2.12	0.2194	
BC	388.09	1	388.09	1.18	0.3378	
A^2	154.49	1	154.49	0.4712	0.5302	
B^2	595.99	1	595.99	1.82	0.2489	
C^2	1038.54	1	1038.54	3.17	0.1497	
ABC	1518.56	1	1518.56	4.63	0.0977	
A^2B	275.73	1	275.73	0.8410	0.4110	
A^2C	0.3725	1	0.3725	0.0011	0.9747	
AB^2	15.60	1	15.60	0.0476	0.8380	
AC^2	0.0000	0				
B^2C	0.0000	0				
BC^2	0.0000	0				
A^3	0.0000	0				
B^3	0.0000	0				
C^3	0.0000	0				
Residual	1311.42	4	327.86			
Lack of Fit	56.40	1	56.40	0.1348	0.7379	not significant
Pure Error	1255.02	3	418.34			
Cor Total	5669.84	17				

Table 4.9: ANOVA for Young's modulus analysis for the reduced cubic model of first DoE (0% water, 100% methanol and 100% water,0% methanol)

Source	**Sum of Squares**	**df**	**Mean Square**	**F-value**	**p-value**	
Model	4053.68	9	450.41	2.23	0.1363	not significant
A-volume	46.31	1	46.31	0.2292	0.6449	
B-voltage	42.97	1	42.97	0.2127	0.6569	
C-time	3.77	1	3.77	0.0187	0.8947	
AB	11.28	1	11.28	0.0558	0.8191	
AC	607.96	1	607.96	3.01	0.1210	
BC	123.40	1	123.40	0.6108	0.4570	
B^2	1499.83	1	1499.83	7.42	0.0261	
C^2	1095.57	1	1095.57	5.42	0.0483	
ABC	1518.56	1	1518.56	7.52	0.0254	
Residual	1616.15	8	202.02			
Lack of Fit	361.13	5	72.23	0.1726	0.9559	not significant
Pure Error	1255.02	3	418.34			
Cor Total	5669.84	17				

Table 4.10: ANOVA for tensile strength analysis for the full cubic model of second DoE (20% water, 80% methanol and 80% water,20% methanol)

Source	Sum of Squares	df	Mean Square	F-value	p-value	
Model	42.99	13	3.31	9.57	0.0211	significant
A-Volume	4.38	1	4.38	12.67	0.0236	
B-Voltage	0.0011	1	0.0011	0.0033	0.9571	
C-Time	2.92	1	2.92	8.44	0.0439	
AB	4.00	1	4.00	11.58	0.0272	
AC	0.1638	1	0.1638	0.4740	0.5290	
BC	0.0346	1	0.0346	0.1000	0.7676	
A^2	0.6847	1	0.6847	1.98	0.2320	
B^2	4.04	1	4.04	11.70	0.0268	
C^2	11.34	1	11.34	32.81	0.0046	
ABC	4.29	1	4.29	12.42	0.0244	
A^2B	1.66	1	1.66	4.81	0.0933	
A^2C	0.6978	1	0.6978	2.02	0.2284	
AB^2	2.23	1	2.23	6.46	0.0639	
AC^2	0.0000	0				
B^2C	0.0000	0				
BC^2	0.0000	0				
A^3	0.0000	0				
B^3	0.0000	0				
C^3	0.0000	0				
Residual	1.38	4	0.3456			
Lack of Fit	0.7948	1	0.7948	4.06	0.1374	not significant
Pure Error	0.5877	3	0.1959			
Cor Total	44.37	17				

Table 4.11: ANOVA for tensile strength analysis for the reduced cubic model of second DoE (20% water, 80% methanol and 80% water,20% methanol)

Source	Sum of Squares	df	Mean Square	F-value	p-value	
Model	41.61	11	3.78	8.21	0.0087	significant
A-Volume	4.38	1	4.38	9.50	0.0216	
B-Voltage	0.0011	1	0.0011	0.0025	0.9621	
C-Time	4.62	1	4.62	10.01	0.0195	
AB	4.00	1	4.00	8.69	0.0257	
AC	0.1638	1	0.1638	0.3555	0.5728	
BC	0.0346	1	0.0346	0.0750	0.7934	
B^2	3.37	1	3.37	7.32	0.0353	
C^2	15.33	1	15.33	33.27	0.0012	
ABC	4.29	1	4.29	9.31	0.0225	

Table 4.11 continued

AC^2	2.23	1	2.23	4.84	0.0700	
BC^2	1.66	1	1.66	3.61	0.1062	
Residual	2.76	6	0.4608			
Lack of Fit	2.18	3	0.7258	3.70	0.1553	not significant
Pure Error	0.5877	3	0.1959			
Cor Total	44.37	17				

Table 4.12: ANOVA for Young's modulus analysis for the full cubic model of second DoE (20% water, 80% methanol and 80% water,20% methanol)

Source	**Sum of Squares**	**df**	**Mean Square**	**F-value**	**p-value**	
Model	8823.74	13	678.75	1.11	0.5098	not significant
A-Volume	249.98	1	249.98	0.4077	0.5579	
B-Voltage	262.66	1	262.66	0.4284	0.5485	
C-Time	3135.53	1	3135.53	5.11	0.0866	
AB	163.62	1	163.62	0.2669	0.6327	
AC	92.62	1	92.62	0.1510	0.7173	
BC	122.62	1	122.62	0.2000	0.6779	
A^2	691.19	1	691.19	1.13	0.3482	
B^2	90.80	1	90.80	0.1481	0.7200	
C^2	988.90	1	988.90	1.61	0.2730	
ABC	0.1405	1	0.1405	0.0002	0.9886	
A^2B	109.96	1	109.96	0.1793	0.6937	
A^2C	657.07	1	657.07	1.07	0.3591	
AB^2	434.94	1	434.94	0.7093	0.4471	
AC^2	0.0000	0				
B^2C	0.0000	0				
BC^2	0.0000	0				
A^3	0.0000	0				
B^3	0.0000	0				
C^3	0.0000	0				
Residual	2452.67	4	613.17			
Lack of Fit	101.03	1	101.03	0.1289	0.7434	not significant
Pure Error	2351.64	3	783.88			
Cor Total	11276.41	17				

Table 4.13: ANOVA for Young's modulus analysis for the reduced linear model of second DoE (20% water, 80% methanol and 80% water,20% methanol)

Source	Sum of Squares	df	Mean Square	F-value	p-value	
Model	5467.65	1	5467.65	15.06	0.0013	significant
C-Time	5467.65	1	5467.65	15.06	0.0013	
Residual	5808.77	16	363.05			
Lack of Fit	3457.12	13	265.93	0.3393	0.9277	not significant
Pure Error	2351.64	3	783.88			
Cor Total	11276.41	17				

4.5.3 Fit statistics of the reduced ANOVA models

Table 4.14 lists the fit statistics of the reduced models for both experimental designs. R^2 (square of correlation coefficient) was also used as a tool to assess how well the proposed model fits the experimental data besides the probability value (p-value) (Yahaya et al., 2016). The R^2 coefficient indicated the proportion of change of the response variable (y) in the region of y that the regression model defined. This coefficient ranges from 0 to 1 (Madondo et al., 2022). From the table, it can be seen that apart from Young's modulus of the second DoE (reduced linear model), the other model, which was the reduced cubic model, had a reasonably high R^2 value ($R^2 > 0.7$), implying that only less than 30% of the data that cannot be described by the created models (Uche et al., 2022). However, a low R^2 value does not always indicate the absence of a relationship. Instead, the dependent variable's variability cannot be well explained by the explanatory variable alone (Ijomah & Azubuike, 2019). The p-value can still be statistically significant even if the R^2 value is small, as proven by the p-value of the reduced linear model (Young's modulus of second DoE). Even if it might not account for a huge portion of the variation in the response, the relationship between the predictors and response may be of considerable importance (Colton & Bower, 2002).

The Adjusted R^2 was used to represent a rectified value for R^2 after excluding unnecessary model terms. Insignificant terms had been contained in the model in case of massive differences between the R^2 and Adjusted R^2 (Breig & Luti, 2021; Nur Sabreena et al., 2016). Only one reduced model showed significant differences between the two values, i.e., Young's modulus of the first DoE. The other three reduced models demonstrated minor differences between the two values. Thus, for these three reduced models, the possibility that the inclusion of insignificant terms in the model was said to be invalid (Lessoued et al., 2017).

The Adjusted and Predicted R2 discrepancy was used to assess the model's suitability and fitness further. For there to be a good agreement between those values, the difference must be within 20% (0.2) of one another (Elganidi et al., 2022; Uche et al., 2022). It can be seen from the table that only the reduced linear model had differences between the Adjusted and Predicted R^2 values lesser than 0.2, indicating that the variable of response was predictably acceptable (Adedeji et al., 2022). Meanwhile, for the other three reduced cubic models, the differences were greater than 0.2, which may indicate a significant block effect or issues with the models or data (Rajewski & Dobrzyńska-Inger, 2021).

Additionally, the low Predicted R^2 value suggests that the model might not be able to accurately anticipate how the process would behave (Joe et al., 2015). Meanwhile, the negative predicted R^2 value indicated that the overall mean could be a better response predictor (Yunardi et al., 2011).

The Adequate Precision (AP), which includes the anticipated value at the design points and the average prediction error, measured the signal-to-noise ratio (Behera et al., 2018). Ratios greater than 4 indicate the signal's precision in finding model design space. For this study, the AP values obtained in all reduced models were more than 4, meaning that there was enough signal present and the model has excellent predictive accuracy (Darvishmotevalli et al., 2019). Meanwhile, the coefficient of variation (CV) refers to the standard deviation to mean ratios. CV also demonstrated great accuracy and reliability of the experimental results. The model was reproducible when the value of CV was less than 10 (Adedeji et al., 2022; Isam et al., 2019). In this study, 2 CV values were less than 10, while the others were slightly more than 10.

The error variation was computed using the predicted residual error sum of squares (PRESS). This statistical coefficient specifically demonstrated how the regression model cannot account for the variance in the process variable of a model equation. The model is typically the best fit when the PRESS value is very low (Madondo et al., 2022). In addition, a small value of PRESS was desired because it is used to determine the ability of the model to be used for future prediction (Breig & Luti, 2021). In this study, only two PRESS values demonstrated relatively low numbers (22.67 and 112.31), while the other two were relatively high.

Table 4.14: Fit statistics of the responses for reduced models (First and Second DoE)

Statistical Parameter	**First DoE (0% water, 100% methanol and 100% water,0% methanol)**		**Second DoE 20% water, 80% methanol and 80% water,20% methanol)**	
Response (Type of reduced model)	**Tensile strength (Cubic)**	**Young's modulus (Cubic)**	**Tensile strength (Cubic)**	**Young's modulus (Linear)**
R^2	0.8902.	0.7150	0.9377	0.4849
Adjusted R^2	0.7334	0.3943	0.8234	0.4527
Predicted R^2	0.3814	-0.9398	-1.5312	0.3722
Adequate Precision (AP)	8.5696	5.1972	10.2571	7.3633
Coefficient of Variation (CV)	13.44	5.72	12.19	7.80
PRESS	22.67	10998.26	112.31	7079.89

4.5.4 Mathematical model of reduced models for composites' tensile strength and Young's modulus (in terms of coded factors)

Second-order polynomial equations were used in presenting the effect of variables on the responses. For the study, three variables were used (k=3); hence additional cubic interaction effects were included in the polynomial equation as shown in **Equation 4.1** below:

$$Y = \beta_0 + \beta_1 x_1 + \beta_2 x_2 + \beta_3 x_3 + \beta_{11} x_1^2 + \beta_{22} x_2^2 + \beta_{33} x_3^2 + \beta_{12} x_1 x_2 + \beta_{13} x_1 x_3 + \beta_{23} x_2 x_3 + \beta_{112} x_1^2 x_2 + \beta_{113} x_1^2 x_3 + \beta_{122} x_1 x_2^2 + \beta_{123} x_1 x_2 x_3$$

Equation 4.1

where the equations' coefficients were represented by β_0 (the intercept), β_1, β_2, β_3 (the main linear), β_{11}, β_{22}, β_{33} (quadratic), β_{112}, β_{113}, β_{122}, β_{123} (cubic) and β_{12}, β_{13}, β_{23}, β_{112}, β_{113}, β_{122}, β_{123} (the interaction). The experimental data were found to be well fit by implementing the reduced model (Talib et al., 2017). The mathematical model represents the factors of volume ratio (in %), voltage, and time as A, B, and C, respectively.

The following equations were the final mathematical models (in terms of coded factors) for the first DoE (0% water, 100% methanol and 100% water,0% methanol):

Tensile strength, TS:

$$TS_{Reduced} = 5.37 – 0.2134A – 1.55B – 1.9181C + 0.2492AB – 0.2050AC + 1.99A^2 – 1.5C^2 + 2.25A^2B + 1.52A^2C + 1.03AC^2$$

Equation 4.2

Young Modulus, E:

$$E_{Reduced} = 246.74 + 2.15A - 2.07B + 0.6140C - 1.19AB + 8.72AC - 3.93BC + 22B^2 - 18.80C^2 - 13.78ABC$$

Equation 4.3

Similarly, the following equations were the final mathematical models for tensile strength and Young's modulus (in terms of coded factors) for the second DoE (20% water, 80% methanol and 80% water, 20% methanol):

Tensile strength, TS:

$$TS_{Reduced} = 6.32 + 1.48A - 0.0238B - 0.6793C + 0.7073AB - 0.1431AC + 0.0657BC + 1.04B^2 - 2.22C^2 + 0.7324ABC - 1.18AC^2 + 1.02BC^2$$

Equation 4.4

Young Modulus, E:

$$E_{Reduced} = 244.43 - 23.38C$$

Equation 4.5

For any given level of each factor, predictions about the response can be made using these equations in terms of coded factors. By default, the components' high and low levels correspondingly were coded as +1 and –1. By comparing the factor coefficients, the coded equations assisted in determining the relative importance of the factors (Derawi, 2016). Apart from that, the prediction of a parameter's positive or negative impact could be obtained through the analysis of the polynomial equations in terms of coded factors. When a parameter's coefficient was positive, the response increased as the parameter value improved, and when it was negative, the response decreased as the parameter value reduced. Furthermore, the significance of the corresponding factor was demonstrated by the absolute value of a coefficient (Mueanmas, 2022).

4.6 Graphical analysis of composites' mechanical properties

4.6.1 Response surface graphical analysis of tensile properties

Contour plots (two-dimensional (2D) plots) and surface response plots (three-dimensional (3D) graphical representation) were used to visualise the regression model. Evaluating the nature of the response at various factor levels was easier with the help of the graphical plots (Nair et al., 2014). **Figures 4.10, 4.11,** and **4.12** showed the effects of the interaction between the volume ratio of the suspension medium and the deposition voltage on their respective response under the fixed conditions of 10 minutes of deposition time. Meanwhile, for **Figure 4.13**, the deposition voltage was fixed at 15V, while the interaction between the deposition time and volume ratios of the suspension medium onto Young's modulus of the second DoE. This was because, for that linear model, time was the only term that showed a significant effect on the response; hence the effect of time was investigated.

Figure 4.10 and **Figure 4.11** correspond to the first experimental design (0% water, 100% methanol and 100% water,0% methanol). From **Figure 4.10(a)**, it can be seen that at the conditions of 0% water and 100% water, the maximum tensile strength (7.9 N/mm^2) was obtained at the highest voltage (20V). This finding was further verified by the contour plot in **Figure 4.10(b)**, where the red colour indicated the maximum interaction between the two variables. The significant model term B (voltage) proved that voltage influenced the tensile properties. However, the contour plot shown indicates that the maximum point would be outside the region of the experiment (Nair et al., 2014). This was true as the experimental maximum tensile strength value was 7.725 N/mm2, slightly lower than the ideal maximum value obtained from the 3D graph.

Additionally, for **Figure 4.11(a)**, initially, at a volume ratio of 0% water, Young's modulus was approximately 249 N/mm^2. However, the maximum Young's modulus was obtained as the volume ratio increased to 100% water. **Figure 4.11(b)** validates this point where the colour becomes warmer at a higher volume ratio and voltage.

Meanwhile, **Figure 4.12** and **Figure 4.13** correspond to the second experimental design (20% water, 80% methanol and 80% water, 20% methanol). **Figure 4.12(a)** showed that at constant deposition time (10 minutes), the tensile strength increased as the volume ratio and voltage increased (approaching volume ratio of 80% water, 20% methanol and voltage of 20V, respectively). The maximum tensile strength was obtained at the suspension medium's high deposition voltage and volume ratio. The significant model terms AB proved the combined effect of the volume ratios and voltage and was validated by the contour plot illustrated in **Figure 4.12(b)**.

As for **Figure 4.13**, as the reduced model was linear, with time as the significant variable, the deposition voltage was fixed instead of time at 15V. **Figure 4.13(a)** demonstrated that the plateau shape shown by the surface plot indicates that the volume ratio had no significant interaction with Young's modulus (Nazeri Abdul Rahman et al., 2023). The reduced linear model showed that the only significant variable was C (time), which verified the plateau shape. The maximum value of Young's modulus was obtained at a deposition time of approximately 5 minutes. When the time increased beyond 5 minutes, Young's modulus value would be reduced. This data implied that the deposition time and Young's modulus were inversely proportional to one another, as Young's modulus would decrease as time increased. The contour plot illustrated in **Figure 4.13(b)** confirmed this relationship with the colour becomes cooler as time increased.

For all the contour plots of the reduced models, the red area was known as the high response value area that showed the optimum points for factors. The prediction value for the response optimization would be extracted from the plot in the high response area (Abdullah et al., 2020). Thus, it can be deduced that the response surface graphical analysis and the numerical optimization had correlation with one another.

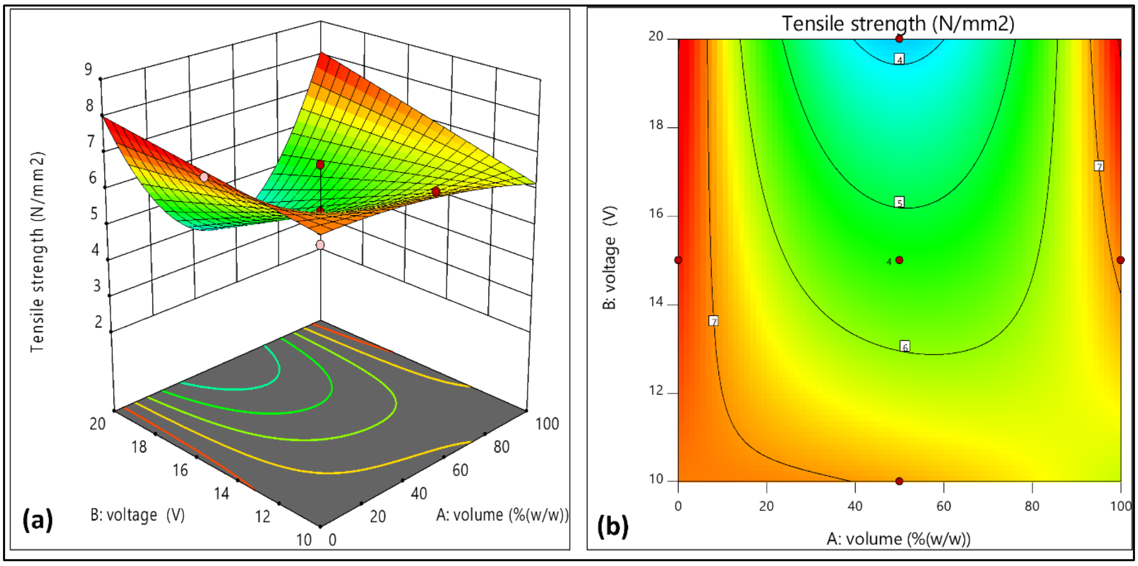

Figure 4.10: The response surface plot of tensile strength for first DoE (0% water, 100% methanol and 100% water,0% methanol) (a) surface response (b) contour plot

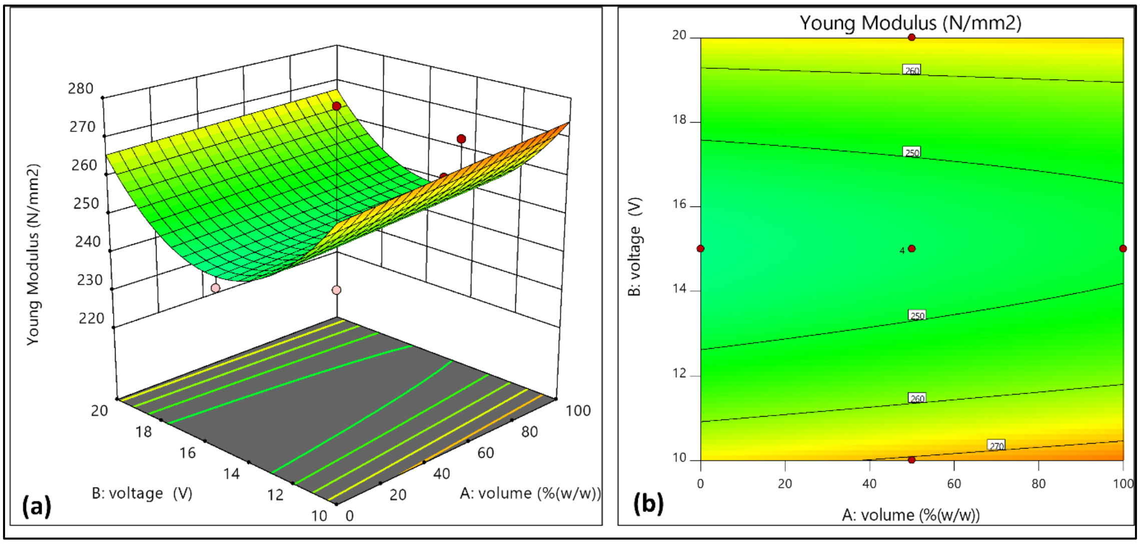

Figure 4.11: The response surface plot of Young's modulus for first DoE (0% water, 100% methanol and 100% water,0% methanol) (a) surface response (b) contour plot

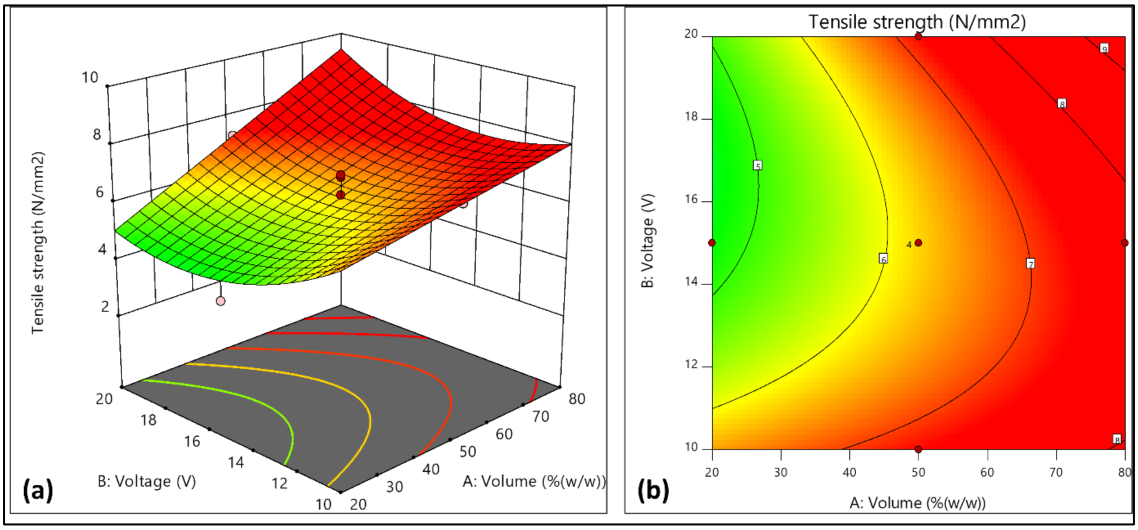

Figure 4.12: The response surface plot of tensile strength for second DoE (20% water, 80% methanol and 80% water, 20% methanol) (a) surface response (b) contour plot

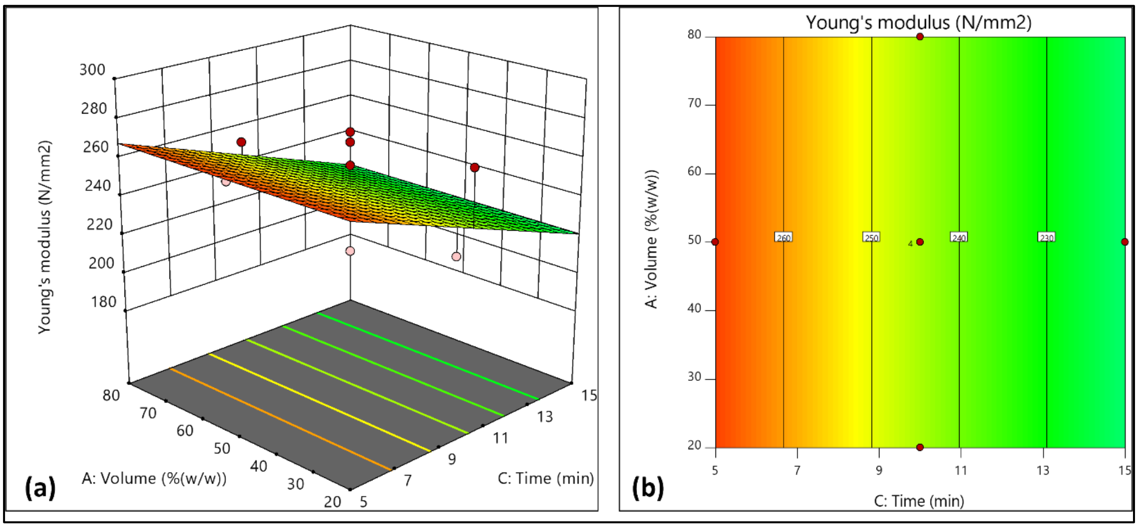

Figure 4.13: The response surface plot of Young's modulus for second DoE (20% water, 80% methanol and 80% water, 20% methanol) (a) surface response (b) contour plot

4.6.2 Validation, verification, and normality test of the modified or reduced models

Diagnostic plots such as the predicted versus actual values, normal probability of residuals, and residual versus predicted values plots were used to evaluate the goodness-of-fit of the proposed model (Ghelich et al., 2019). These model fit errors were also known as the residual plot, as the distribution of residuals was checked using the plots (Abdullah et al., 2020; Ocholi et al., 2018). In statistics, the diagnostic tests are crucial to ensure that the assumptions of ANOVA test are met; regression model validation must be done (Madondo et al., 2022). The graphs would also assess the transformation choice and evaluate the model fit (Abdullah et al., 2020).

Table 4.15 and **Table 4.16** showed the experimental and predicted results of the response, i.e., tensile strength and Young's modulus. The residual values indicate the deviation between the actual and predicted values. When the experimental errors are random, the residuals are expected to be in a normal distribution (Liu et al., 2018).

The responses of prediction versus actual plots of the modified or reduced model were demonstrated in **Figure 4.14** and **Figure 4.15**. From **Figure 4.14(a & b)** and **Figure 4.15 (a)**, the experimental range studied were expressed adequately as the modified model had realistic fitting parameter. The measured results for individual experimental runs were shown by the actual values and the evaluation of the independent variables in the regression model represented by the predicted value (Muhamad et al., 2020). The centre of the graph was where most of the data was plotted, forming a perpendicular line at a 45-degree angle. These outcomes demonstrated the model's capacity for accurate response prediction (Abdullah et al., 2020). Whereas in **Figure 4.15(b)**, the scattering of the values was quite random, but most of the residual points were still close to the straight line. Except for a few points, the residuals in **Figure 4.15(b)** were thought to follow the normal distribution.

Meanwhile, **Figure 4.16** and **Figure 4.17** demonstrated the normal probability plot of residuals, where the standard deviations between the actual (experimental) and the predicted values were calculated using internally studentized residuals. Since the residuals were nearly straight-lined, the residuals followed a normal distribution, suggesting that deviations from normality had no significant impact on the outcomes. Appropriate normal error terms were also obtained (Abdullah et al., 2020; Welu et al., 2020).

In addition, **Figure 4.18** and **Figure 4.19** illustrate the plot for residual versus predicted values. These plots were used for confirmation or identification of the constant variance assumption (Vaka et al., 2020). These were models that were used to validate the significance outlier of the points. Outlier points were any points that were placed outside the red lines. All the points for all the figures lie well within the red lines, showing that the models were fitted well (Radhwan et al., 2019). Apart from that, the model's accuracy and predictability were shown by the random distribution of residuals inside the red bounds of the graph (Rahman & Dzulkarnain, 2021). The proposed models were acceptable and did not violate the assumptions of independence or constant variance, as those plots showed a random scatter of data (Krishnan et al., 2020). The well-fitting of the models was further verified by the non-significant lack-of-fit values demonstrated in ANOVA.

Table 4.15: Experimental and predicted results of the output response for experimental design of first DoE (0% water, 100% methanol and 100% water,0% methanol)

Run	Volume ratio	Voltage	Time	Tensile strength (TS)			Young's modulus (E)		
				Actual	Pred	Residual	Actual	Pred	Residual
1	0	20	15	6.60	6.31	0.2900	252.66	248.64	4.02
2	100	20	5	7.72	7.23	0.4950	260.16	257.20	2.96
3	0	10	15	5.19	5.40	-0.2126	229.48	230.72	-1.24
4	50	10	10	7.05	6.91	0.1406	277.86	270.81	7.05
5	50	20	10	3.96	3.82	0.1406	252.71	266.66	-13.95
6	0	10	5	4.07	3.78	0.2900	265.58	266.62	-1.04
7	100	10	5	4.91	5.33	-0.4177	226.02	228.31	-2.29
8	100	15	10	6.99	7.15	-0.1547	250.91	248.89	2.02
9	50	15	10	6.70	5.37	1.34	243.25	246.74	-3.49
10	0	20	5	4.47	4.69	-0.2126	249.36	245.15	4.21
11	50	15	15	2.80	2.95	-0.1547	225.49	228.55	-3.06
12	0	15	10	7.42	7.57	-0.1547	241.61	244.59	-2.98
13	50	15	5	4.63	4.79	-0.1547	223.49	227.33	-3.84
14	50	15	10	4.48	5.37	-0.8839	230.14	246.74	-16.60
15	100	10	15	6.63	6.13	0.4950	279.90	282.38	-2.48
16	50	15	10	4.90	5.37	-0.4673	243.50	246.74	-3.24
17	100	20	15	7.61	8.03	-0.4177	243.22	240.45	2.77
18	50	15	10	5.41	5.37	0.0421	277.92	246.74	31.18

Table 4.16: Experimental and predicted results of the output response for experimental design of second DoE (20% water, 80% methanol and 80% water,20% methanol)

Run	Volume ratio	Voltage	Time	Tensile strength (TS)			Young's modulus (E)		
				Actual	Pred	Residual	Actual	Pred	Residual
1	50	10	10	7.28	7.29	-0.0157	251.96	244.43	7.53
2	20	20	5	6.11	6.24	-0.1282	240.39	267.82	-27.43
3	50	15	10	6.92	6.23	0.6904	211.87	244.43	-32.56
4	20	15	10	4.05	4.75	-0.6967	273.44	244.43	29.01
5	20	10	15	4.72	4.59	0.1360	223.92	221.05	2.87
6	80	10	5	5.13	5.26	-0.1282	271.98	267.82	4.16
7	20	20	15	3.97	3.83	0.1360	216.10	221.05	-4.95
8	50	15	5	5.19	4.68	0.5126	266.78	267.82	-1.04
9	50	15	10	6.30	6.23	0.0767	268.28	244.43	23.85
10	50	20	10	7.23	7.24	-0.0157	229.04	244.43	-15.39
11	80	10	15	2.16	2.02	0.1360	218.42	221.05	-2.63
12	20	10	5	4.20	4.33	-0.1282	263.34	267.82	-4.48
13	50	15	10	7.00	6.23	0.7740	256.43	244.43	12.00
14	80	20	15	7.16	7.02	0.1360	229.22	221.05	8.17
15	80	15	10	7.01	7.70	-0.6967	251.08	244.43	6.65
16	80	20	5	6.94	7.07	-0.1282	266.59	267.82	-1.23
17	50	15	15	2.78	3.32	-0.5440	187.59	221.05	-33.46
18	50	15	10	6.11	6.23	-0.1164	273.39	244.43	28.96

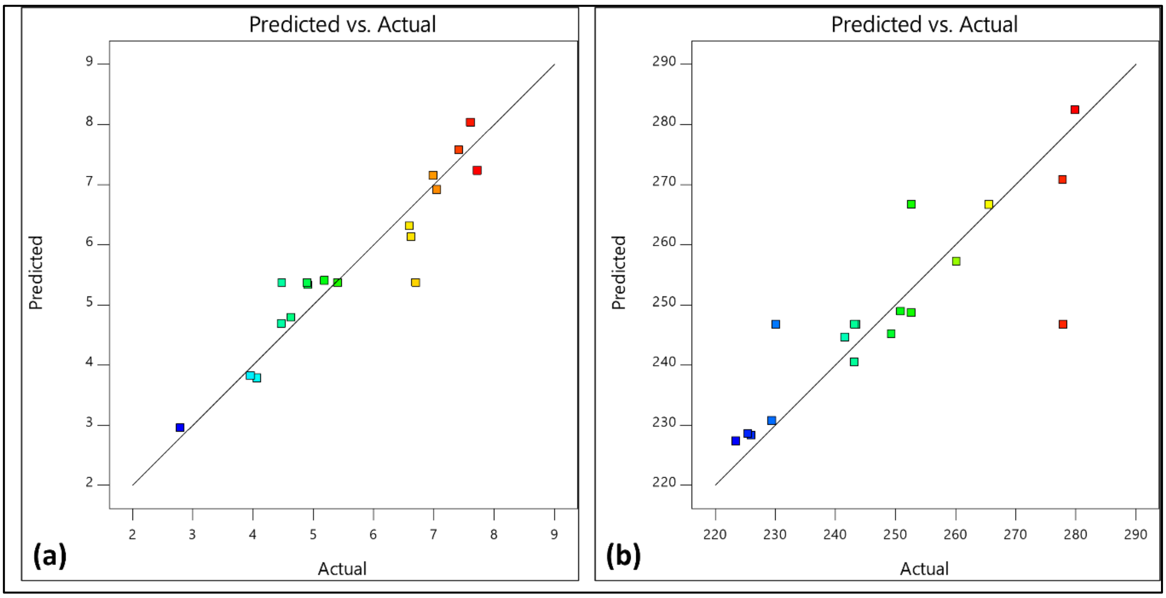

Figure 4.14: Prediction versus actual graph for first DoE (0% water, 100% methanol and 100% water,0% methanol) (a) Tensile strength, (b) Young's modulus

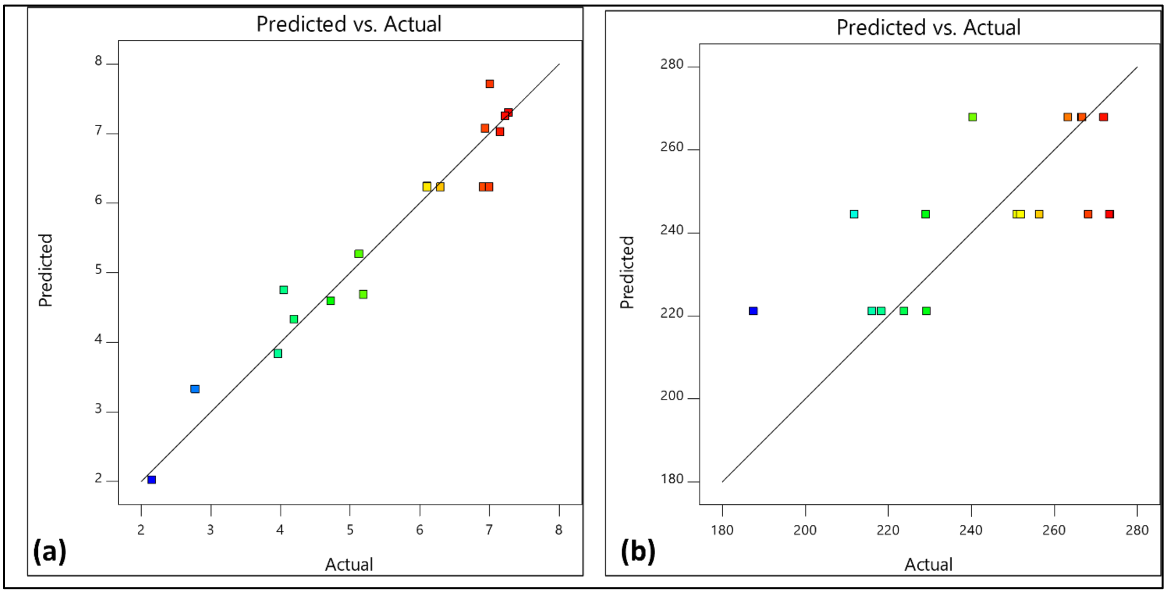

Figure 4.15: Prediction versus actual graph for second DoE (20% water, 80% methanol and 80% water, 20% methanol) (a) Tensile strength, (b) Young's modulus

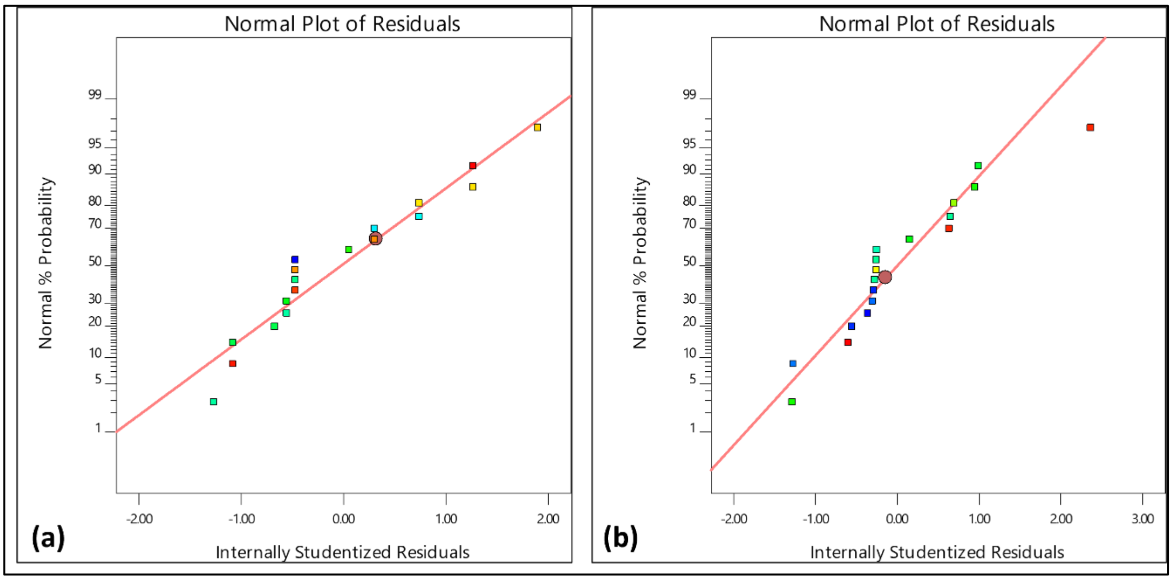

Figure 4.16: The normal plot of residual for first DoE (0% water, 100% methanol and 100% water,0% methanol) (a) Tensile strength, (b) Young's modulus

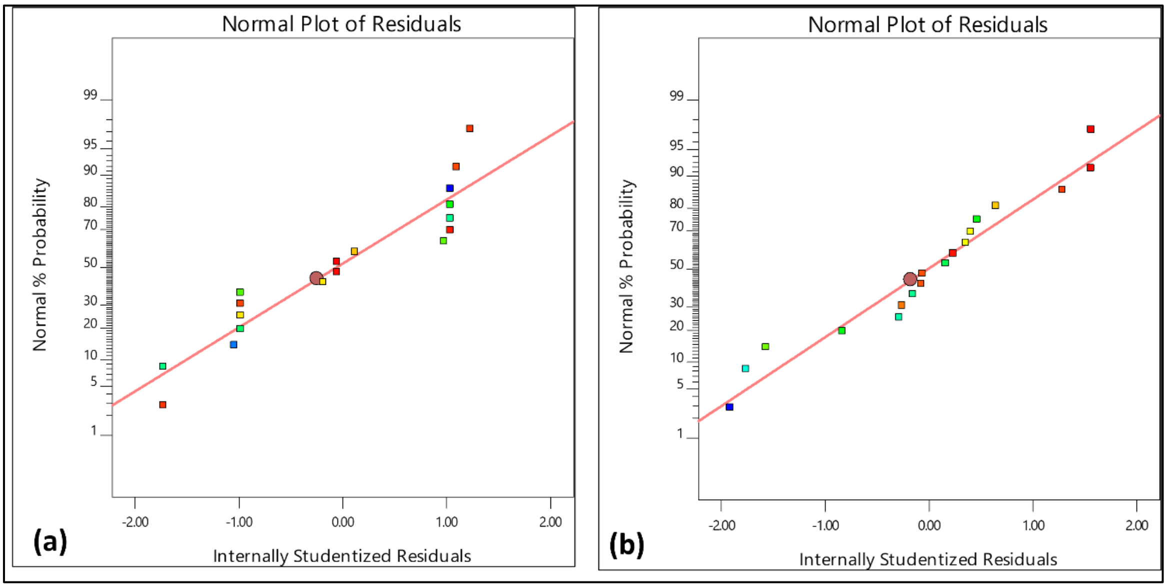

Figure 4.17: The normal plot of residual for second DoE (20% water, 80% methanol and 80% water, 20% methanol) (a) Tensile strength, (b) Young's modulus

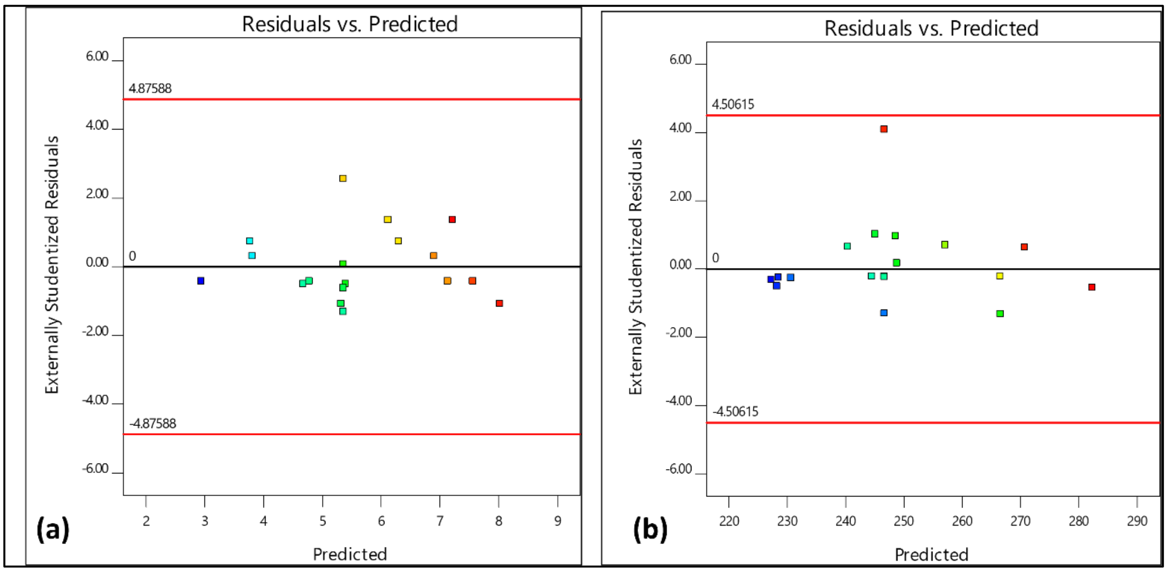

Figure 4.18: The residual versus predicted graph for first DoE (0% water, 100% methanol and 100% water,0% methanol) (a) Tensile strength, (b) Young's modulus

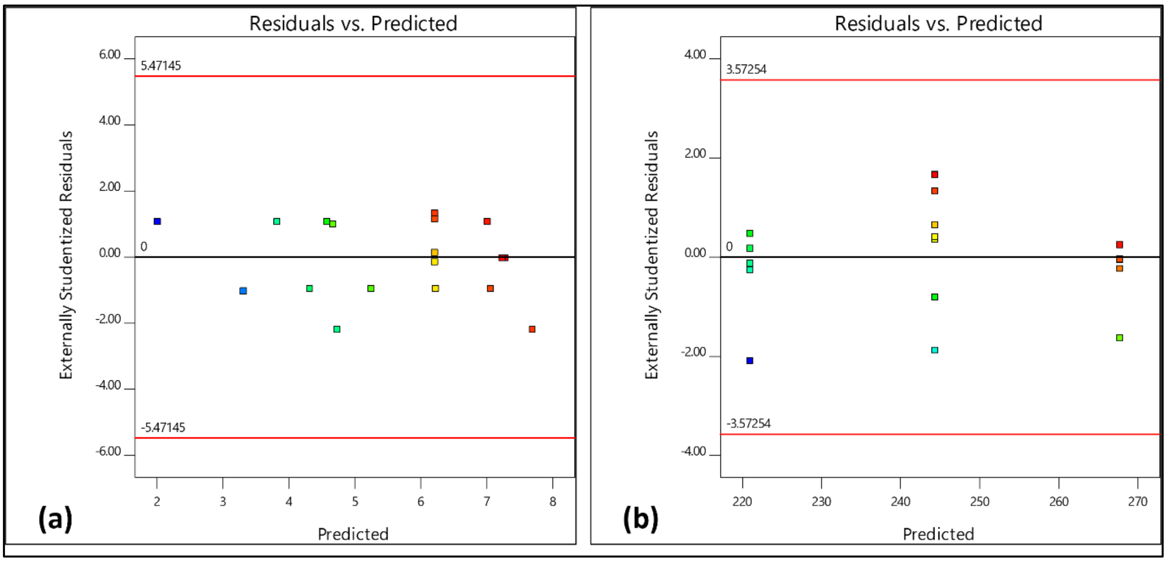

Figure 4.19: The residual versus predicted graph for second DoE (20% water, 80% methanol and 80% water, 20% methanol) (a) Tensile strength, (b) Young's modulus

4.6.3 Determination of optimum condition using numerical optimization and desirability function

Process optimization was the final goal of RSM. Using the developed models, simulation and optimization were done (Jokić et al., 2016). The desired responses and the corresponding ideal conditions can be obtained by analysing the response surface. When all the parameters simultaneously satisfy the desired criteria, the optimal conditions for multiple responses can be achieved. The ideal conditions can be represented graphically by overlaying the contours of the regression models' response surfaces. The regions that meet the criteria of optimization were shown in graphical optimization along with the feasible response values' area in the factor space. However, when the independent variables were more than three, obtaining the conditions that can satisfy all the responses at once would be hard. Hence, multicriteria methodology, such as the desirability function, can be used (Nair et al., 2014).

An overall desirability function was created by the combination of the goals (Sadhukhan et al., 2016). Desirability is a tool used to describe how closely the best solution proposed adhered to the response's goals. When the desirability value is 1, it denotes the ideal scenario, whereas a desirability value of 0 implies the need to discard the response (Rohajatien et al., 2023).

In order to optimize the responses of the study, numerical optimization ramps were utilized to determine the ideal input variables (volume ratios of suspension medium, deposition voltage and time). The target values of the three input variables for the study were selected as the "in-range" option while the target of the responses was set to "maximize". A stationary point that was considered to be the ideal response was the optimal point for each variable (Rohajatien et al., 2023). Additionally, the goal priority was set to three pluses (+++)

because all goals in the investigation were equally important (Madondo et al., 2022). **Table 4.17** and **Table 4.18** listed the constraints for optimising the EPD process, while **Figure 4.20** and **Figure 4.21** illustrated the results of the numerical optimization results in the form of ramp graphs, which corresponded to the third objective of the study.

The optimum conditions for the first DoE (0% water, 100% methanol and 100% water,0% methanol) for the reduced model in numerical optimization were volume ratios of suspension medium = 99.99% water, voltage = 20V, and time = 8.88 minutes, with the desirability of 0.894. Under these optimal operating conditions, tensile strength of 7.983 N/mm^2 and Young's modulus of 268.558 N/mm^2 were predicted, as shown in **Table 4.17** and **Figure 4.20**. The finding in the response surface graphical analysis validated the ideal maximum condition of the responses.

For the second DoE (20% water, 80% methanol and 80% water, 20% methanol), the numerical optimization of the reduced models were volume ratios of suspension medium = 79.99% water, voltage = 20V, and time = 5.22 minutes. The maximum tensile strength and Young's modulus obtained under these optimum conditions were 7.2766 N/mm^2 and 266.778 N/mm^2, respectively, were shown in **Table 4.18** and **Figure 4.21**. The desirability for the optimization was 0.96, which was very close to 1. These findings were also analogous to the response surface analysis data.

Overall, both desirability values indicated that the formulation was desirable to fulfil the responses' objective, as the desirability value was close to one (Mohmad Noor et al., 2020).

Table 4.17: Constraint for optimization for experimental design of first DoE (0% water, 100% methanol and 100% water,0% methanol)

Constraints	Conditions	Lower limit	Upper limit	Solution	Importance
Volume ratio, % (w/w)	In range	0	100	99.99	3
Voltage (V)	In range	10	20	20	3
Time (min)	In range	5	15	8.88	3
Tensile strength	Maximize	2.79761	7.72467	7.98289	3
Young's modulus	Maximize	223.49	279.9	268.558	3

Table 4.18: Constraint for optimization for experimental design of second DoE (20% water, 80% methanol and 80% water,20% methanol)

Constraints	Conditions	Lower limit	Upper limit	Solution	Importance
Volume ratio, % (w/w)	In range	20	80	79.999	3
Voltage (V)	In range	10	20	20	3
Time (min)	In range	5	15	5.22	3
Tensile strength	Maximize	2.15553	7.27661	7.27661	3
Young's modulus	Maximize	187.59	273.44	266.778	3

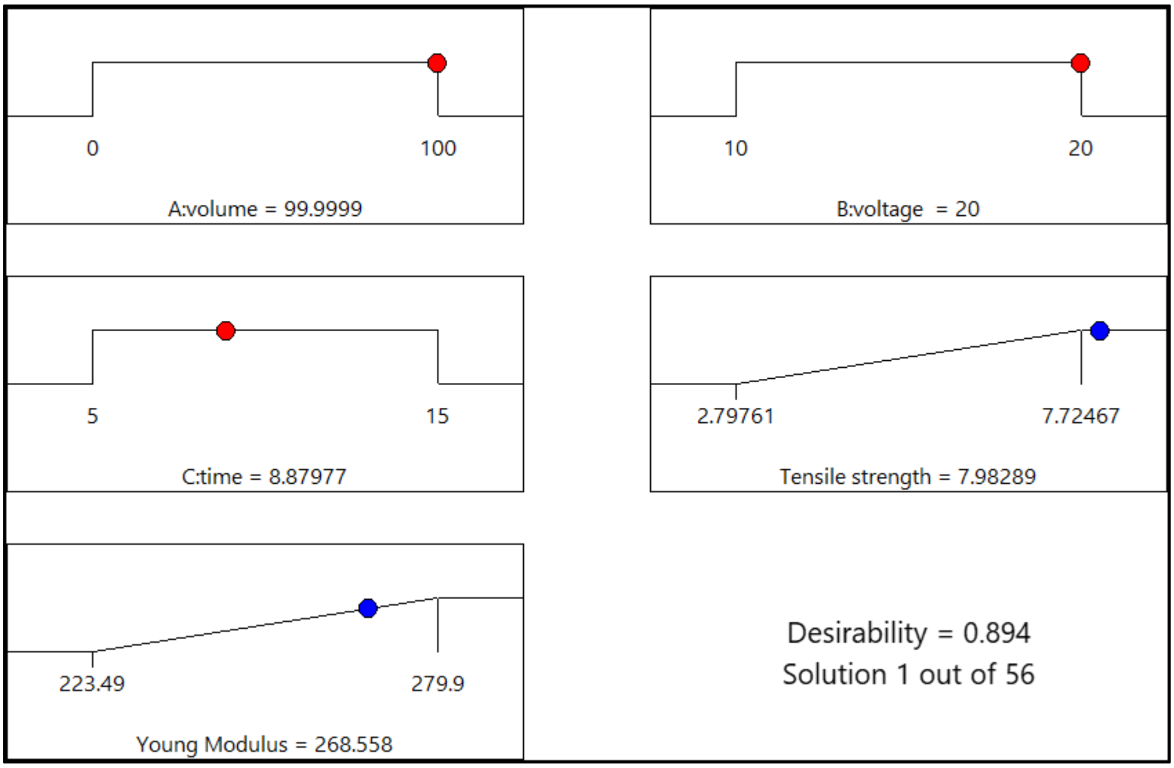

Figure 4.20: Numerical ramp graph for statistically optimized factors and response for first experimental design (0% water, 100% methanol and 100% water,0% methanol)

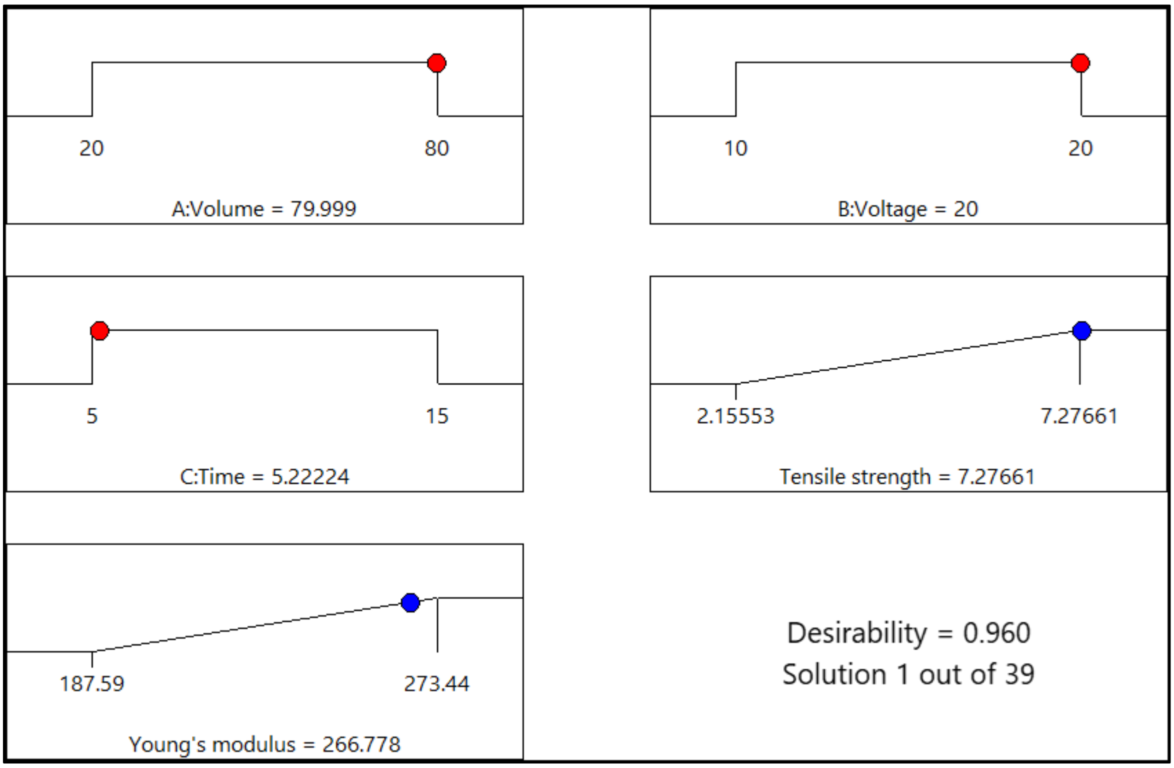

Figure 4.21: Numerical ramp graph for statistically optimized factors and response for second experimental design (20% water, 80% methanol and 80% water,20% methanol)

4.7 Chapter Summary

The objectives of the study were achieved and discussed in this chapter. The RSM in the Design Expert software was used to conduct the analysis, and the central composite design (CCD) response surface study was used to investigate the interaction between the parameters of the EPD, i.e., volume ratio of the suspension medium, deposition voltage, and deposition time, on the responses (tensile strength and Young's modulus of the composites). Through the optical observations, the mediums with dispersed MWCNTs are suitable to be used in the EPD process because, up until 30 minutes of dispersion, the MWCNTs are still well distributed. Apart from that, the effects of the three EPD input parameters can be seen through the FTIR, SEM, and tensile properties analyses. When MWCNTs were added to the composite, the FTIR peak shifted from 3288 cm^{-1} to 3313 cm^{-1}, indicating that the matrix and reinforcement had formed good interactions with one another. Additionally, through SEM, the CF can be seen to be closely packed in the composites when deposited with MWCNTs. As for the tensile properties analysis, there are significant improvements in the tensile strength and Young's modulus of the composites with the addition of MWCNTs. This proved that the interaction between the three input parameters helped to deposit MWCNTs successfully. Meanwhile, the ideal parameter for obtaining maximum responses had been determined by analysing the response surface graphical analysis. The optimum conditions for the first DoE (0% water, 100% methanol and 100% water,0% methanol) were when the volume ratio was 99.99% water, the voltage was 20V, and the time was 8.88 minutes, which obtained the maximum tensile strength of 7.98 N/mm^2 and the Young's modulus of 268.56 N/mm^2. As for the second DoE (20% water, 80% methanol and 80% water,20% methanol), tensile strength and Young's modulus of 7.28 N/mm^2 and 266.78 N/mm^2, respectively, were achieved when the ideal conditions were: volume ratio of 79.99% water, deposition voltage of 20V, and time of 5.22 minutes. In the end, composites with good tensile properties were obtainable as the three EPD parameters interacted well with one another.

CHAPTER 5

CONCLUSION AND RECOMMENDATION

5.1 Conclusion

This research aimed to analyse the tensile properties of the MWCNT-CF/Epoxy laminated composites when the input parameters of the EPD process vary. The data collection was done in accordance with the objectives of the study. Firstly, the MWCNTs' dispersion in the suspension medium was stable to be used in the deposition process. This was proven via the optical observation that was done before the EPD process. Secondly, the study demonstrated that the input parameters affect the laminated composites' tensile properties. The deposition voltage significantly influenced the tensile properties for the first DoE (0% water, 100% methanol and 100% water, 0% methanol). This had been further supported by significant model terms in the ANOVA analysis and the response surface graphical analysis. Meanwhile, for the second DoE (20% water,80% methanol and 80% water,20% methanol), the deposition time directly influenced the tensile properties as denoted by the significant model terms in the ANOVA analysis. Lastly, the third objective, the optimization study, was achieved by using RSM. The ideal input parameter conditions were essential to obtain composites with high tensile properties. The aim and objectives of the study had been achieved, as proven by the study's findings. The obtained results also confirmed the hypothesis of the study.

5.2 Recommendation

Based on the study's conclusions, a few recommendations can be considered for future studies to improve the study. Future studies using different types of solvents, such as acetone, tetrahydrofuran and dichloromethane for the deposition process are recommended to compare the capability of those solvents with the current medium. Continuous ultrasonication throughout the EPD process is also suggested to minimize the agglomeration of the MWCNTs in the medium. Lastly, based on the findings of the optimization study for both DoE, it is proposed that only ratios ranging from 20% water, 80% methanol until 80% water, 20% methanol is used in similar future studies to check and compare the tensile properties of laminated composites.

REFERENCES

Aamir, M., Tolouei-Rad, M., Giasin, K., & Nosrati, A. (2019). Recent advances in drilling of carbon fiber–reinforced polymers for aerospace applications: a review. *International Journal of Advanced Manufacturing Technology*, *105*(5–6), 2289–2308.

Abdul Rahman, N., Muhammad Firdaus Kumar, N. K., Gilan, U. J., Jihed, E. E., Phillip, A., Linus, A. A., Nen@Shahinan, D., & Ismail, V. (2020). Kinetic Study & Statistical Modelling of Sarawak Peat Water Electrocoagulation System using Copper and Aluminium Electrodes. *Journal of Applied Science & Process Engineering*, *7*(1), 439–456.

Abdul Rahman, Nazeri, Jose Jol, C., Albania Linus, A., Wan Borhan, W. W. S., Abdul Jalal, N. S., Baharuddin, N., Samsul, S. N. A., & Abdul Mutalip, N. (2023). Statistical analysis of salinity reduction in Borneo tropical brackish peat water with continuous electrocoagulation treatment system. *Journal of Hazardous Materials Advances*, *10*(January), 100265.

Abdullah, N., Saidur, R., Zainoodin, A. M., & Aslfattahi, N. (2020). Optimization of electrocatalyst performance of platinum–ruthenium induced with MXene by response surface methodology for clean energy application. *Journal of Cleaner Production*, *277*(2020), 123395.

Adedeji, J. A., Tetteh, E. K., Amo-Duodu, G., Armah, E. K., Rathilal, S., & Chetty, M. (2022). Central Composite Design Optimisation of Banana Peels/Magnetite for Anaerobic Biogas Production from Wastewater. *Applied Sciences (Switzerland)*, *12*(23), 1–14.

Ahmad, A., Lajis, M. A., Yusuf, N. K., & Ab Rahim, S. N. (2020). Statistical optimization by the response surface methodology of direct recycled aluminum-alumina metal matrix composite (MMC-AlR) employing the metal forming process. *Processes*, *8*(805), 1–19.

Ahmad, H., Markina, A. A., Porotnikov, M. V., & Ahmad, F., 2020. A review of carbon fiber materials in automotive industry. In Sevastopol State University, National Research Technological University, Altai State Technical University, Limited Liability Company "Inlink," & International Union of Mechanical Engineers (Eds.), *IOP Conference Series: Materials Science and Engineering*, Sevastopol, Russia, 7-11 September 2020. IOP Publishing Ltd.

Akca, E., & Gursel, A. (2015). *A Review on the Matrix Toughness of Thermoplastic Materials*. *3*(2), 1–8.

Alshehri, R., Ilyas, A. M., Hasan, A., Arnaout, A., Ahmed, F., & Memic, A. (2016). Carbon Nanotubes in Biomedical Applications: Factors, Mechanisms, and Remedies of Toxicity. *Journal of Medicinal Chemistry*, *59*(18), 8149–8167.

Altin Karataş, M., & Gökkaya, H. (2018). A review on machinability of carbon fiber reinforced polymer (CFRP) and glass fiber reinforced polymer (GFRP) composite materials. *Defence Technology*, *14*(4), 318–326.

Amrollahi, P., Krasinski, J. S., Vaidyanathan, R., Tayebi, L., & Vashaee, D. (2016). Electrophoretic Deposition (EPD): Fundamentals and Applications from Nano- to Microscale Structures Pouya. In *Handbook of Nanoelectrochemistry: Electrochemical Synthesis Methods, Properties, and Characterization Techniques* (Aliofkhazraei, M. & Makhlouf, A. S. H., 1st ed.) pp. 561–591. Switzerland: Springer International

Publishing Switzerland 2016.

Aqel, A., El-Nour, K. M. M. A., Ammar, R. A. A., & Al-Warthan, A. (2012). Carbon nanotubes, science and technology part (I) structure, synthesis and characterisation. *Arabian Journal of Chemistry*, *5*(1), 1–23.

Atiq Ur Rehman, M., Chen, Q., Braem, A., Shaffer, M. S. P., & Boccaccini, A. R. (2020). Electrophoretic deposition of carbon nanotubes: recent progress and remaining challenges. *International Materials Reviews*, *66*(8), 533–562.

Atmakuri, A., Palevicius, A., Kolli, L., Vilkauskas, A., & Janusas, G. (2021). Development and analysis of mechanical properties of caryota and sisal natural fibers reinforced epoxy hybrid composites. *Polymers*, *13*(6), 1–19.

Attar, S., & Ranveer, A. (2015). Carbon Nanotubes and Its Environmental Applications. *Journal of Environmental Science , Computer Science and Engineering & Technology*, *4*(2), 304–311.

Avcu, E., Baştan, F. E., Abdullah, H. Z., Rehman, M. A. U., Avcu, Y. Y., & Boccaccini, A. R. (2019). Electrophoretic deposition of chitosan-based composite coatings for biomedical applications: A review. *Progress in Materials Science*, *103*(January), 69–108.

Awais, H., Nawab, Y., Amjad, A., Anjang, A., Md Akil, H., & Zainol Abidin, M. S. (2021). Environmental benign natural fibre reinforced thermoplastic composites: A review. *Composites Part C: Open Access*, *4*(August 2020), 1–18.

Awasthi, S., Pandey, S. K., Pandey, C. P., & Balani, K. (2019). Progress in Electrochemical and Electrophoretic Deposition of Nickel with Carbonaceous Allotropes: A Review. *Advanced Materials Interfaces*, *7*(1), 1–33.

Aznam, I., Mah, J. C. W., Muchtar, A., Somalu, M. R., & Ghazali, M. J. (2018). A review of key parameters for effective electrophoretic deposition in the fabrication of solid oxide fuel cells. *Journal of Zhejiang University: Science A*, *19*(11), 811–823.

Azri, F. A., Sukor, R., Hajian, R., Yusof, N. A., Bakar, F. A., & Selamat, J. (2017). Modification strategy of screen-printed carbon electrode with functionalized multi-walled carbon nanotube and chitosan matrix for biosensor development. *Asian Journal of Chemistry*, *29*(1), 31–36.

Bahmani, M., Zarghami, S., Mohammadi, T., Asadi, A. A., & Khanlari, S. (2021). PES electrospun fibrous membrane for oily wastewater treatment: Fabrication condition optimization using response surface methodology. *Polymers for Advanced Technologies*, *32*(2), 886–899.

Banerjee, A., Chitnis, U., Jadhav, S., Bhawalkar, J., & Chaudhury, S. (2009). Hypothesis testing, type I and type II errors. *Industrial Psychiatry Journal*, *18*(2), 127–131.

Bassiouny, L., Samir, T., Abdallah, S., Ashour, H., & Anwar, A., 2021. Enhancement of carbon fiber/epoxy composite electrical, optical and thermal properties by using different types of nano-additives. In The Military Technical College (Ed.), *IOP Conference Series: Materials Science and Engineering*, Cairo, Egypt, 6-8 April 2021. IOP Publishing.

Batool, S. A., Wadood, A., Hussain, S. W., Yasir, M., & Rehman, M. A. U. (2021). A Brief Insight to the Electrophoretic Deposition of PEEK- , Chitosan- , Gelatin- , and Zein-Based Composite Coatings for Biomedical Applications : Recent Developments and Challenges. *Surfaces*, *4*(1), 205–239.

Behera, S. K., Meena, H., Chakraborty, S., & Meikap, B. C. (2018). Application of response surface methodology (RSM) for optimization of leaching parameters for ash reduction from low-grade coal. *International Journal of Mining Science and Technology*, *28*(4), 621–629.

Beiramzadeh, Z., Baqersad, M., & Aghababaei, M. (2019). Application of the response surface methodology (RSM) in heavy metal removal from real power plant wastewater using electrocoagulation. *European Journal of Environmental and Civil Engineering*, *26*(1), 1–20.

Bera, B. (2017). A Review on Polymer, Graphene and Carbon Nanotube: Properties, Synthesis and Applications. *Imperial Journal of Interdisciplinary Research (IJIR)*, *3*(10), 61–70.

Bhattacharya, S. (2021). Central Composite Design for Response Surface Methodology and Its Application in Pharmacy. In *Response Surface Methodology in Engineering Science* (Kayaroganam P., 1st ed.) pp. 1–19. London: IntechOpen.

Bhowmik, K., Khutia, N., Tarfaoui, M., Jana, M., Das, K., Roy, T., Bandyopadhyay, A., & Roy Chowdhury, A. (2022). Influence of multiwalled carbon nanotube on progressive damage of epoxy/carbon fiber reinforced structural composite. *Polymer Composites*, *43*(11), 7751–7772.

Bilisik, K., & Syduzzaman, M. (2021). Carbon nanotubes in carbon/epoxy multiscale textile preform composites: A review. *Polymer Composites*, *42*(4), 1670–1697.

Breig, S. J. M., & Luti, K. J. K., 2021. Response surface methodology: A review on its applications and challenges in microbial cultures. In Al-Nahrain University, Universiti Malaysia Perlis, Universiti Sains Malaysia, & MIE University (Eds.), *Materials Today: Proceedings*, Kuala Lumpur, Malaysia, 28-30 December 2020. Elsevier Ltd.

Cecen, V., Seki, Y., Sarikanat, M., & Tavman, I. H. (2008). FTIR and SEM analysis of polyester- and epoxy-based composites manufactured by VARTM process. *Journal of Applied Polymer Science*, *108*(4), 2163–2170.

Chavez-Valdez, A., Shaffer, M. S. P., & Boccaccini, A. R. (2013). Applications of graphene electrophoretic deposition. A review. *Journal of Physical Chemistry B*, *117*(6), 1502–1515.

Chen, K. J., Oswald, J., & Krüger, T. (2018). Electrophoretic deposition of dielectric film on stimulation electrodes for the use in intraoperative neuromonitoring. *Current Directions in Biomedical Engineering*, *4*(1), 521–524.

Chen, Z., Zhang, A., Wang, X., Zhu, J., Fan, Y., Yu, H., & Yang, Z. (2017). The Advances of Carbon Nanotubes in Cancer Diagnostics and Therapeutics. *Journal of Nanomaterials*, *2017*(3418932), 1–14.

Colton, J. A., & Bower, K. M. (2002). Some Misconceptions About R2. *EXTRA Ordinary Sense*, *January 2002*, 1–12.

Cordero-Arias, L., Cabanas-Polo, S., Gao, H., Gilabert, J., Sanchez, E., Roether, J. A., Schubert, D. W., Virtanen, S., & Boccaccini, A. R. (2013). Electrophoretic deposition of nanostructured-TiO2/chitosan composite coatings on stainless steel. *RSC Advances*, *3*(28), 11247–11254.

Dai, C. A., Hsiao, C. C., Weng, S. C., Kao, A. C., Liu, C. P., Tsai, W. B., Chen, W. S., Liu, W. M., Shih, W. P., & Ma, C. C. (2009). A membrane actuator based on an ionic polymer network and carbon nanotubes: The synergy of ionic transport and mechanical properties. *Smart Materials and Structures*, *18*(8), 1–13.

Darvishmotevalli, M., Zarei, A., Moradnia, M., Noorisepehr, M., & Mohammadi, H. (2019).

Optimization of saline wastewater treatment using electrochemical oxidation process: Prediction by RSM method. *MethodsX*, *6*, 1101–1113.

de León-Martínez, P. A., Sáenz-Galindo, A., Ávila-Orta, C. A., Castañeda-Facio, A. O., Andrade-Guel, M. L., Sierra, U., Alvarado-Tenorio, G., & Bernal-Martínez, J. (2021). Ultrasound-assisted surface modification of mwcnt using organic acids. *Materials*, *14*(72), 1–13.

de Oliveira, L. G., de Paiva, A. P., Balestrassi, P. P., Ferreira, J. R., da Costa, S. C., & da Silva Campos, P. H. (2019). Response surface methodology for advanced manufacturing technology optimization: theoretical fundamentals, practical guidelines, and survey literature review. *International Journal of Advanced Manufacturing Technology*, *104*(5–8), 1785–1837.

Derawi, D. (2016). Experimental design using response surface methods for palm olein-based hydroxy-ether systhesis. *Sains Malaysiana*, *45*(7), 1149–1154.

Deshpande, P., & Mahendru, A. (2018). A review of single wall carbon nanotube: Structure and preparation. *International Journal of Scientific and Technology Research*, *7*(4), 132–135.

Diba, M., Fam, D. W. H., Boccaccini, A. R., & Shaffer, M. S. P. (2016). Electrophoretic deposition of graphene-related materials: A review of the fundamentals. *Progress in Materials Science*, *82*, 83–117.

Do Amaral Montanheiroa, T. L., Cristóvan, F. H., Machado, J. P. B., Tada, D. B., Durán, N., & Lemes, A. P. (2015). Effect of MWCNT functionalization on thermal and electrical properties of PHBV/MWCNT nanocomposites. *Journal of Materials Research*, *30*(1), 55–65.

dos Santos, A. S., de Oliveira, T. C., Rodrigues, K. F., Silva, A. A. C., Coppio, G. J. L., da Silva Fonseca, B. C., Simonetti, E. A. N., & Cividanes, L. D. S. (2021). Amino-functionalized carbon nanotubes for effectively improving the mechanical properties of pre-impregnated epoxy resin/carbon fiber. *Journal of Applied Polymer Science*, *138*(46), 1–18.

Du Prel, J. B., Hommel, G., Röhrig, B., & Blettner, M. (2009). Confidence Interval or P-Value? *Deutsches Arzteblatt Int*, *106*(19), 335–339.

Dumée, L., Sears, K., Schütz, J., Finn, N., Duke, M., & Gray, S. (2013). Influence of the sonication temperature on the debundling kinetics of carbon nanotubes in propan-2-ol. *Nanomaterials*, *3*(1), 70–85.

Eatemadi, A., Daraee, H., Karimkhanloo, H., Kouhi, M., Zarghami, N., Akbarzadeh, A., Abasi, M., Hanifehpour, Y., & Joo, S. W. (2014). Carbon nanotubes: properties, synthesis, purification, and medical applications. *Nanoscale Research Letters*, *9*(1), 1–13.

Ebrahimi, S., Mohd Nasri, C. S. S., & Bin Arshad, S. E. (2021). Hydrothermal synthesis of hydroxyapatite powders using Response Surface Methodology (RSM). *PLoS ONE*, *16*(5), 1–24.

Elganidi, I., Elarbe, B., Ridzuan, N., & Abdullah, N. (2022). Optimisation of reaction parameters for a novel polymeric additives as flow improvers of crude oil using response surface methodology. *Journal of Petroleum Exploration and Production Technology*, *12*(2), 437–449.

Erden, S., & Ho, K. (2017). Fiber reinforced composites. In *Fiber Technology for Fiber-Reinforced Composites* (Seydibeyoğlu, M. Ö., Mohanty, A. K., & Misra, M., 1st eds.), pp. 51–79. Duxford: Elsevier Ltd.

Ervina, J., Ghaleb, Z. A., Hamdan, S., & Mariatti, M. (2019). Colloidal stability of water-based carbon nanotube suspensions in electrophoretic deposition process: Effect of applied voltage and deposition time. *Composites Part A: Applied Science and Manufacturing*, *117*(November 2018), 1–10. h

Ervina, J., Mariatti, M., & Hamdan, S. (2017). Mechanical, electrical and thermal properties of multi-walled carbon nanotubes/epoxy composites: effect of post-processing techniques and filler loading. *Polymer Bulletin*, *74*(7), 2513–2533.

Farrokhi-Rad, M. (2016). Electrophoretic deposition of hydroxyapatite nanoparticles in different alcohols: Effect of Tris (tris(hydroxymethyl)aminomethane) as a dispersant. *Ceramics International*, *42*(2), 3361–3371.

Frackowiak, E., Khomenko, V., Jurewicz, K., Lota, K., & Béguin, F. (2006). Supercapacitors based on conducting polymers/nanotubes composites. *Journal of Power Sources*, *153*(2), 413–418.

Gharib, D. H., Malherbe, F., & Moulton, S. E. (2018). Debundling, Dispersion, and Stability of Multiwalled Carbon Nanotubes Driven by Molecularly Designed Electron Acceptors. *Langmuir*, *34*(40), 12137–12144.

Ghasempour, R., & Narei, H. (2018). CNT basics and characteristics. In *Carbon Nanotube-Reinforced Polymers: From Nanoscale to Macroscale* (Rafiee, R., 1st ed.), pp. 1–24. Amsterdam: Elsevier Inc.

Ghelich, R., Jahannama, M. R., Abdizadeh, H., Torknik, F. S., & Vaezi, M. R. (2019). Central composite design (CCD)-Response surface methodology (RSM) of effective electrospinning parameters on PVP-B-Hf hybrid nanofibrous composites for synthesis of HfB2 -based composite nanofibers. *Composites Part B: Engineering*, *166*(February), 527–541.

Gravis, D., Moisan, S., & Poncin-Epaillard, F. (2021). Characterization of surface physico-chemistry and morphology of plasma-sized carbon fiber. *Thin Solid Films*, *721*(March 2021), 1–35.

Guo, J., Lu, C., An, F., & He, S. (2012). Preparation and characterization of carbon nanotubes/carbon fiber hybrid material by ultrasonically assisted electrophoretic deposition. *Materials Letters*, *66*(1), 382–384.

Harussani, M. M., Sapuan, S. M., Nadeem, G., Rafin, T., & Kirubaanand, W. (2022). Recent applications of carbon-based composites in defence industry: A review. *Defence Technology*, *18*(8), 1281–1300.

Hashim, A. B., Giwa, S. O., Ibrahim, M., & Giwa, A. (2015). Finding The Optimum Parameters For Oil Extraction From Sesame Seed Using Response Surface Methodology. *International Journal of Scientific Research and Management Studies*, *2*(1), 1–13.

Hsissou, R., Seghiri, R., Benzekri, Z., Hilali, M., Rafik, M., & Elharfi, A. (2021). Polymer composite materials: A comprehensive review. *Composite Structures*, *262*(January), 113640–113654.

Hu, S., Li, W., Finklea, H., & Liu, X. (2020). A review of electrophoretic deposition of metal oxides and its application in solid oxide fuel cells. *Advances in Colloid and Interface Science*, *276*, 102102.

Ighalo, J. O., Adelodun, A. A., Adeniyi, A. G., & Igwegbe, C. A. (2020). Modelling the Effect of Sorbate-Sorbent Interphase on the Adsorption of Pesticides and Herbicides by

Historical Data Design. *Iranian Journal of Energy and Environment*, *11*(4), 253–259.

Ijomah, & Azubuike, M. (2019). On the Misconception of R2 for (r)2 in a Regression Model. *International Journal of Research and Scientific Innovation (IJRSI)*, *VI*(Xii), 71–76.

Imtiaz, S., Siddiq, M., Kausar, A., Muntha, S. T., Ambreen, J., & Bibi, I. (2018). A Review Featuring Fabrication, Properties and Applications of Carbon Nanotubes (CNTs) Reinforced Polymer and Epoxy Nanocomposites. *Chinese Journal of Polymer Science (English Edition)*, *36*(4), 445–461. https://doi.org/10.1007/s10118-018-2045-7

Isam, M., Baloo, L., Kutty, S. R. M., & Yavari, S. (2019). Optimisation and modelling of Pb(II) and Cu(II) biosorption onto red algae (Gracilaria changii) by using response surface methodology. *Water (Switzerland)*, *11*(2325), 1–18.

Isopencu, G., Stroescu, M., Brosteanu, A., Chira, N., Pârvulescu, O. C., Busuioc, C., & Stoica-Guzun, A. (2019). Optimization of ultrasound and microwave assisted oil extraction from sea buckthorn seeds by response surface methodology. *Journal of Food Process Engineering*, *42*(1), 1–12.

Jafar, A., Alshatti, Y., & Ahmad, A. (2016). Carbon nanotube toxicity: The smallest biggest debate in medical care. *Cogent Medicine*, *3*(1), 1–12.

Jafari, S. (2018). Engineering applications of carbon nanotubes. In *Carbon Nanotube-Reinforced Polymers: From Nanoscale to Macroscale* (Rafiee, R., 1st ed.), pp. 25–40. Amsterdam: Elsevier Inc.

Jena, G. K., Sahoo, S. K., Patra, C. N., Panigrahi, K. C., Sahu, S., & Dixit, P. K. (2017). Design, optimization, and evaluation of capecitabine-loaded chitosan microspheres for colon targeting. *Asian Journal of Pharmaceutics*, *11*(3), S592–S602.

Joe, B. M., Giwa, S. O., Ibrahim, M., Raji, Y. O., & Giwa, A. (2015). Optimization of the

Operating Conditions of Turbidity Removal from Synthesized Dairy Wastewater Using Pumpkin Seed as a Coagulant. *International Journal of Scientific & Engineering Research*, *6*(2), 1266–1277.

Jokić, S., Bijuk, M., Aladić, K., Bilić, M., & Molnar, M. (2016). Optimisation of supercritical CO2 extraction of grape seed oil using response surface methodology. *International Journal of Food Science and Technology*, *51*(2), 403–410.

Kassem, M. A., Shaboury, K. M. El, & Mohamed, A. I. (2019). Application of Central Composite Design for the Development and Evaluation of Chitosan-based Colon Targeted Microspheres and in vitro Characterization. *Indian Journal of Pharmaceutical Sciences*, *81*(2), 354–364.

Kaur, B., & Kaur, R. (2013). Application of response surface methodology for optimizing arginine deiminase production medium for Enterococcus faecium sp. GR7. *The Scientific World Journal*, *2013*(Article ID 892587), 1–12.

Kaur, R., Vatta, P., & Kaur, M. (2018). Carbon Nanotubes: A Review Article. *International Journal for Research in Applied Science and Engineering Technology*, *6*(4), 5075–5079.

Kausar, A., Rafique, I., & Muhammad, B. (2016). Review of Applications of Polymer/Carbon Nanotubes and Epoxy/CNT Composites. *Polymer - Plastics Technology and Engineering*, *55*(11), 1167–1191.

Keyte, J., Pancholi, K., & Njuguna, J. (2019). Recent Developments in Graphene Oxide/Epoxy Carbon Fiber-Reinforced Composites. *Frontiers in Materials*, *6*(224), 1–30.

Kim, H. Il, Han, W., Choi, W. K., Park, S. J., An, K. H., & Kim, B. J. (2016). Effects of maleic anhydride content on mechanical properties of carbon fibers-reinforced maleic anhydride-grafted-poly-propylene matrix composites. *Carbon Letters*, *20*(1), 39–46.

Kim, M., Lee, J., Cho, M., & Kim, J. (2022). Improvement of thermal and abrasion resistance performance of polyphenylene sulfide composite through 3-mercaptopropyl trimethoxysilane treatment of carbon fiber and graphene oxide fillers. *Polymer Testing*, *108*(2022), 1–10.

Kingston, C., Zepp, R., Andrady, A., Boverhof, D., Fehir, R., Hawkins, D., Roberts, J., Sayre, P., Shelton, B., Sultan, Y., Vejins, V., & Wohlleben, W. (2014). Release characteristics of selected carbon nanotube polymer composites. *Carbon*, *68*(March 2014), 33–57.

Konneh, M., Sudin, I., Dzahi Padil, M. E., & Roszat, R., 2014. Surface Roughness Study Of Milled Carbon Fiber Reinforced Polymer (CFRP) Composite Using 4 mm 2-Flute Titanium Aluminum Nitride (TiAlN) Coated Carbide End Mills. In: Z. Jiang, X. Liu, & J. Han (Eds.), *Advances in Materials and Materials Processing IV*, Kunming, China, 18-19 December 2013. Trans Tech Publication, Ltd.

Krishnan, S., Suzana, B. N., Wahid, Z. A., Nasrullah, M., Abdul Munaim, M. S., Din, M. F. B. M., Taib, S. M., & Li, Y. Y. (2020). Optimization of operating parameters for xylose reductase separation through ultrafiltration membrane using response surface methodology. *Biotechnology Reports*, *27*, e00498.

Kumar, A., Sharma, K., & Dixit, A. R. (2020). Carbon nanotube- and graphene-reinforced multiphase polymeric composites: review on their properties and applications. *Journal of Materials Science*, *55*(7), 2682–2724.

Lamberti, M., Pedata, P., Sannolo, N., Porto, S., De Rosa, A., & Caraglia, M. (2015). Carbon nanotubes: Properties, biomedical applications, advantages and risks in patients and occupationally-exposed workers. *International Journal of Immunopathology and Pharmacology*, *28*(1), 4–13.

Lamidi, S., Olaleye, N., Bankole, Y., Obalola, A., Aribike, E., & Adigun, I. (2023). Applications of Response Surface Methodology (RSM) in Product Design, Development, and Process Optimization. In *Response Surface Methodology - Research Advances and Applications* (Kayaroganam, P., 1st ed.), pp. 1–19. London: IntechOpen.

Leão, S. G., Martins, M. G. de M., Menezes, N. C. F., Lima, F. L. R. de M., Silva, C. F., Arantes, G. C., & Ávila, A. F. (2017). Experimental Multi-scale analysis of Carbon / Epoxy Composites Nano-Reinforced by Carbon Nanotubes / Multi-layer Graphene. *Materials Research*, *20*(Suppl.1), 134–142.

Lu. H., Khalina, A., Nurazzi, N. M., Norli, A., Harussani, M. M., Rafiqah, S. A., Aisyah, H. A., & Ramli, N. (2021). The challenges and future perspective of woven kenaf reinforcement in thermoset polymer composites in malaysia: A review. *Polymers*, *13*(1390), 1–25.

Lee, S. H., Woo, S. P., Kakati, N., Kim, D. J., & Yoon, Y. S. (2018). A comprehensive review of nanomaterials developed using electrophoresis process for high-efficiency energy conversion and storage systems. *Energies*, *11*(3122), 1–81.

Lessoued, R., Souahi, F., & Pelaez, L. C. (2017). Assessment of coagulation pretreatment of leachate by response surface methodology. *Water Science and Technology*, *76*(9), 2321–2327.

Li, J., Zhang, Z., Fu, J., Liang, Z., & Ramakrishnan, K. R. (2021). Mechanical properties and structural health monitoring performance of carbon nanotube-modified FRP composites: A review. *Nanotechnology Reviews*, *10*(1), 1438–1468.

Li, M., Gu, Y., Liu, Y., Li, Y., & Zhang, Z. (2013). Interfacial improvement of carbon fiber/epoxy composites using a simple process for depositing commercially functionalized carbon nanotubes on the fibers. *Carbon*, *52*, 109–121.

Li, S., Tzeng, S. S., Cherng, D. H., & Chiu, H. T., 2015. Mechanical properties of CNT/carbon fiber/epoxy hierarchical composites prepared using electrophoretic deposition. In Scandinavian Organizing and Scientific Committee (Ed.), *ICCM International Conferences on Composite Materials*, Copenhagen, Denmark, 19-24 July 2015. International Committee on Composite Materials.

Liu, J., Wang, J., Leung, C., & Gao, F. (2018). A multi-parameter optimization model for the evaluation of shale gas recovery enhancement. *Energies*, *11*(654), 1–29.

Liu, X., Wang, M., Zhang, S., & Pan, B. (2013). Application potential of carbon nanotubes in water treatment: A review. *Journal of Environmental Sciences (China)*, *25*(7), 1263–1280.

Ma, Y., Han, J., Wang, M., Chen, X., & Jia, S. (2018). Electrophoretic deposition of graphene-based materials: A review of materials and their applications. *Journal of Materiomics*, *4*(2), 108–120.

Madondo, N. I., Rathilal, S., & Bakare, B. F. (2022). Utilization of Response Surface Methodology in Optimization and Modelling of a Microbial Electrolysis Cell for Wastewater Treatment Using Box–Behnken Design Method. *Catalysts*, *12*(9), 1–20.

Masilamani, R., Dhandapani, N. V, Kumar, K. V., & Mani, K. T. (2017). A Review on Usage of Carbon Fiber Reinforced Plastics in Automobiles. *International Journal of Pure and Applied Mathematics*, *117*(20), 537–544.

McNulty, R. (2022). A logical analysis of null hypothesis significance testing using popular terminology. *BMC Medical Research Methodology*, *22*(1), 1–9.

Menezes, B. R. C. De, Rodrigues, K. F., Fonseca, B. C. D. S., Ribas, R. G., Montanheiro, T. L. D. A., & Thim, G. P. (2019). Recent advances in the use of carbon nanotubes as smart biomaterials. *Journal of Materials Chemistry B*, *7*(9), 1343–1360.

Merck KGaA. (2023). *Methanol CAS 67-56-1 | 106009*.[online] Available at: https://www.merckmillipore.com/MY/en/product/Methanol,MDA_CHEM-106009 [Assessed on 18 July 2023]

Misra, A., Tyagi, P. K., Rai, P., & Misra, D. S. (2007). FTIR spectroscopy of multiwalled carbon nanotubes: A simple approach to study the nitrogen doping. *Journal of Nanoscience and Nanotechnology*, *7*(6), 1820–1823.

Mittal, G., Dhand, V., Rhee, K. Y., Park, S. J., & Lee, W. R. (2015). A review on carbon nanotubes and graphene as fillers in reinforced polymer nanocomposites. *Journal of Industrial and Engineering Chemistry*, *21*(January 2015), 11–25.

Moaseri, E., Karimi, M., Baniadam, M., & Maghrebi, M. (2016). Enhancement in mechanical properties of multi-walled carbon nanotube–carbon fiber hybrid epoxy composite: effect of electrostatic repulsion. *Applied Physics A: Materials Science and Processing*, *122*(49), 1–8.

Mohan, S. K., Viruthagiri, T., & Arunkumar, C. (2014). Statistical optimization of process parameters for the production of tannase by Aspergillus flavus under submerged fermentation. *3 Biotech*, *4*(2), 159–166.

Mohd Nurazzi, N., Asyraf, M. R. M., Khalina, A., Abdullah, N., Sabaruddin, F. A., Kamarudin, S. H., Ahmad, S., Mahat, A. M., Lee, C. L., Aisyah, H. A., Norrrahim, M.

N. F., Ilyas, R. A., Harussani, M. M., Ishak, M. R., & Sapuan, S. M. (2021). Fabrication, functionalization, and application of carbon nanotube-reinforced polymer composite: An overview. *Polymers*, *13*(7), 1–44.

Mohmad Noor, B. N. A. B., Abdul Rojab, N. N. B., Bin Wahab, M. A., Mat, K. B., Binti Rusli, N. D., Al-Amsyar, S. M., Mahmud, M., & Harun, H. C. (2020). Feed Formulation of Improved Egg Custard formulation using Response Surface Methodology (RSM). In Universiti Malaysia Kelantan (UMK) (Ed.), *IOP Conference Series: Earth and Environmental Science*, Kelantan, Malaysia, 10 September 2020. IOP Publishing.

Moon, M., Yun, Y., Yoo, M., Song, J., & Oh, J. (2019). Carbon Fiber Manufacturing and Applications as a Benchmark for Nanotube Superfiber Development. In *Nanotube Superfiber Materials* (Schulz, M. J., Shanov, V., Yin, Z., & Cahay, M., 2nd ed.), pp. 879–896.Amsterdam: Elsevier Inc.

Mueanmas, C. (2022). The Optimization and Parameters Effect on Distilled Product from Pyrolysis of LDPE based on RSM for Liquid Fuel Production. In Hanoi University of Science and Technology (Ed.), *IOP Conference Series: Earth and Environmental Science*, Hanoi, Vietnam, 25-27 February 202, IOP Publishing.

Muhamad, M. S., Osman, M. H., Yasser, M., Mohamad, R. N., Sunar, N. M., Ali, R., Hamidon, N., Abdul, N. H., & Harun, H. (2020). Response Surface Methodology Optimization of Concrete Strength Using Hydroxyapatite Nanopowder As Admixture. *Progress in Engineering Application and Technology*, *1*(1), 134–141.

Nair, A. T., Makwana, A. R., & Ahammed, M. M. (2014). The use of response surface methodology for modelling and analysis of water and wastewater treatment processes: A review. *Water Science and Technology*, *69*(3), 464–478.

Nandiyanto, A. B. D., Oktiani, R., & Ragadhita, R. (2019). How to read and interpret ftir spectroscope of organic material. *Indonesian Journal of Science and Technology*, *4*(1), 97–118.

Niazmand, R., Jahani, M., Sabbagh, F., & Rezania, S. (2020). Optimization of electrocoagulation conditions for the purification of table olive debittering wastewater using response surface methodology. *Water (Switzerland)*, *12*(6), 1–18.

Njoku, C. N., & Otisi, S. K. (2023). Application of Central Composite Design with Design Expert v13 in Process Optimization. In *Response Surface Methodology - Research Advances and Applications* (Kayaroganam, P., 1st ed.), pp. 1–34. London:IntechOpen.

Nur Sabreena, A. H., Nor Azma, Y., & Mohamad, O. (2016). Response Surface Methodology for Optimisation of Parameters for Extraction of Stevia Rebaudiana Using Water, H2O. | *Iioabj* |, *7*(Suppl 1), 459–466.

Nurazzi, N. M., Sabaruddin, F. A., Harussani, M. M., Kamarudin, S. H., Rayung, M., Asyraf, M. R. M., Aisyah, H. A., Norrrahim, M. N. F., Ilyas, R. A., Abdullah, N., Zainudin, E. S., Sapuan, S. M., & Khalina, A. (2021). Mechanical performance and applications of cnts reinforced polymer composites—a review. *Nanomaterials*, *11*(2186), 1–25.

Obregón, S., Amor, G., & Vázquez, A. (2019). Electrophoretic deposition of photocatalytic materials. *Advances in Colloid and Interface Science*, *269*(July 2019), 236–255.

Ocholi, O., Menkiti, M., Auta, M., & Ezemagu, I. (2018). Optimization of the operating parameters for the extractive synthesis of biolubricant from sesame seed oil via response surface methodology. *Egyptian Journal of Petroleum*, *27*(3), 265–275.

Ouedraogo, B., & Savadogo, O. (2013). Electrophoretic Deposition of Alumina and Nickel Oxide Particles. *Journal of Scientific Research and Reports*, *2*(1), 190–205.

Ozkan, D., Gok, M. S., & Karaoglanli, A. C. (2020). Carbon Fiber Reinforced Polymer (CFRP) Composite Materials, Their Characteristic Properties, Industrial Application Areas and Their Machinability. In *Engineering Design Applications III* (Öchsner, A. & Altenbach, H., 1st ed.), pp. 235–253. Switzerland:Springer, Cham.

Park, S. J., & Park, S. J. (2020). Effect of ozone-treated single-walled carbon nanotubes on interfacial properties and fracture toughness of carbon fiber-reinforced epoxy composites. *Composites Part A: Applied Science and Manufacturing*, *137*, 105937.

Pei, B., Wang, W., Dunne, N., & Li, X. (2019). Applications of carbon nanotubes in bone tissue regeneration and engineering: Superiority, concerns, current advancements, and prospects. *Nanomaterials*, *9*(10), 1–39.

Pereira, L. M. S., Milan, T. M., & Tapia-Blácido, D. R. (2021). Using Response Surface Methodology (RSM) to optimize 2G bioethanol production: A review. *Biomass and Bioenergy*, *151*(June), 106166.

Prajapati, S. K., Malaiya, A., Kesharwani, P., Soni, D., & Jain, A. (2020). Biomedical applications and toxicities of carbon nanotubes. *Drug and Chemical Toxicology*, *45*(9), 1–16.

Qiu, P., Cui, M., Kang, K., Park, B., Son, Y., Khim, E., Jang, M., & Khim, J. (2014). Application of Box-Behnken design with response surface methodology for modeling and optimizing ultrasonic oxidation of arsenite with H2O2. *Central European Journal of Chemistry*, *12*(2), 164–172.

Radhwan, H., Shayfull, Z., Farizuan, M. R., Effendi, M. S. M., & Irfan, A. R., 2019. Optimization parameter effects on the quality surface finish of the three-dimensional printing (3D-printing) fused deposition modeling (FDM) using RSM. In Center Of

Excellence Geopolymer & Green Technology & School of Materials Engineering UniMAP (Eds.), *AIP Conference Proceedings*, Bandung, Indonesia, 29-30 April 2019. AIP Publishing.

Rahman, G., Najaf, Z., Mehmood, A., Bilal, S., Shah, A. ul H. A., Mian, S. A., & Ali, G. (2019). An Overview of the Recent Progress in the Synthesis and Applications of Carbon Nanotubes. *C Journal of Carbon Research*, *5*(1), 1–31.

Rahman, M., & Dzulkarnain, I. (2021). RSM for Modelling the CO2 Effect in the Interfacial Tension Between Brine and Waxy Dulang Crude Oil During LSW-WAG EOR. *Journal of Advanced Research in Fluid Mechanics and Thermal Sciences*, *85*(2), 159–174.

Rajewski, J., & Dobrzyńska-Inger, A. (2021). Application of response surface methodology (Rsm) for the optimization of chromium(iii) synergistic extraction by supported liquid membrane. *Membranes*, *11*(11), 1–17.

Ranjbar, Z., & Bakhtiary-Noodeh, M. (2020). Electrophoretic deposition of waterbome colloidal dispersions. In *Handbook of Waterborne Coatings* (Zarras, P., Soucek, M. D., & Tiwari, A., 1st ed.), pp. 181–194. Elsevier Inc.

Rao, R., Pint, C. L., Islam, A. E., Weatherup, R. S., Hofmann, S., Meshot, E. R., Wu, F., Zhou, C., Dee, N., Amama, P. B., Carpena-Nuñez, J., Shi, W., Plata, D. L., Penev, E. S., Yakobson, B. I., Balbuena, P. B., Bichara, C., Futaba, D. N., Noda, S., … Hart, A. J. (2018). Carbon Nanotubes and Related Nanomaterials: Critical Advances and Challenges for Synthesis toward Mainstream Commercial Applications. *ACS Nano*, *12*(12), 11756–11784.

Raunika, A., Raj, S. A., Jayakrishna, K., & Sultan, M. T. H., 2017. Carbon nanotube: A review on its mechanical properties and application in aerospace industry. In Aerospace

Society Malaysia (AEROS Malaysia) (Ed.), *IOP Conference Series: Materials Science and Engineering*, Putrajaya, Malaysia, 12 December 2017. Institute of Physics Publishing.

Rege, K., Raravikar, N. R., Kim, D., Schadler, L. S., Ajayan, P. M., & Dordick, J. S. (2003). Enzyme − Polymer − Single Walled Carbon Nanotube Composites as Biocatalytic Films. *Nano Letters*, *3*(6), 829–832.

Reji, M., & Kumar, R. (2022). Response surface methodology (RSM): An overview to analyze multivariate data. *Indian Journal of Microbiology Research*, *9*(4), 241–248.

Rodríguez-González, J. A., & Rubio-González, C. (2019). Influence of sprayed multi-walled carbon nanotubes on mode I and mode II interlaminar fracture toughness of carbon fiber/epoxy composites. *Advanced Composite Materials*, *28*(sup1), 1–18.

Rohajatien, U., Estiasih, T., Devi, M., Soekopitojo, S., Imron, A., Nor, N. B. M., Shah, L. A., Setyobudi, R. H., & Damat, D. (2023). Optimization of the Process of Reducing the Bitterness of Bitter Melon with Response Surface Methodology. *Jordan Journal of Biological Sciences*, *16*(1), 85–92.

Sabri, F. N. A. M., Zakaria, M. R., & Akil, H. M., 2020. Dispersion and stability of multiwalled carbon nanotubes (MWCNTs) in different solvents. In M. Jaafar & N. M. Sharif (Eds.), *AIP Conference Proceedings*, Nibong Tebal, Malaysia, 31 October-1 November 2019. American Institute of Physics Inc.

Sadhukhan, B., Mondal, N. K., & Chattoraj, S. (2016). Optimisation using central composite design (CCD) and the desirability function for sorption of methylene blue from aqueous solution onto Lemna major. *Karbala International Journal of Modern Science*, *2*(3), 145–155.

Saifuddin, N., Raziah, A. Z., & Junizah, A. R. (2013). Carbon nanotubes: A review on structure and their interaction with proteins. *Journal of Chemistry*, *2013*(Article ID 676815), 1–18.

Salahuddin, B., Faisal, S. N., Baigh, T. A., Alghamdi, M. N., Islam, M. S., Song, B., Zhang, X., Gao, S., & Aziz, S. (2021). Carbonaceous Materials Coated Carbon Fibre Reinforced Polymer Matrix Composites. *Polymers*, *13*(2771), 1–23.

Sarath Kumar, P., Jayanarayanan, K., & Balachandran, M., 2020. Thermal and Mechanical Behavior of Functionalized MWCNT Reinforced Epoxy Carbon Fabric Composites. In Amrita School of Engineering (Ed.), *Materials Today: Proceedings*, Bengaluru, India, 16-18 August 2018. Elsevier Ltd.

Sarfraz, M. S., Hong, H., & Kim, S. S. (2021). Recent developments in the manufacturing technologies of composite components and their cost-effectiveness in the automotive industry: A review study. *Composite Structures*, *266*(June 2021), 113864.

Sarrai, A. E., Hanini, S., Merzouk, N. K., Tassalit, D., Szabó, T., Hernádi, K., & Nagy, L. (2016). Using central composite experimental design to optimize the degradation of Tylosin from aqueous solution by Photo-Fenton reaction. *Materials*, *9*(6), 428.

Shahidi, S., & Moazzenchi, B. (2018). Carbon nanotube and its applications in textile industry–A review. *Journal of the Textile Institute*, *109*(12), 1653–1666.

Sheth, D., Maiti, S., Patel, S., Kandasamy, J., Chandan, M. R., & Rahaman, A. (2020). Enhancement of mechanical properties of carbon fiber reinforced epoxy matrix laminated composites with multiwalled carbon nanotubes. *Fullerenes Nanotubes and Carbon Nanostructures*, *29*(4), 288–294.

SkySpring Nanomaterials Inc. (2023). *MWNTs 95% <8 nm*.[online] Available at:

https://www.ssnano.com/inc/sdetail/mwnts_95___8_nm_/864 [Assessed on 18 July 2023]

Stat-Ease Inc. (2023). *Stat-Ease » v11 » Pre-Experiment » Summary Screen*.[online] Available at: https://www.statease.com/docs/v11/contents/design/summary-screen/[Assessed on 18 July 2023]

Talib, N. A. A., Salam, F., Yusof, N. A., Alang Ahmad, S. A., & Sulaiman, Y. (2017). Optimization of peak current of poly(3,4-ethylenedioxythiophene)/multi-walled carbon nanotube using response surface methodology/central composite design. *RSC Advances*, *7*(18), 11101–11110.

Tsushima, E. (2022). Interpreting Results from Statistical Hypothesis Testing: Understanding the Appropriate P-value. *Physical Therapy Research*, *25*(2), 49–55.

Tzetzis, D., Tsongas, K., & Mansour, G. (2017). Determination of the mechanical properties of epoxy silica nanocomposites through FEA-supported evaluation of ball indentation test results. *Materials Research*, *20*(6), 1571–1578.

Uche, O. A., Kelechi, S. E., Adamu, M., Ibrahim, Y. E., Alanazi, H., & Okokpujie, I. P. (2022). Modelling and Optimizing the Durability Performance of Self Consolidating Concrete Incorporating Crumb Rubber and Calcium Carbide Residue Using Response Surface Methodology. *Buildings*, *12*(4), 398.

Vaka, M., Walvekar, R., Jagadish, P., Khalid, M., Mubarak, N. M., & Panchal, H. (2020). High-temperature molten salts optimisation using mixture design for energy storage application. *Journal of Energy Storage*, *32*(June), 101981.

Veza, I., Spraggon, M., Fattah, I. M. R., & Idris, M. (2023). Response surface methodology (RSM) for optimizing engine performance and emissions fueled with biofuel: Review of RSM for sustainability energy transition. *Results in Engineering*, *18*(June), 101213.

Wang, H., Li, J., Zhang, X., Ouyang, Z., Li, Q., Su, Z., & Wei, G. (2013). Synthesis, characterization and drug release application of carbon nanotube-polymer nanosphere composites. *RSC Advances*, *3*(24), 9304–9310.

Welu, K. T., Beyan, S. M., Balakrishnan, S., & Admassu, H. (2020). Chicken feathers based Keratin extraction process data analysis using response surface-box-Behnken design method and characterization of keratin product. *Current Applied Science and Technology*, *20*(2), 163–177.

Wu, Y., Dhamodharan, D., Wang, Z., Wang, R., & Wu, L. (2020). Effect of electrophoretic deposition followed by solution pre-impregnated surface modified carbon fiber-carbon nanotubes on the mechanical properties of carbon fiber reinforced polycarbonate composites. *Composites Part B: Engineering*, *195*(2020), 108093.

Wulan, P. P. D. K., Ulwani, S. H., Wulandari, H., Purwanto, W. W., & Mulia, K., 2018. The effect of hydrochloric acid addition to increase carbon nanotubes dispersibility as drug delivery system by covalent functionalization. In Faculty of Engineering Universitas Indonesia (Ed.), *IOP Conference Series: Materials Science and Engineering*, Bali, Indonesia, 24-27 July 2017. Institute of Physics Publishing.

Xiao, C., Tan, Y., Wang, X., Gao, L., Wang, L., & Qi, Z. (2018). Study on interfacial and mechanical improvement of carbon fiber/epoxy composites by depositing multi-walled carbon nanotubes on fibers. *Chemical Physics Letters*, *703*(2018), 8–16.

Yahaya, S., Giwa, S. O., Ibrahim, M., & Giwa, A. (2016). Extraction of oil from jatropha seed kernels: Optimization and characterization. *International Journal of ChemTech Research*, *9*(5), 758–770.

Yao, X., Gao, X., Jiang, J., Xu, C., Deng, C., & Wang, J. (2018). Comparison of carbon nanotubes and graphene oxide coated carbon fiber for improving the interfacial properties of carbon fiber/epoxy composites. *Composites Part B: Engineering, 132*(2018), 170–177.

Yassin, K., & Hojjati, M. (2018). Processing of thermoplastic matrix composites through automated fiber placement and tape laying methods: A review. *Journal of Thermoplastic Composite Materials*, *31*(12), 1676–1725.

Ye, L., Wen, K., Zhang, Z., Yang, F., Liang, Y., Lv, W., Lin, Y., Gu, J., Dickerson, J. H., & He, W. (2016). Highly Efficient Materials Assembly Via Electrophoretic Deposition for Electrochemical Energy Conversion and Storage Devices. *Advanced Energy Materials*, *6*(7), 1–15.

Youssry, M., Al-Ruwaidhi, M., Zakeri, M., & Zakeri, M. (2020). Physical functionalization of multi-walled carbon nanotubes for enhanced dispersibility in aqueous medium. *Emergent Materials*, *3*(1), 25–32.

Yunardi, Zulkifli, & Masrianto. (2011). Response Surface Methodology Approach to Optimizing Process Variables for the Densification of Rice Straw as a Rural Alternative Solid Fuel. *Journal of Applied Sciences*, *11*(7), 1192–1198.

Zakaria, M. R., Akil, H. M., Omar, M. F., Abdullah, M. M. A. B., Rahman, A. A. A., & Othman, M. B. H. (2020). Improving flexural and dielectric properties of carbon fiber epoxy composite laminates reinforced with carbon nanotubes interlayer using electrospray deposition. *Nanotechnology Reviews*, *9*(1), 1170–1182.

Zakaria, M. R., Md Akil, H., Abdul Kudus, M. H., Ullah, F., Javed, F., & Nosbi, N. (2019). Hybrid carbon fiber-carbon nanotubes reinforced polymer composites: A review.

Composites Part B: Engineering, *176*(2019), 107313.

Zakaria, M. R., Md Akil, H., Omar, M. F., Abdul Kudus, M. H., Mohd Sabri, F. N. A., & Abdullah, M. M. A. B. (2020). Enhancement of mechanical and thermal properties of carbon fiber epoxy composite laminates reinforced with carbon nanotubes interlayer using electrospray deposition. *Composites Part C: Open Access*, *3*(August), 100075.

Zakaria, M. R., Omar, M. F., Akil, H. M., & Abdullah, M. M. A. B. (2020). Study of carbon nanotubes stability in different types of solvents for electrospray deposition method. *Evergreen - Joint Journal of Novel Carbon Resource Sciences & Green Asia Strategy*, *7*(4), 538–543.

Zhang, C., Liu, L., Xu, Z., Lv, H., Wu, N., Zhou, B., Mai, W., Zhao, L., Tian, X., & Guo, X. (2018). Improvement for interface adhesion of epoxy/carbon fibers endowed with carbon nanotubes via microwave plasma-enhanced chemical vapor deposition. *Polymer Composites*, *39*(S2), E1262–E1268.

Zhang, L., De Greef, N., Kalinka, G., Van Bilzen, B., Locquet, J. P., Verpoest, I., & Seo, J. W. (2017). Carbon nanotube-grafted carbon fiber polymer composites: Damage characterization on the micro-scale. *Composites Part B: Engineering*, *126*, 202–210.

Zhou, Q., Ding, L., Zhu, Y., Zhong, M., & Yang, C. (2020). Process parameters optimization of gallic acid removal from water by MIEX resin based on response surface methodology. *Processes*, *8*(273), 1–11.

Zhuang, J., Li, M., Pu, Y., Ragauskas, A. J., & Yoo, C. G. (2020). Observation of potential contaminants in processed biomass using fourier transform infrared spectroscopy. *Applied Sciences (Switzerland)*, *10*(4345), 1–13.

Zulkifle, N. T., Saat, M. N., & Ariffin, Z. Z. (2022). A Review on Response Surface

Methodology Optimization in Microbial Biotransformation. *Science Letters*, *16*(2), 64–72.

APPENDICES

Appendix A: Journal Publications

1. Rahman, M.R., Taib, N.-A.A.B., Matin, M.M., Alexanrovich, T.P., Vladimirovich, S.V., Sanaullah, K., Tazeddinova, D., Khan, A. (2022) Optimization of Tensile Strength and Young's Modulus of CNT – CF/ Epoxy Composites Using Response Surface Methodology (RSM). *Materials*, *15*(19), 6746. https://doi.org/10.3390/ma15196746